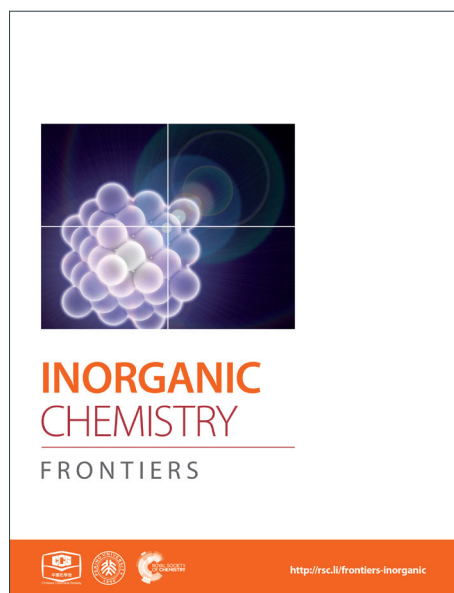
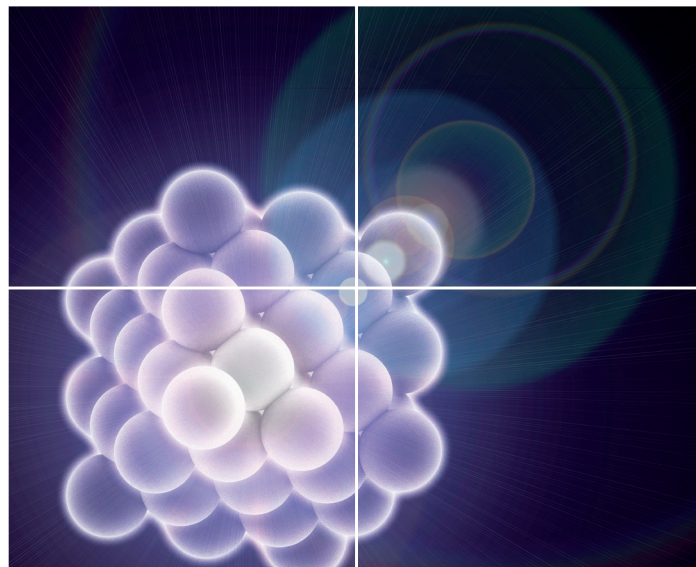


INORGANIC CHEMISTRY

FRONTIERS

Accepted Manuscript



This is an *Accepted Manuscript*, which has been through the Royal Society of Chemistry peer review process and has been accepted for publication.

Accepted Manuscripts are published online shortly after acceptance, before technical editing, formatting and proof reading. Using this free service, authors can make their results available to the community, in citable form, before we publish the edited article. We will replace this *Accepted Manuscript* with the edited and formatted *Advance Article* as soon as it is available.

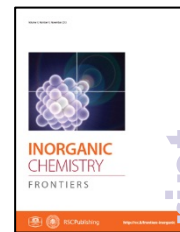
You can find more information about *Accepted Manuscripts* in the [Information for Authors](#).

Please note that technical editing may introduce minor changes to the text and/or graphics, which may alter content. The journal's standard [Terms & Conditions](#) and the [Ethical guidelines](#) still apply. In no event shall the Royal Society of Chemistry be held responsible for any errors or omissions in this *Accepted Manuscript* or any consequences arising from the use of any information it contains.



Frontiers is a unique collaboration between the Chinese Chemical Society and the Royal Society of Chemistry, aiming to publish a series of high impact quality chemistry journals that showcase the very best research from China, Asia and the rest of the world to an international audience. Each journal title is launched in collaboration with a top Chinese institute in the relevant field. For *Inorganic Chemistry Frontiers*, this is Peking University.

<http://rsc.li/frontiers-inorganic>



Guidelines for Referees - Paper Submission

Inorganic Chemistry Frontiers is a high impact Journal publishing research into inorganic and organometallic molecules and solids with explicit applications. This includes inorganic chemistry research at the interfaces of materials science, energy, nanoscience, catalysis and bio-inorganic chemistry. Papers should be of high significance and answer fundamental questions relevant to interdisciplinary applications. Structural reports, such as papers exclusively dealing with synthesis and characterization, will not be considered.

Full papers contain high impacting and original scientific work that has not been published previously. We ask you to only recommend work for publication which demonstrates a significant advance in the field; routine and incremental work – however competently researched and reported should not be recommended for publication.

Thank you very much for your assistance in evaluating this manuscript.

Best wishes

Song GAO, 高松, Peking University

Editor-in-Chief, *Inorganic Chemistry Frontiers*, InorgChemFrontiersED@rsc.org

General Guidance - Please be aware of our [Ethical Guidelines](#), which contain full information on the responsibilities of referees and authors, and our [Refereeing Procedure and Policy](#).

When preparing your report, please:

- Comment on the originality, significance, impact and scientific reliability of the work;
- State clearly whether you would like to see the article accepted or rejected and give detailed comments (with references, as appropriate) that will both help the Editor to make a decision on the article and the authors to improve it.

For confidentiality reasons, please:

- Treat the work and the report you prepare as confidential; the work may not be retained (in any form), disclosed, used or cited prior to publication; if you need to consult colleagues to help with the review, please inform them that the manuscript is confidential, and inform the Editor;
- Do not communicate directly with authors; *NB* your anonymity as a referee will be strictly preserved from the authors.

Please inform the Editor if:

- There is a conflict of interest;
- There is a significant part of the work which you are not able to referee with confidence;
- The work, or a significant part of the work, has previously been published or is currently submitted elsewhere;
- The work represents part of an unduly fragmented investigation.

When submitting your report, please:

- Provide your report rapidly and within **two weeks**, or inform the Editor immediately if you cannot do so. We welcome suggestions of alternative referees.

If you have any questions about reviewing this manuscript, please contact InorgChemFrontiersPROD@rsc.org

Submit your report at <http://mc.manuscriptcentra.com/inorgcf>

Dear editor,

Thank you for allowing us to revise the manuscript. We have addressed all the point of the referee and point by point replies are included. We have re-determined the temperature dependent fluorescence profiles of complexes 1-3 and added as new figures replacing earlier ones as suggested. The text is elaborated and made adequate. I hope you will find the revision adequate.

Regards.

J.B. Baruah

Comments to the Author

This manuscript reports structures and fluorescence properties of metal complexes with N-(3-imidazol-1-yl-propyl)-1,8-naphthalimide (L). The characterization of the complexes has been well done by means of NMR, IR, elemental analysis, thermal analysis, and X-ray analysis. The relation between the orientation and fluorescence spectral change would be an informative finding. However, there are many inappropriate description and questionable points concerning fluorescence in this manuscript. Thus, before the paper is recommended for publication in Inorganic Chemistry Frontiers, the manuscript should be fully revised in light of the comments below.

1. "Low and high wavelength" should be changed to "shorter and longer wavelength".

Reply: This is changed as suggested.

2. Figure 4 and related sentences in the text: The authors should show the information of the intensity of fluorescence. Why the increase or decrease in the emission intensity can be said from the solid state spectra? What are the quantum yields of these samples?

Reply: In solid state it is not possible to find out quantum yield. We have done the quantum yield in solution and values are given in table 2S of supporting material. The method of determination of quantum yield is also mentioned in the experimental section. Discussion on this part is made in text. To show the information on the relative intensity we have shown the normalised plots now along the Y-axis. The method of measurement of fluorescence in solid state is mentioned in experimental section to show that the measurements were carried out in uniform manner.

3. Scheme 2: this should be a scheme for the tetrahedral complexes. However, the complex indicated by M = Cd, X = SCN (i.e. complex 7) is octahedral.

Reply: We have corrected the scheme by omitting the extra ion which was put by mistake.

4. There are no comments and discussion for the complexes 4 and 5 though the fluorescence spectra are shown in Figure 4.

Reply: It is discussed now in text. These two complexes causes reduction of fluorescence intensity which is attributed to the paramagnetic ions.

5. Why the emission spectra of 2 and 3 in Figure 7 at 30 deg. are very different from the corresponding spectra in Figure 6?

Reply: It was measured elsewhere as facility was not with us, now we have the facility hence recorded once again and identical features are show. The additional results on the change of fluorescence emission of complex 1 with temperature are added. New figure 7 is provided and text is rewritten to make it clear.

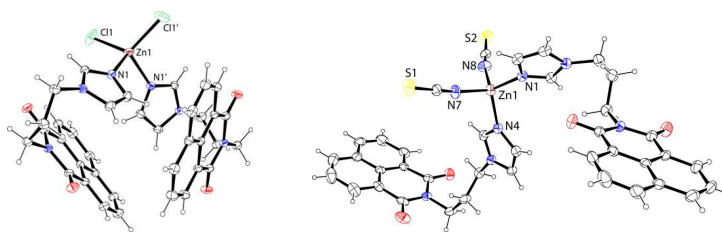
6. Page 13, line 10 from the bottom: figures 6a and 6b -> figures 7a and 7b.

Reply: Corrected.

7. The result of the elemental analysis of the complex 7 exceeds the tolerance.

Reply: Thank you for the finding. Infact there was a mistake in calculation of the theoretical one which should have read as Elemental anal calcd. $C_62H_59N_{13}O_8S_2Cd$, C, 57.69, H, 4.61, N, 14.11; found C, 60.02; H, 5.03; N, 12.82 (deviation could be due to loss of DMF outside the coordination during combustion). We express our inability to get the complete matching of elemental analysis in this case. We come across such problem often in related samples too. Since we are not being able to get the correct composition from the elemental analysis we dropped. We had a re-look at the NMR and the thermogram which supports the composition. These are discussed in text. The NMR assignment had small error which is now corrected. We have provided experimentally determined powder-XRD and the indexed simulated PXRD which matches nicely.

Twisted conformations in complexes of N-(3-imidazol-1-yl-propyl)-1,8-naphthalimide and fluorescence properties



Shorter-wavelength emission

Longer-wavelength emission

Jayanta Kumar Nath and Jubaraj B. Baruah

Twisted conformations in complexes of N-(3-imidazol-1-yl-propyl)-1,8-naphthalimide and fluorescence properties

Jayanta Kumar Nath and Jubaraj B. Baruah*

Department of Chemistry, Indian Institute of Technology Guwahati, Guwahati 781 039
Assam, India, Fax: +91-361-2690762; Ph. +91-361-2582311; email: juba@iitg.ernet.in

<http://www.iitg.ernet.in/juba>

Keywords:

Naphthalimide; Imidazole, Isomorphous structures; fluorescence; Metal-imidazole complexes.

Abstract:

A series of complexes of N-(3-imidazol-1-yl-propyl)-1,8-naphthalimide (**L**) with divalent ions of manganese, cobalt, zinc, cadmium and mercury are structurally characterized. The metal complexes $[ML_2Cl_2]$ $\{M = Zn$ (**1**), Cd (**2**), Hg (**3**) $\}$ are isomorphous and have distorted tetrahedral geometry with bent conformation of **L**. The thiocyanate complex $[ZnL_2(SCN)_2]$ has a distorted tetrahedral geometry with **L** in bent but different geometry from that in the structure of complex **1**. The manganese and cobalt thiocyanate complexes $[ML_4(SCN)_2] \cdot 2CH_3CN$ ($M = Mn, Co$) are isomorphous and have distorted octahedral geometry with the thiocyanate ligands occupying the axial positions. The cadmium complex $CdL_3(SCN)_2DMF \cdot DMF$ has a distorted octahedral geometry with thiocyanate ligands in the axial positions. The tetrahedral complexes $[ML_2Cl_2]$ $\{M = Zn$ (**1**), Cd (**2**) $\}$ in solid state shows emission at shorter wavelength than the single emission peak observed from the ligand; whereas the fluorescence emission of $[ML_2(SCN)_2]$ $\{M = Zn$ (**1**), Cd (**2**) $\}$ occurred at longer wavelength than **L**. On the other hand, $[HgL_2Cl_2]$ (**3**) showed single emission peak with higher intensity but at 31 nm shorter wavelength

than the emission peak of the parent ligand. Two types of bend orientations of the ligand **L** namely, parallel arrangement of imidazole with 1,8-naphthalimide ring and non-parallel arrangement in the tetrahedral complexes are observed. Former case favors intra-molecular charge transfer to shows **shorter** wavelength emission, whereas the non-parallel arrangements facilitate exciplex leading to emission at **longer** wavelength.

Introduction:

Naphthalimide derivatives are commonly used as fluorescence probes¹ and optical materials.² Structurally modified naphthalimide compounds show selectivity in binding ions.³ The nature of self-assemblies formed by naphthalimide derivatives are guided by functional groups.⁴ Study on chromogenic properties of naphthalimide derivatives helps to understand biological interactions.⁵ Naphthalimides have vast photochemistry⁶ and they are used to make bio-model for anion transport.⁷ Solar cells are developed based on ruthenium complexes of naphthalimides.⁸ Stacking interactions between naphthalimides generate interesting structures.⁹ Naphthalimides also bind to DNA¹⁰ and act as anticancer agents.¹¹ Naphthalimide based dyads are potent inhibitor against human N-acetyl-D-hexosaminidase.¹² Imidazole based naphthalimide has been shown to have interesting DNA binding and anticancer activity.¹³ Beside these, the N-functionalised 1,8-naphthalimide compounds having nitrogen-heterocyclic tether finds special interest for their interesting dual fluorescence properties. Such compounds show dual fluorescence originating from charge transfer via excited state with extended conjugation (ESEC).¹⁴ In such cases it was shown that the different orientation of N-heterocyclic ring

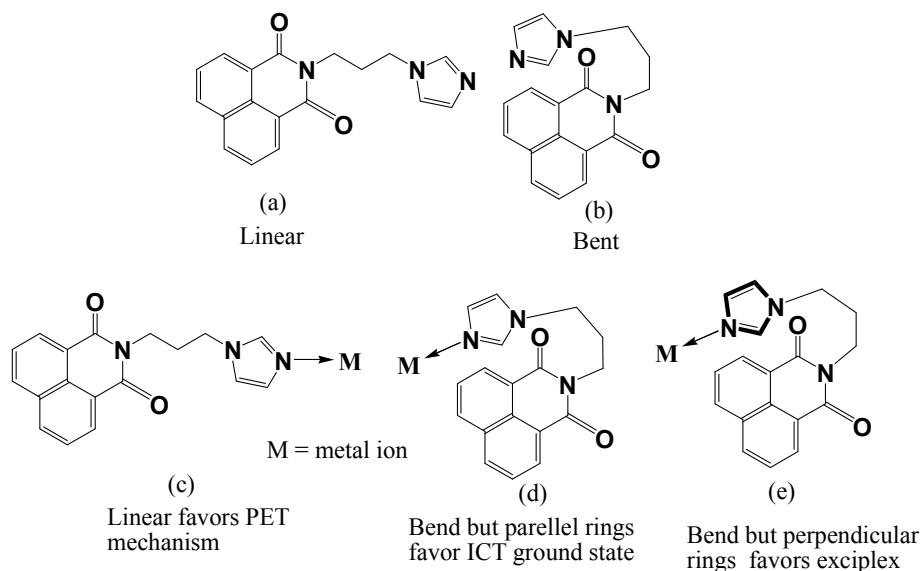


Figure 1: (a) linear and (b) bend form of the ligand **L**. Geometries of ligand **L** attached to a metal ion (c) linear form; and bend forms having (d) parallel or (e) non-parallel orientation of imidazole ring over 1,8-naphthalimide ring.

over a 1,8-naphthalimide ring can change the intensity as well as position of the absorptions. It was earlier shown by us that the anion- π interactions guide the fluorescence emission of imidazole tethered 1,8-naphthalimide derivatives. Since variation of anions resulted in change of fluorescence, it is essential to understand the role of cation in stabilization of different geometries of ligand such as **L** (figure 1) and understand their fluorescence properties. So far, such observations are not related to coordination effect of metal ions, as for example an N-functionalised 1,8-naphthalimide ligand such as **L** having flexible chain to connect the 1,8-naphthalimide with an imidazole ring would have provision to adopt linear or bend structure as illustrated in figure 1. Such geometry may be guided by a metal ion coordinating the orientation of the ligand to affect the intramolecular charge transfer or photo-electron transfer mechanism operative in such system to show characteristic fluorescence emission.³ While pursuing our study with metal complexes of **L**, we observe such structures in metal complexes of the ligand **L** and as a consequence characteristic fluorescence emissions are observed. Thus, we present here the results of such a study to establish correlation between the fluorescence and structures.

Experimental

All reagents and solvents were obtained from commercial sources. The IR spectra were recorded on a Perkin-Elmer SpectrumOne FT-IR spectrometer in the range 4000-400 cm^{-1} . The $^1\text{H-NMR}$ spectra were recorded using a Varian Mercury plus 400 MHz and Bruker 600 MHz instrument. Powder X-ray Diffraction (PXRD) were recorded using a Bruker D2 phaser with Cu- $K\alpha$ source ($\lambda = 154 \text{ \AA}$) on glass surfaces of air dried samples. Thermogravimetric analyses (TGA) were performed on a Mettler Toledo TGA/SDTA 851e module. Samples were placed in open alumina pans in the temperature range 25-600 $^{\circ}\text{C}$ and were purged with a stream of dry N_2 flowing at 100 mL min^{-1} with heating rate 5 $^{\circ}\text{C}$. The UV-Vis and solid state fluorescence emission spectra were recorded on a Perkin-Elmer-Lambda 750 UV-Vis spectrometer and Fluoromax-4 fluorimeter respectively at room temperature. The solid state fluorescence emission spectra of the samples were recorded of powdered samples in each case of equal weight (30 mg).

The quantum yield of fluorescence was determined by using quinine sulphate as a reference in water at room temperature.

$$\text{Quantum Yield} = \frac{\text{Area of the compound}}{\text{Area of Q.S}} \times \frac{\text{Absorbance at 333nm (Q.S)}}{\text{Absorbance at 333nm (Compound)}} \times \frac{\text{R.I of DMF}}{\text{R.I of water}} \times 0.54$$

The Q.S, DMF and R.I are quinine sulphate, dimethylformamide and refractive index respectively. And area means the area covered by fluorescence curve of the respective compound.

The N-(3-imidazol-1-yl-propyl)-1,8-naphthalimide (**L**) was synthesized by a reported procedure^{3f} using DMF as solvent and refluxing at 100 °C for 12 hs. Then the reaction mixture was cooled and ice cold water was added to it. Silky white precipitate of **L** formed was filtered and dried.

[ZnL₂Cl₂] (1): The ligand, **L** (0.61 g, 2 mmol) was dissolved in warmed DMF and added to a methanolic solution of zinc chloride (0.136 g, 1 mmol). The reaction mixture was refluxed for 4 hours and cooled it to room temperature and the filtered solution was kept undisturbed for crystallization. After one week white crystals appeared. Yield, 51%. Elemental anal calcd. For C₃₆H₃₀Cl₂N₆O₄Zn, C, 57.89; H, 4.05; N, 11.25; found C, 57.95, H, 4.07, N, 11.45. IR (KBr, cm⁻¹): 3414 (br), 2963 (s), 1695 (s), 1653 (s), 1586 (s), 1441 (m), 1344 (m), 1261 (s), 1242 (m), 1170 (w), 1098 (s), 1057 (w), 1026 (w), 850 (w), 801 (m), 785 (m), 654 (w), 544 (w). ¹H-NMR (600 MHz, DMSO-d₆): 8.48(d, 1H, 6.6 Hz), 8.42(br, 1H), 7.84(t, 1H, 7.8 Hz), 7.44(s, 1H), 7.02(s, 1H), 4.17(t, 2H, 6.6Hz), 4.10(t, 2H, 5.4Hz), 2.12(m, 2H, 6.6Hz).

[CdL₂Cl₂] (2): Complex **2** was prepared by a similar procedure as that of the complex **1**. Cadmium chloride was used instead of zinc chloride. One week later colourless crystals of **2** were obtained. Yield, 39 %. Elemental anal calcd. C₃₆H₃₀Cl₂N₆O₄Cd; C, 54.46; H,3.81; N, 10.58 found C, 54.51, H, 3.82, N, 10.61. IR (KBr, cm⁻¹): 3140 (m), 1694 (m), 1653 (s), 1586 (m), 1440 (w), 1342 (m), 1242 (s), 1170 (w), 1097 (m), 849 (m), 783 (s), 750 (w), 544 (w). ¹H-NMR (600 MHz, DMSO-d₆): 8.51(d, 1H, 24Hz), 7.87 (bs, 1H), 7.71(br, 1H), 7.22(s, 1H), 6.88(s, 1H), 4.08(t, 2H, 6Hz), 4.05 (t, 2H, 7.2Hz), 2.08 (bs, 2H).

[HgL₂Cl₂] (3): Complex **3** was prepared by the similar procedure as that of the complex **1** but **mercuric chloride was used instead of cadmium chloride**. On standing for 6-7 days, colorless crystals were observed. Isolated yield, 41%. Elemental anal calcd. C₃₆H₃₀Cl₂N₆O₄Hg, C, 49.01; H, 3.43; N, 9.53; found C, 49.10; H, 3.44; N, 9.61. IR (KBr, cm⁻¹): 3139 (s), 2123 (w), 1693 (m), 1654 (m), 1625 (s), 1518 (m), 1440 (m), 1342 (m), 1241 (s), 1096 (m), 1170 (w), 1096 (m), 1056 (w), 848 (s), 782 (s), 543 (m). ¹HNMR (600 MHz, DMSO-d₆): 8.47 (d, 1H, 7.2 Hz), 8.42 (d, 1H, 8.5Hz), 7.83 (t, 1H, 7.8Hz), 7.31 (s, 1H), 6.93 (s, 1H), 4.10 (t, 2H, 7.2 Hz), 4.03 (t, 2H, 7.2Hz), 2.08 (m, 2H, 7.2Hz).

[MnL₄(SCN)₂].2CH₃CN (4): To a binary mixture solution of acetonitrile and methanol of **L** (0.61 g, 2 mmol), manganese chloride tetrahydrate (0.10 g, 0.5 mmol) was added. After stirring the mixture for five minutes, potassium thiocyanate (0.10 g, 1 mmol) was added. Refluxing the reaction mixture for 4 hours, it was cooled, filtered and allowed to evaporate at room temperature. Brown colored crystals were observed after a week. Isolated yield, 54 %. Elemental anal calcd. C₇₈H₆₆N₁₆O₈S₂Mn C, 63.53, H, 4.51; N, 15.20 found C, 63.73, H, 4.61; N, 16.01. IR (KBr, cm⁻¹): 3466 (bs), 3121 (m), 2958 (w), 2059 (s), 1698 (m), 1661(s), 1591 (s), 1515 (s), 1443 (s), 1349 (s), 1238(s), 1174 (w), 1088 (w), 931 (m), 844

(s), 775 (s), 661 (m), 537 (w). Thermogravimetry: loss of 5.11% weight in the temperature range 70-170 °C (calcd 5.56 % for loss of acetonitrile molecules).

[CoL₄(SCN)₂].2CH₃CN (5): Complex **5** was synthesized in the same procedure as that of the complex **4**, cobalt chloride hexahydrate (0.12g, 0.5mmol) was used instead of MnCl₂.4H₂O. Yield, 51%. Elemental anal. calcd. C₇₈H₆₆N₁₆O₈S₂Co; C, 63.36, H, 4.50; N, 15.16; found C, 63.38; H, 4.51; N, 15.34. IR (KBr, cm⁻¹): 3444 (br), 3126 (w), 2071 (s), 1698 (s), 1660 (s), 1591 (s), 1515 (s), 1442 (s), 1349 (s), 1237 (s), 1174 (m), 1104 (w), 1089 (w), 935 (w), 844 (m), 775 (s), 661 (m), 537 (w). Thermogravimetry: Loss of the 5.39 % weight for acetonitrile molecules in the range 88-200 °C (calcd. 5.55 %).

[ZnL₂(SCN)₂] (6): It was synthesized by a similar procedure as that of the compound **6** where zinc nitrate hexahydrate was used. Colorless crystals were obtained after 7-8 days. Isolated yield, 39%. Elemental anal. calcd. C₃₇H₃₀N₈O₄S₂Zn, C, 56.96; H, 3.88; N, 14.36; found C, 56.49; H, 3.87; N, 14.23. IR(KBr, cm⁻¹): 3130 (m), 2954 (w), 2075 (s), 1691 (w), 1657 (m), 1588 (m), 1535 (m), 1438 (s), 1346 (w), 1237 (s), 1173 (w), 844 (s), 755 (s), 653 (s), 630 (m), 539 (w), 409 (w). ¹H-NMR (600 MHz, DMSO-d₆): 8.42-8.39 (m, 6H, naphthalene protons), 7.81-7.56 (m, 3H, imidazole protons), 4.19 (m, 2H N-CH₂), 4.04 (t, 2H, 4.8Hz N-CH₂), 2.15 (m, 2H, -CH₂-).

[CdL₃(SCN)₂DMF].DMF (7): It was synthesized by a similar procedure as that of the compound **7** where cadmium nitrate tetrahydrate was used instead of zinc nitrate hexahydrate. Brown crystals were formed after 8 days. Isolated yield, 45 %. IR (KBr, cm⁻¹): 3112 (w), 2954 (w), 2062 (s), 1702 (m), 1661 (s), 1590 (m), 1513 (s), 1443 (s), 1236 (s), 1091 (m), 843 (m), 774 (s), 659 (s), 539 (m). ¹H-NMR (600 MHz, DMSO-d₆): 8.45-8.41 (m, 18H, naphthalene protons), 7.94 (s, 2H, OC-H of DMF), 7.83 - 7.43 (m, 9H imidazole protons), 4.15 (t, 6H, 6.6Hz, NCH₂), 4.02 (t, 6H, 7.2Hz, NCH₂), 2.88 (s, 6H CH₃ of DMF), 2.72 (s, 6H, CH₃ of DMF), 2.10 (m, 6H -CH₂-). Thermogravimetry: Weight loss of 8.34 % in the range of 120-182 °C corresponds to the loss of two dimethylformamide molecules (calcd. 8.98 %).

Structure determination:

The X-ray single crystal diffraction data for the complex **1**, complex **3**, complex **4** and the complex **7** were collected at 298 K with Mo K α radiation ($\lambda = 0.71073 \text{ \AA}$) with the use of a Bruker Nonius SMART APEX CCD diffractometer equipped with a graphite monochromator an Apex CCD camera; SMART software was used for data collection and also for indexing the reflections and determining the unit cell parameters^{15a}; whereas the data of complex **2**, **5** and **6** were collected on a Oxford SuperNova diffractometer. For the data collected on the SuperNova diffractometer, data refinement and cell reductions were carried out by CrysAlisPro.^{15b} Data reduction and cell refinement were performed using SAINT software.^{15a} The structures were solved by direct methods

and refined by full-matrix least-squares calculations using SHELXTL software. All the non-H atoms were refined in the anisotropic approximation against F^2 of all reflections. The H-atoms were placed at their calculated positions and refined in the isotropic approximation; those attached to nitrogen and oxygen atoms were located in the difference Fourier maps and refined with isotropic displacement coefficients. Crystallographic data collection was done at room temperature, and the data are tabulated in Table 1.

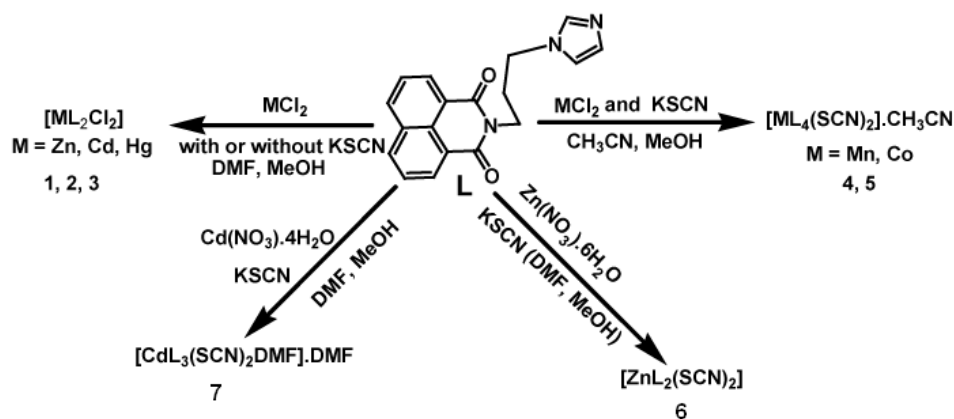
Table 1: Crystallographic parameters of complexes **1-7**

Compound No	Complex 1	Complex 2	Complex 3	Complex 4	Complex 5	Complex 6	Complex 7
Formulae	C ₃₆ H ₃₀ Cl ₂ N ₆ O ₄ Zn	C ₃₆ H ₃₀ Cl ₂ N ₆ O ₄ Cd	C ₃₆ H ₃₀ Cl ₂ N ₆ O ₄ Hg	C ₇₈ H ₆₆ N ₁₆ O ₈ S ₂ Mn	C ₇₈ H ₆₆ N ₁₆ O ₈ S ₂ Co	C ₃₈ H ₃₀ N ₈ O ₄ S ₂ Zn	C ₆₂ H ₅₉ N ₁₃ O ₈ S ₂ Cd
CCDC Nos.	928185	928178	928182	928183	928180	928184	928179
Mol. wt.	746.93	793.96	882.15	1474.53	1478.52	792.19	1290.74
Crystal system	Monoclinic	Monoclinic	Monoclinic	Triclinic	Triclinic	Monoclinic	Triclinic
Space group	<i>C2/c</i>	<i>C2/c</i>	<i>C2/c</i>	<i>P-1</i>	<i>P-1</i>	<i>P2₁/c</i>	<i>P-1</i>
<i>a</i> / Å	14.6120(18)	14.6314(6)	14.7824(3)	10.6242(7)	10.6146(8)	14.5214(4)	10.3324(3)
<i>b</i> / Å	11.9825(18)	11.9993(4)	12.0395(3)	11.2787(6)	11.2239(12)	14.1478(5)	16.9948(4)
<i>c</i> / Å	19.488(3)	19.7572(8)	19.7994(5)	15.7505(9)	15.7625(14)	22.8454(8)	17.5964(4)
α / °	90.00	90.00	90.00	95.575(4)	95.493(8)	90.00	91.4080(10)
β / °	104.612(11)	105.630(4)	104.923(2)	103.794(4)	104.366(7)	128.618(2)	95.6650(10)
γ / °	90.00	90.00	90.00	99.258(4)	99.105(8)	90.00	106.9570(10)
V / Å ³	3276.9(8)	3340.4(2)	3404.91(14)	1790.86(18)	1778.3(3)	3667.1(2)	2936.48(13)
Z	4	4	4	1	1	4	2
Density g.cm ⁻³	1.514	1.579	1.721	1.367	1.381	1.435	1.460
Abs. Coeff. /mm ⁻¹	0.964	0.864	4.727	0.312	0.370	0.836	0.511
F(000)	1536	1608	1736	767	769	1632	1332
Total no. of reflections	2919	3032	3066	6370	6422	6629	10470
Reflections, <i>I</i> > 2 σ (<i>I</i>)	2156	2638	2402	4095	4116	4765	7921
Max. 2 θ / °	50.50	50.50	50.48	50.50	50.50	50.50	50.50
Ranges (h, k, l)	-16 ≤ h ≤ 17 -14 ≤ k ≤ 12 -22 ≤ l ≤ 22	-17 ≤ h ≤ 17 -14 ≤ k ≤ 10 -23 ≤ l ≤ 23	-17 ≤ h ≤ 17 -13 ≤ k ≤ 14 -23 ≤ l ≤ 23	-12 ≤ h ≤ 12 -13 ≤ k ≤ 13 -18 ≤ l ≤ 18	-12 ≤ h ≤ 12 -11 ≤ k ≤ 13 -18 ≤ l ≤ 18	-16 ≤ h ≤ 17 -16 ≤ k ≤ 16 -26 ≤ l ≤ 27	-12 ≤ h ≤ 12 -19 ≤ k ≤ 18 -21 ≤ l ≤ 20
Complete to 2 θ (%)	98.1	99.8	99.0	98.3	99.8	99.8	98.3
Data/							
Restraints/Parameters	2919/0/222	3032/0/255	3066/0/222	6370/0/476	6422/0/476	6629/0/478	10470/0/779
Goof (F^2)	0.984	1.043	1.104	1.005	1.019	1.114	1.044
R indices [<i>I</i> > 2 σ (<i>I</i>)]	0.0488	0.0351	0.0720	0.0433	0.0699	0.0473	0.0320
R indices (all data)	0.0627	0.0427	0.1093	0.0790	0.1076	0.0732	0.0450
WR ₂ [<i>I</i> > 2 σ (<i>I</i>)]	0.1353	0.0793	0.1346	0.0676	0.1426	0.0774	0.0714
WR ₂ (all data)	0.1446	0.0835	0.1432	0.0781	0.1624	0.0863	0.0811

Results and discussion:

A series of divalent metal (M = Mn, Co, Zn, Cd, Hg) complexes of the ligand **L** with various compositions as depicted in scheme 1 were synthesized and characterized by various spectroscopic techniques and finally by single crystal X-ray diffraction. The powder XRD of all samples were recorded and compared with the simulated spectra; which showed the purity of the bulk samples in solid state. For the sake of comparison the powder pattern of the complex **1** is shown figure 1a and

others are available as supporting information. The metal chlorides of zinc, cadmium and mercury independently reacted with **L** led to a series of isomorphous complexes $[ML_2Cl_2]$ $\{M = Zn$ (**1**), Cd (**2**), Hg (**3**) $\}$. Each of the three complexes adopts distorted tetrahedral geometry. Since these three



Scheme 1: Different metal complexes of **L**

complexes are structurally similar, only the representative structure of the zinc complex (**1**) is shown in figure 2. In the solid state structure the zinc ion lies on a two-fold axis. The ligand **L** in these cases adopts a bend structure and such bend form of the ligand is stabilized by weak C-H \cdots O and π -

Table 1: The metal-ligand bond parameters in complexes **1-3**

Complex	M-L	Bond-length(Å)	< L-M-L	Angle (°)	< L-M-L	Angle (°)
Complex 1	Zn1- N1	2.028(2)	N1- Zn1- N1	99.41(13)	N1- Zn1- Cl1	112.63(7)
	Zn1- Cl1	2.2378(11)	N1- Zn1- Cl1	107.74(7)	Cl1- Zn1- Cl1	115.58(8)
Complex 2	Cd1- N1	2.231(2)	N1- Cd1- N1	94.99(12)	N1- Cd1- Cl1	112.84(7)
	Cd1 Cl1	2.4131(10)	N1-Cd1- Cl1	107.93(7)	Cl1 -Cd1- Cl1	118.00(7)
Complex 3	Hg1 -N1	2.268(7)	N1 -Hg1- N1	92.3(4)	N1 -Hg1- Cl1	111.5(2)
	Hg1- Cl1	2.451(5)	N1- Hg1-Cl1	106.3(2)	Cl1 -Hg1-Cl1	124.2(3)

stacking interactions (supporting figure 2S). Such interactions arise from intermolecular interactions between the carbonyl group of 1,8-naphthalimide with one C-H of the propylene attached to an imidazole unit. Another C-H bond of the propylene group at the α -position next to the imidazole also interacts with carbonyl group of 1,8-naphthalimide group. The formation of intra-molecular stacks of imidazole and naphthalene rings is favored by flexible propylene group. The metal-ligand bond parameters of the complexes **1-3** are listed in table 1. From the table 1 it is clear that metal-ligand bond distances are in the sequence Zn < Cd < Hg. The observed trend is due to the increase in the size of the metal ions.

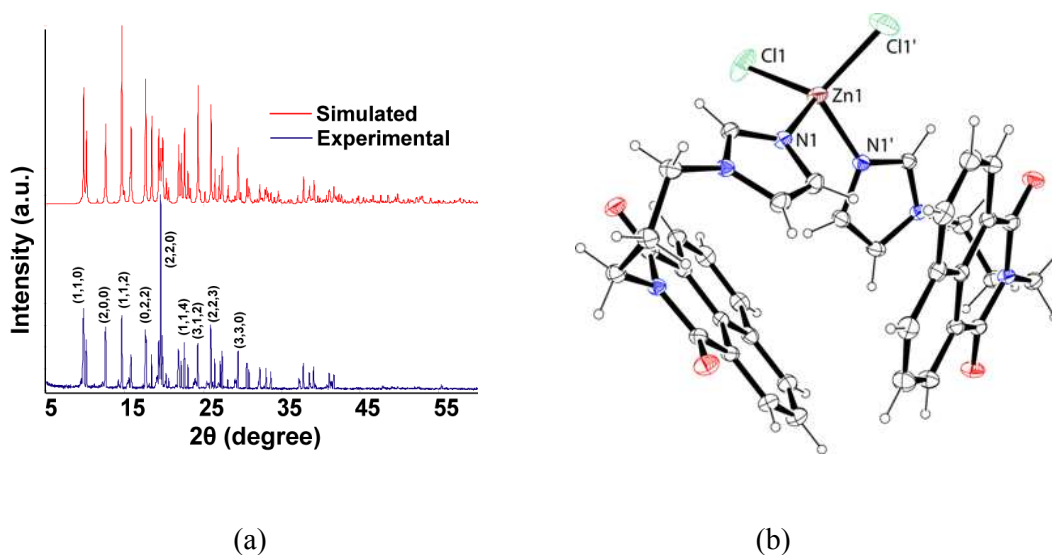


Figure 2: (a) Powder-XRD of the complex **1** (top : simulated, bottom : experimental). (b) Crystal structure of the complex **1** (ORTEP drawn with 30 % probability; equivalent symmetry is generated through $2-x, y, 1/2-z$)

Table 2: The Metal-ligand bond parameters of complexes **4-7**

Complex No.	M-X	Bond-length (Å)	< L-M-L	Angle (°)	< L-M-L	Angle (°)
Complex 4	Mn1- N1	2.2758(19)	N1- Mn1- N4	88.12	N1'- Mn1- N4'	91.88
	Mn1- N4	2.2606(19)	N1- Mn1- N7	89.67	N1'- Mn1- N7	90.33
	Mn1- N7	2.236(2)	N4- Mn1- N7	92.67	N4'- Mn1- N7	87.33
Complex 5	Co1- N1	2.169(4)	N1- Co1- N4	88.92	N1'- Mn1- N4	91.08
	Co1- N4	2.161(4)	N1- Co1- N7	90.37	N1'- Mn1- N7	89.63
	Co1- N7	2.157(4)	N4- Co1- N7	92.64	N4'- Mn1- N7	87.46
Complex 6	Zn1-N1	1.986(3)	N1-Zn1 -N4	114.52(10)	N4 -Zn1-N8	102.27(11)
	Zn1-N4	1.997(3)	N1-Zn1 -N7	103.77(11)	N7- Zn1-N8	111.58(12)
	Zn1-N7	1.972(3)	N1-Zn1 -N8	115.03(12)		
	Zn1-N8	1.940(3)	N4-Zn1 -N7	109.85(12)		
Complex 7	Cd1-N1	2.327(2)	N1-Cd1-N4	178.09(7)	N4-Cd1-N11	90.36(8)
	Cd1-N4	2.335(2)	N1-Cd1-O7	88.72(8)	N4-Cd1-N7	87.37(7)
	Cd1-N7	2.339(2)	N1-Cd1-N11	91.18(9)	N4-Cd1-N10	90.92(8)
	Cd1-N10	2.340(3)	N1-Cd1-N7	93.77(7)	N7-Cd1-N10	92.63(9)
	Cd1-N11	2.343(3)	N1-Cd1-N10	87.50(9)	N11-Cd1-N10	177.69(9)
	Cd1-O7	2.337(2)	N4-Cd1-O7	90.20(8)	O7-Cd1-N7	176.79(8)
			O7-Cd1-N11	88.57(9)	O7-Cd1-N10	89.50(9)

In the thiocyanate containing metal complexes the ratio of the ligand to the metal ions varies. For example 1: 2 complex was formed in the case of zinc, 1 : 3 in cadmium and 1 : 4 in the case of manganese and cobalt. The metal complexes bearing thiocyanate ligand has special interest from their ease of degradability and due to their labile nature.¹⁶ The manganese complex **4** and cobalt complex **5** have a similar compositions, namely $[\text{ML}_4(\text{SCN})_2] \cdot 2\text{CH}_3\text{CN}$ and they are isomorphous (Figure 3).

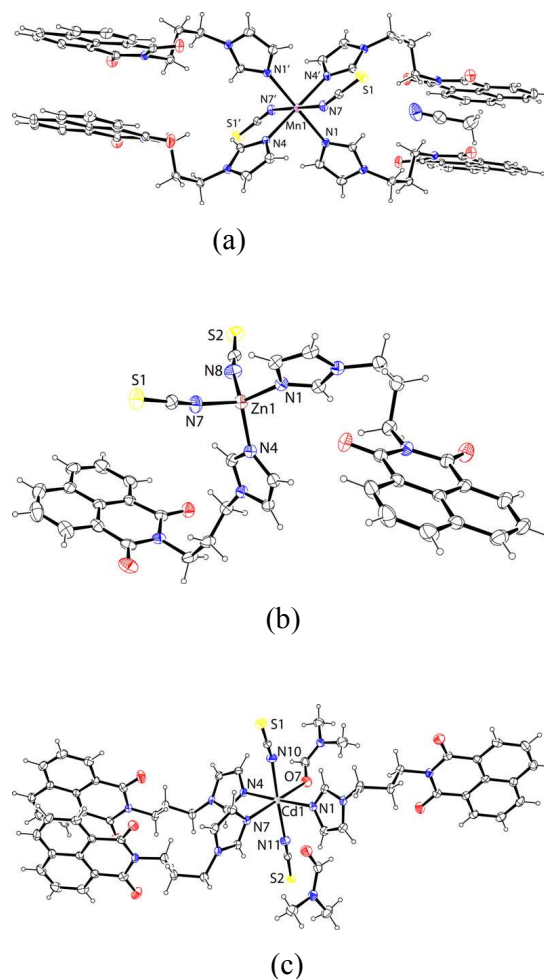


Figure 3: The structure of the complex (a) **4** (symmetry of equivalent atoms $-x, 1-y, -z$); (b) **6** and (c) **7** (ORTEP drawn with 30% thermal ellipsoid)

The manganese atom in the complex **4** and the cobalt atom in the complex **5** lies on an inversion centre. These hexa-coordinated complexes **4** and **5** have distorted octahedral geometry with four nitrogen atoms of the imidazole in one plane forming dative bond with a metal ion (Figure 3a). The monodentate thiocyanate ligands coordinating through nitrogen atoms occupy the axial positions. The structure of the complex **4** contains a center of inversion. The interesting feature of the structure is that the naphthalimide rings are π -stacked with another naphthalimide ring of neighboring molecules on each side so that layered structures are formed. The ligand **L** adopts a linear structure in the complex. While forming such structure the imidazole rings are not in one plane with respect to each other across the metal centers. The zinc thiocyanate complex $[\text{ZnL}_2(\text{SCN})_2]$ (**6**) is a tetra-coordinated complex (Figure 3b) with a distorted tetrahedral geometry. **The complex is stable in solution and the $^1\text{H-NMR}$ show significant shift from the parent ligand, the spectra is shown in figure 21s of supporting information.** On the other hand the $[\text{CdL}_3(\text{SCN})_2]\cdot\text{DMF}$ (**7**) is a hexa-coordinated complex with three ligands (**L**) and one DMF occupying one plane and two thiocyanate occupying the axial positions

of a distorted octahedron (Figure 3c). The complex **7** is also characterized by its $^1\text{H-NMR}$ which is shown in the supporting figure 22S. It shows methyl signals for two DMF molecules, one corresponding to coordinated other free dimethylformamide appears at 2.88 and 2.72 ppm. This is supportive of the structure determined by X-ray crystallography. From the integration compound shows presence of two molecules of DMF per molecule. In thermogravimetry complex **7** shows weight loss of 8.34 wt % (calcd. 8.98 wt %) in the range of 120-182 °C corresponds to the loss of one lattice dimethylformamide molecule and one coordinated dimethylformamide molecule. The IR spectra of thiocyanate complexes showed characteristic stretching frequencies in the region of 2051-2075 cm^{-1} . The values support the coordination thiocyanate through nitrogen atom in each case.¹⁷

The complexes have UV-visible absorptions in the range of 315-360 nm originating from the ligand. By comparing with analogous compound it may be suggested to originate from $n \rightarrow \pi^*$ transition.¹⁸ The naphthalimide derivatives are fluorescent¹⁹ and in solid state the ligand **L** shows a strong emission at 461 nm. The solid samples of the complexes **1-5** showed emissions in the range of 425-481 nm upon excitation at 350 nm [Figure 4(i)-(ii)]. The complexes **3**, **6** or **7** show fluorescence enhancement with

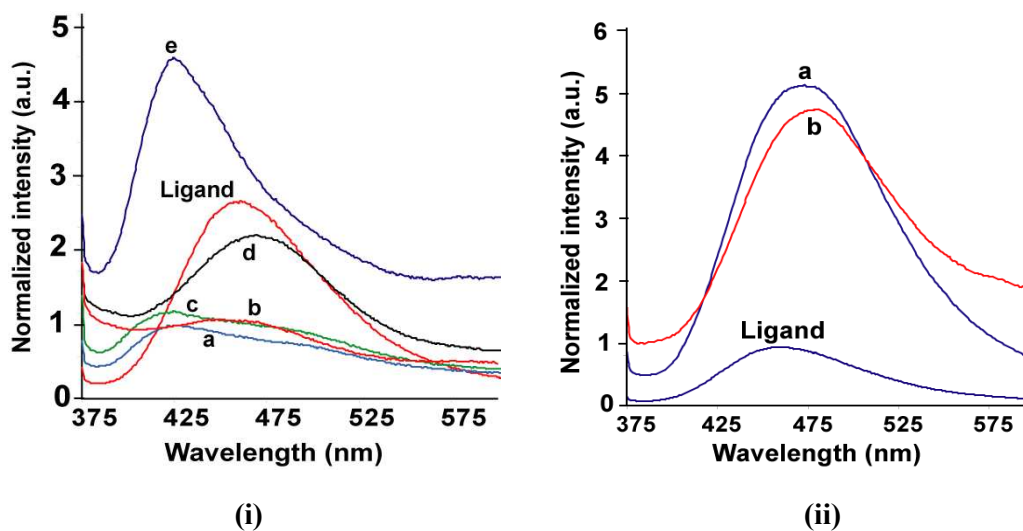
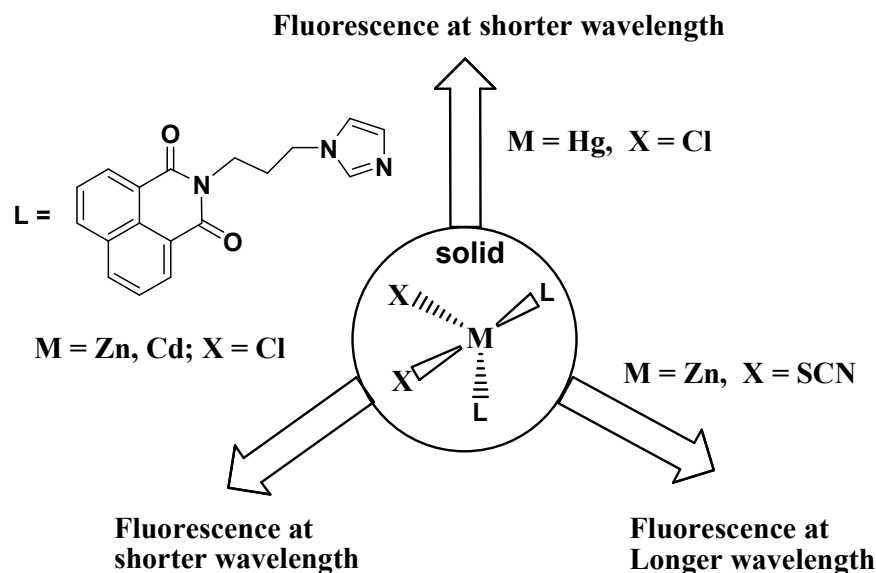


Figure 4: (i) Solid state fluorescence emission of ligand **L** and complexes (a) complex **1**; (b) complex **5**; (c) complex **2** ; (d) complex **4**, (e) complex **3**. In each case the intensity are normalized with respect to the lowest emission intensity shown by complex **1**. (ii) Solid state fluorescence emission of (a) complex **6**; (b) complex **7** at room temperature ($\lambda_{\text{ex}} = 350$ nm) with intensities normalised with respect to ligand.

respect to the ligand (**L**). On the other hand the complex **4** and **5** shows quenching of fluorescence with a small shift towards longer wavelength. The central metal ion in the complex **4** and complex **5** are manganese (d^5 , high-spin) and cobalt (d^7) in +2 oxidation state respectively, which are paramagnetic

Both complexes show lower fluorescence intensity than the parent ligand due to the paramagnetic nature of the ions^{1f}. These complexes have stretched conformations of the ligand; hence follow conventional fluorescence emission resembling the emission of parent ligand.



Scheme 2: The fluorescence selectivity in four coordinated complexes of L

The fluorescence emission changes of solid samples of these tetrahedral complexes are interesting; they show characteristic emission on variation of anions and cations. The increase and decrease in intensity of fluorescence emission shown by these complexes are schematically presented in scheme 2.

The complexes 1-3 have chloride ions, among them, the complex 1 or 2 show fluorescence emission at 428 nm and 425 nm respectively which are lower than the fluorescence emission of the ligand at 461 nm. The emission peak of mercury complex 3 has higher intensity than the free ligand occurs at 430 nm which is 31 nm less than the fluorescence emission of the ligand at solid state. On the other hand, the complexes 6 as well as 7 have fluorescence emission longer wavelength than the parent ligand. A close examination of the structure 1, 2 and 6, shows that the orientation of 1,8-naphthalimide rings are similar in the complex 1 and 2 but different from complexes 6 and 7. Whereas, the complexes 6 has a non-parallel bent orientation, but complex 7 has a stretched orientation of ligand L. Thus, twisting of the ligand to adopt near parallel orientation between the imidazole ring and 1,8-naphthalimide rings favors shorter-wavelength emission due to stabilization of the ground state by intramolecular charge transfer. The stretched orientation or an orientation not favoring stabilization of ground state of L would help in stabilization of inter-molecular charge transfer excited state, taking the emission to longer wavelength. The mercury being large and have more diffused charge have intra-molecular

interaction between imidazole and naphthalimide ring, helps in the stabilization of the ground state, accordingly it emits at **shorter** wavelength.

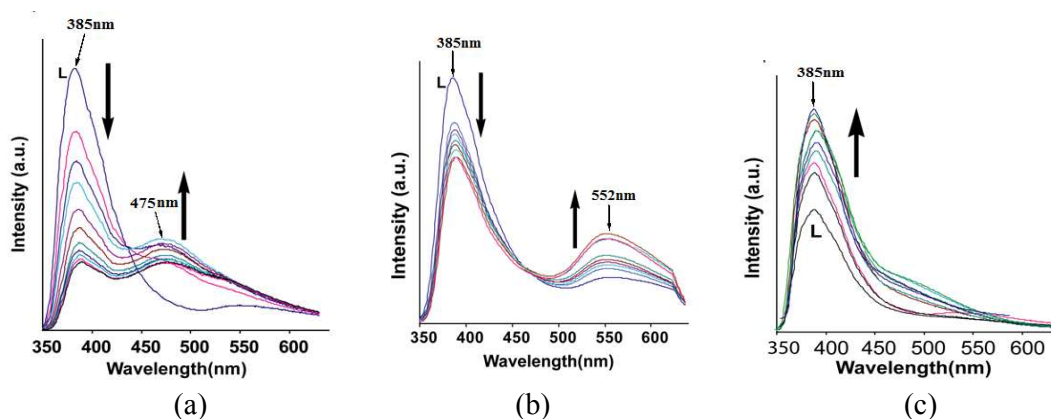


Figure 5: The changes in fluorescence emission intensity of ($\lambda_{\text{ex}} = 340 \text{ nm}$) of the ligand, **L** (2 ml of 10^{-4} M solution in DMF) on addition of (a) zinc chloride, (b) cadmium chloride and (c) mercuric chloride (5 μl aliquots of a 10^{-2} M solution in water).

The fluorescence emission of **L** in DMF solution by adding aqueous solution of chloride salts of zinc, cadmium or mercury were independently studied with complexes **1-3** (figure 5). As anticipated addition of mercury ions showed enhancement of fluorescence whereas the addition of zinc chloride or cadmium chloride quenched the emission causing emission at two wavelengths (Figure 5a, 5b). We find analogy between solution and solid state fluorescence emission study from the observed changes. The ligand single emission peak changed on titration with zinc chloride, and at the end of titration we observed emission at 385 nm and 475 nm; whereas similar titration with cadmium chloride yielded emission at 385 nm and 552 nm respectively. The role of anions in the fluorescence emission of naphthalimide fluorophores interacting with various anions is well established.^{2b} Heagy and coworkers have shown that depending on the orientations of pyridine over a naphthalimide ring causes fluorescence either shift to **shorter** wavelength (SW) or to **longer** wavelength (LW).¹⁴ Thus, in solution the addition zinc ions facilitated the stretching of the ligand leading to emission at **longer** wavelength occur from stabilization of exciplex through intermolecular π - π interactions.^{3f}

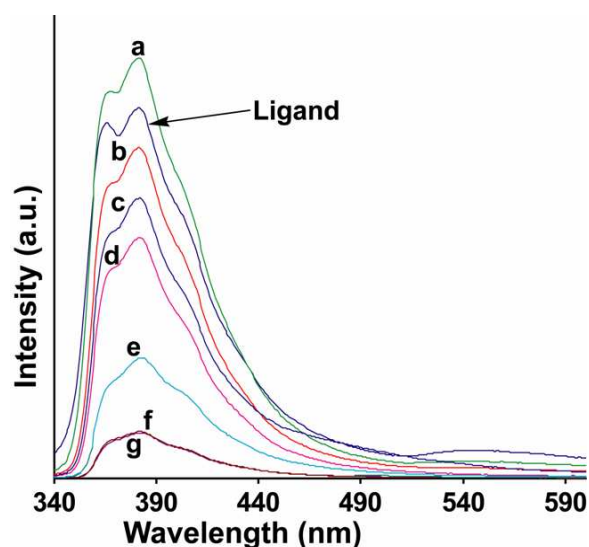


Figure 6 : Fluorescence emission spectra (λ_{ex} 330 nm) of the (a) complex **3**, (b) complex **2**; (c) complex **6**; (d) complex **1**; (e) complex **7**; (f) complex **5**; (g) complex **4** and ligand (**L**) in dimethylformamide (concentration of 10^{-4}M each)

The fluorescence emission spectra of the complexes in solutions were determined and are shown in figure 6. It is clear from the figure 6 that that the fluorescence quenching with respect to the ligand occurred in solution in each metal complex. However the exception was the mercury complex **3** which showed fluorescence enhancement. There are multiple components of fluorescence in each cases pointing out number of orientations present in solutions. This makes clear distinction of mercury from other ions. There are terpyridine ligands distinguish mercury²⁰ in aqueous medium; but, our system also can distinguish mercury in aqueous solution from aqueous solution of cadmium and zinc ions. **The quantum yields of the ligand as well as all the complexes were determined from their respective solution in dimethylfomamide (table 2s of supporting information). The quantum yield of the ligand L is 0.36 and the complexes lies in the range of 0.37-0.50.**

To understand the effect of temperature on the fluorescence changes, we recorded the temperature dependent fluorescence emissions at different temperatures for the complexes **1-3** and compared these data with the ligand. This is carried out with the anticipation that as the thermal energy increases the ligand would open up from a bend geometry, which disfavors intramolecular charge transfer

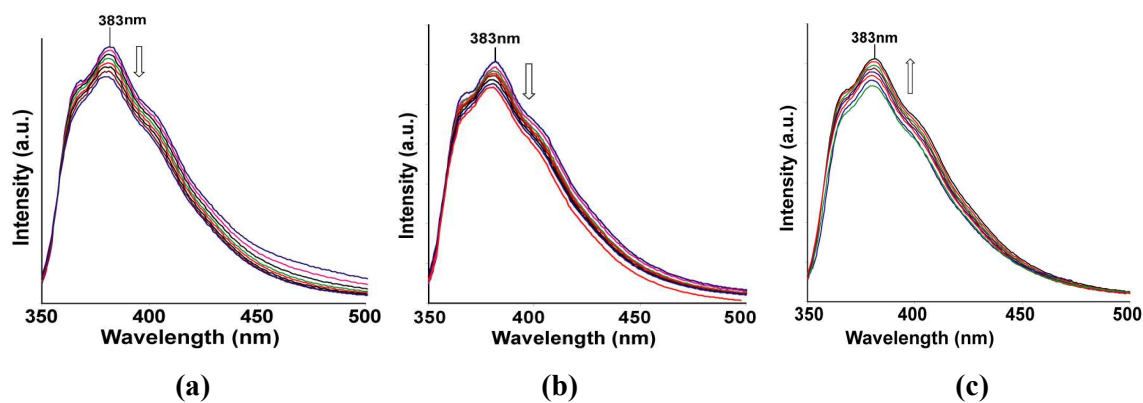


Figure 7: Temperature dependent fluorescence spectra of the (a) complex **1** ; (b) complex **2** and (c) complex **3**. (30 °C to 100 °C at 10 °C interval of temperature; 0.1 mM solution each in DMF; $\lambda_{\text{ex}} = 330$ nm, downward arrow shows decrease in intensity).

interaction. Three illustrative examples on the changes of fluorescence in solution with respect to temperatures are shown figures 7. Quenching of fluorescence in the case of complex **1** and **2** were observed as the temperature was increased. While the mercury complex **3** showed enhancement of fluorescence emission as the temperature was increased. It may be mentioned that the nitrogen heterocycles attached to 1,8-naphthalimides are important as some of them show dual fluorescence and these are related to coplanar or orthogonal geometries of the 1,8-naphthalimide part with respect to the nitrogen containing heterocyclic units attached to them^{2c,14b}. Thus, the complex **1** and **2** shows decrease of fluorescence intensity on heating, suggesting the decrease in photo-electron energy transfer contribution to the emission process by change of orientation. Whereas, the mercury complex having a folded structure, stretches out on heating to show increase in the fluorescence emission intensity. When there is no metal ion to guide the orientation the ligand **L**, the lone pair of electrons present on the nitrogen atom of imidazole contributes to photo-electron energy transfer (PET) mechanism, causing a partially quenched state at start of heating, on heating the orientation of **L** changes, accordingly the intensity grows.

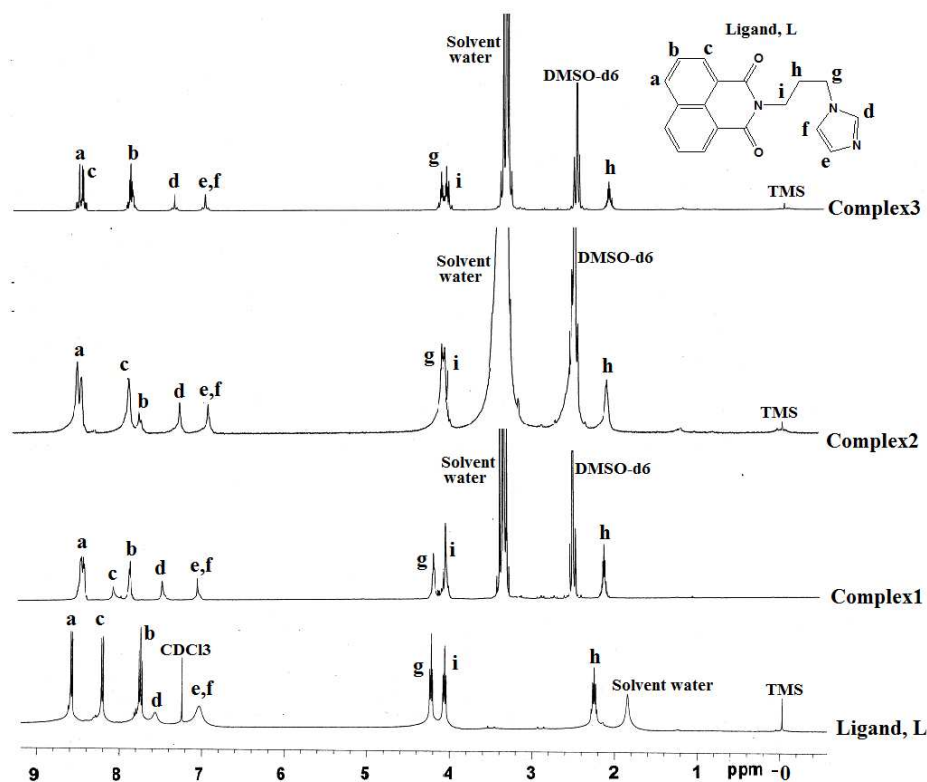


Figure 8: $^1\text{H-NMR}$ spectra of the ligand and (400MHz, CDCl_3) and the complex **1-3** (600MHz, DMSO-d_6)

The stability of the complexes in solution was ascertained from the respective $^1\text{H-NMR}$ spectra of the complexes **1-3**, **6** and **7**. The $^1\text{H-NMR}$ spectra of the complex **1-3** and ligand are compared in figure 8, which clearly indicates, that the complexes are stable in solution and on complexation of the ligand to zinc or cadmium, the chemical shift of the methylene group adjacent to imidazole is affected and so as the protons on the imidazole ring. Analogously, the complexes **6** and **7** also shows clear shifts of the $^1\text{H-NMR}$ peaks and some of the peaks were broadened in these complexes as shown in supporting information (figure 21S and 22S).

In conclusions, the structures in solid state have helped us to explain the fluorescence behavior of such complexes by invoking intramolecular charge-transfer (ICT) to stabilize ground state in bent geometry (d of figure 1) to cause emission at lower wave-length, whereas a stretched ligand helps exciplex through π -stacking of 1,8-naphthalimides to show emission at long wavelength (e of figure 1). The free ligand as well as the complexes in solution shows fluorescence enhancement on heating shows enhancement of fluorescence intensity through a PET mechanism²¹ arising from the lone pair of electrons on nitrogen atom of imidazole. On heating conformational changes disfavor participation of lone pair on nitrogen atom of imidazole in such process, hence enhancement of intensity of fluorescence of the ligand was observed. Whereas, in solid state the coordination of the ligand to d^{10} -

metal ions provide orientation to the ligand so as to favor or disfavor intra-molecular charge-transfer emission (d, e of figure 1). The mercury ions show fluorescence enhancement over the cadmium or zinc ions hence it is distinguishable from the later. From the series of study it is clear that the conformation shown as d of figure 1 favors the low wavelength emission, while the other stretched geometry helps in exciplex formation taking the fluorescence to longer wavelength.

Supporting information: The packing diagrams, powder XRD-patterns and their comparison with simulated patterns, solid state and solution UV-Vis spectra and thermogravimetric analysis are available. The CIF files are deposited to Cambridge Crystallographic database and have the CCDC numbers The CCDC numbers of the CIF of **1-7** are 928178, 928179, 928180, 928182, 928183, 928164 and 9281885.

References:

- (a) R. M. Duke, E. M. Veale, F. M. Pfeffer, P. E. Kruger, T. Gunnlaugsson, *Chem. Soc. Rev.*, 2010, **39**, 3936-3953. (b) T. Gunnlaugsson, P. E. Kruger, P. Jensen, F. M. Pfeffer, G.M. Hussey, *Tetrahedron Lett.*, 2003, **44**, 8909-8913. (c) X. Poteau, A. I. Brown, R. G. Brown, C. Holmes, D. Matthew, *Dyes and Pigments*, 2000, **47**, 91-105. (d) A. P. De Silva, H. Q. N. Gunaratne, T. Gunnlaugsson, A. J. M. Huxley, C. P. McCoy, J. T. Rademacher, T. E. Rice, *Chem. Rev.*, 1997, **97**, 1515-1566. (e) S. Guha, F. S. Goodson, L. J. Corson, S. Saha, *J. Am. Chem. Soc.*, 2012, **134**, 13679-13691. (f) Z. Xu, J. Yoon, D. R. Spring *Chem. Commun.*, 2010, **46**, 2563-2565.
- (a) K-Y. Lee, *Chem. Rev.*, 1993, **93**, 449-486. (b) H. D. P. Ali, P. E. Kruger, T. Gunnlaugsson, *New J. Chem.*, 2008, **32**, 1153-1161. (c) P. Nandhikonda, M. P. Begaye, Z. Cao, M. D. Heagy, *Chem. Commun.*, 2009, 4941-4943. (d) J. Gan, H. Tian, Z. Wang, K. Chen, J. Hill, P. A. Lane, M. D. Rahn, A. M. Fox, D.D.C. Bradley, *J. Organomet. Chem.*, 2002, **645**, 168-175.
- (a) Z. Liu, C. Zhang, X. Wang, W. He, Z. Guo, *Org. Lett.*, 2012, **14**, 4378-4381. (b) M. Formica, V. Fusi, L. Giorgi, M. Micheloni, *Coord. Chem. Rev.*, 2012, **256**, 170-192. (c) V. F. Pais, P. Remon, D. Collado, J. Andersson, E. Perez-Inestros, U. Pischel, *Org. Lett.*, 2011, **13**, 5572-5575. (d) L. Prodi, F. Bolletta, M. Montali, N. Zaccheroni, *Coord. Chem. Rev.*, 2000, **205**, 59-85. (e) S. Guha, S. Saha, *J. Am. Chem. Soc.*, 2010, **132**, 17674-17677. (f) J. K. Nath, J. B. Baruah, *New J. Chem.*, 2013, **37**, 1509-1519. (g) J. Nath, J.B. Baruah, *J. Fluoresc.* DOI 10.1007/s10895-014-1353-8.
- (a) C. Thalacker, A. Miura, S. De Feyter, F. De Schryver, F. Wurthner, *Org. Biomol. Chem.*, 2005, **3**, 414-422. (b) D. L. Reger, J. D. Elgin, R. F. Semeniuc, P. J. Pellechia, M. D. Smith, *Chem. Commun.*, 2005, 4068-4070.
- (a) G. Loving, B. Imperiali, *Bioconjugate Chem.*, 2009, **20**, 2133-2141. (b) M. E. Vazques, J. B. Blanco, B. Imperiali, *J. Am. Chem. Soc.*, 2005, **127**, 1300-1306. (c) G. Loving, B. Imperiali, *J. Am. Chem. Soc.*, 2008, **130**, 13630-13638.

6. (a) D.W. Cho, M. Fujisuka, K. H. Choi, M. J. Park, U. C. Yoon, T. Majima, *J. Phys. Chem. B*, 2006, **110**, 4576-4582. (b) Y. Xu, X. Qian, W. Yao, P. Mao, J. Cui, *Bioorg. Med. Chem.*, 2003, **11**, 5427-5433.
7. (a) V. Gorteau, G. Bollot, J. Mareda, A. Perez-valasco, S. Matile, *J. Am. Chem. Soc.*, 2005, **128**, 14788-14789. (b) J. T. Davis, *Nature Chem.*, 2010, **2**, 516-517. (c) R. E. Sawson, A. Hennig, D. P. Weimann, D. Emery, V. Ravikumar, J. Montenegro, T. Takeuchi, S. Gabutti, M. Mayor, J. Mareda, C. A. Schalley, S. Matile, *Nature Chem.*, 2010, **2**, 533-538.
8. D. V. Pogozhev, M. J. Bezdek, P. A. Schauer, C. P. Berlinguette, *Inorg. Chem.*, 2013, **52**, 3001-3006.
- 9.(a) D. L. Reger, A. Debreczeni, B. Reinecke, V. Rasslov, M. D. Smith, *Inorg. Chem.*, 2009, **48**, 8911-8924. (b) D. L. Reger, A. Debreczeni, M. D. Smith, *Inorg. Chim. Acta*, 2010, **364**, 10-15. (c) D. L. Reger, J. J. Horger, A. Debreczeni, M. D. Smith, *Inorg. Chem.*, 2011, **50**, 4669-4670. (d) R. J. Sarma, C. Tamuly, N. Barooah, J. B. Baruah, *J. Mol. Struct.*, 2007, **829**, 29-36. (e) D. Singh, J. B. Baruah, *Cryst. Growth Des.*, 2012, **12**, 2109-2121. (c) D. Singh, J. B. Baruah, *Inorg. Chim. Acta* 2012, **390**, 37-40.
10. (a) I. Saito, M. Takayama, H. Sugiyama, K. Nakatani, *J. Am. Chem. Soc.*, 1995, **117**, 6406-6407. (b) M. F. Brafia, M. Cacho, A. Ramos, M. T. Dominguez, J. M. Pozuelo, C. Abradelo, M. F. Rey-Stolle, M. Yuste, C. Carrasco, C. Bailly, *Org. Biomol. Chem.*, 2003, **1**, 648-654. (c) E. B. Veale, T. Gunnlaugsson, *J. Org. Chem.*, 2010, **75**, 5513-5525.
11. (a) L. Ingrassia, F. Lefranc, R. Kiss, T. Mijatovic, *Curr. Med. Chem.*, 2009, **161**, 192-121. (b) M. Ly, H. Xu, *Curr. Med. Chem.*, 2009, **16**, 797-813. (c) J. L. Nitiss, J. Zhou, A. Rose, Y. Huiung, K. C. Gale, N. Osheroff, *BioChem.*, 1998, **37**, 3078-3085. (d) S. Banerjee, E. B Veale, C. M. Phelan, S. A Murphy, G. M. Tocci, L. J. Gillespie, D. O. Frimannsson, J. M. Kelly, T. Gunnlaugsson, *Chem. Soc. Rev.*, 2013, **42**, 1601-1618. (e) K. Wang, Y. Wang, X. Yan, H. Chen, G. Ma, P. Zhang, J. Li, X. Li, J. Zhang, *Bioorg. Med. Chem. Lett.*, 2012, **22**, 937-941. (f) P. Gasioski, K. S. Danel, M. Matusiewicz, T. Uchacz, W. Kuznik, A. V. Kityk, *J. Fluoresc.*, 2012, 81-91.
12. P. Guo, Q. Chen, T. Liu, L. Xu, Q. Yang, X. Qian, *Med. Chem. Lett.*, 2013, **4**, 527-531.
13. K. J. Kilpin, C. M. Clavel, F. Edefe, P. J. Dyson, *Organometallics*, 2012, **31**, 7031-7039.
14. (a) S. Paudel, P. Nandhikonda, M. D Heagy, *J. Fluoresc.*, 2009, **19**, 681-691. (b) P. Nandhikonda, M. P. Begaye, Z. Chao, M. D. Heagy, *Org. Biomol. Chem.*, 2010, **8**, 3195-3201. (c) L. Biczok, P. Valat, V. Wintgens, *Phys. Chem. Chem. Phys.*, 1999, **1**, 4759-4766. (d) H. Cao, V. Chang, R. Hernandez, M. D. Heagy, *J. Org. Chem.*, 2005, **70**, 4929-4934. (e) J. V. Mello, N. S. Finney, *Angew. Chem. Int. Ed.* 2001, **40**, 1536-1538.

15. (a) G. M. Sheldrick, *Acta Crystallogr.*, 2008, **A64**, 112-122. (b) CrysAlisPro, Oxford Diffraction Ltd., version 1,171. 33. 34d (release crysAlis 171.NET) 2009.
16. A. Abedi, V. Amani, R. Boca, L. Dlhan, H. K. Khavasi, N. Safari, *Inorg. Chim. Acta*, 2013, **395**, 58-66.
17. P. C. H. Mitchell, R. J. P. Williams, *J. Chem. Soc.*, 1960, 1912-1918.
18. P. Kucheryavy, G. Li, S. Vyas, C. Hadad, K. D. Glusac, *J. Phys. Chem. A.*, 2009, **113**, 6453-646.
19. (a) D. L. Reger, A. Debreczeni, J. J. Horger, M. D. Smith, *Cryst. Growth Des.*, 2011, **11**, 4068-4079. (b) D. L. Reger, A. Debreczeni, A. E. Pascui, M. D. Smith, *Polyhedron*, 2013, **52**, 1317-1322. (c) S.-M. Fang, Q. Zhang, M. Hu, X.-G. Yang, L.-M. Zhou, M. Du, C.-S. Liu, *Cryst. Growth Des.*, 2010, **10**, 4773-4785. (d) S.-L. Zheng, J. -H. Yang, X. -L. Yu, X. -M. Chen, W. -T. Wong, *Inorg. Chem.*, 2004, **43**, 830-838.
20. (a) R. Shunmugam, G. J. Gabriel, C. E. Smith, K. A. Aamer, G. N. Tew, *Chem. Eur. J.*, 2008, **14**, 3904-3907. (b) H. N. Kim, W. X. Ren, J. S. Kim, J. Yoon, *Chem. Soc. Rev.*, 2012, **41**, 3210-3244.
21. D.W. Cho, M. Fujisuka, A. Sugimoto, U.C. Yoon, P.S. Mariano, T. Majima, *J. Phys. Chem. B.*, 2006, **110**, 11062-11068.

Twisted conformations in complexes of N-(3-imidazol-1-yl-propyl)-1,8-naphthalimide and
fluorescence properties

J. K. Nath and J. B. Baruah

Supporting Information

Table 1S: Absorption and emission of complexes # 1-7

Complex / ligand	Absorption in solid (nm)	Emission in solid (nm)
L	361	461
1	315, 353	428
2	330	425
3	318, 351	426
4	323	470
5	361	452
6	357	473
7	360	481

Table 2S : The quantum yield of the complexes determined in DMF solution

S.I No.	Compound	Quantum yield
1	Ligand, L	0.36
2	Complex 1	0.37
3	Complex 2	0.35
4	Complex 3	0.40
5	Complex 4	0.38
6	Complex 5	0.41
7	Complex 6	0.50
8	Complex 7	0.46

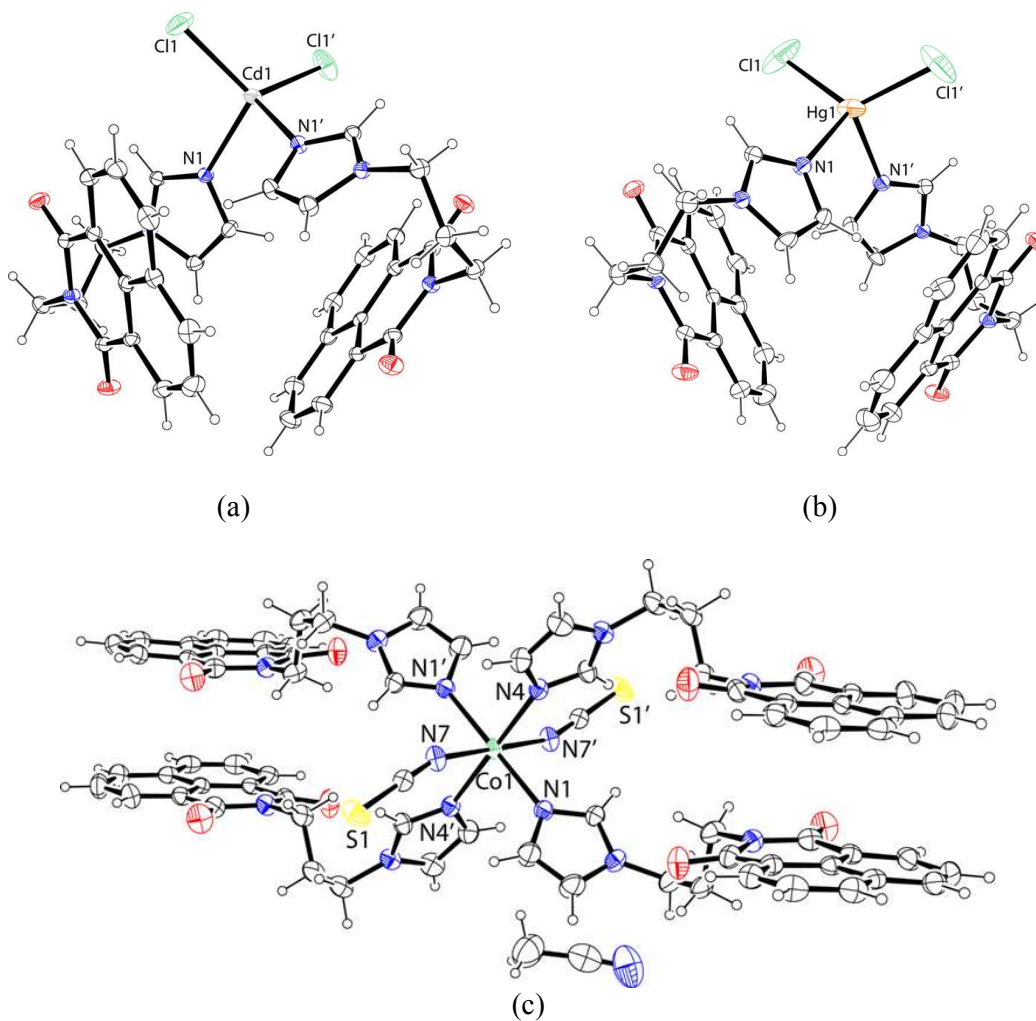


Figure 1S: ORTEP diagram of (a) complex 2, (b) complex 3, (c) complex 5 (symmetry of equivalent atoms $x, -y, -z$)

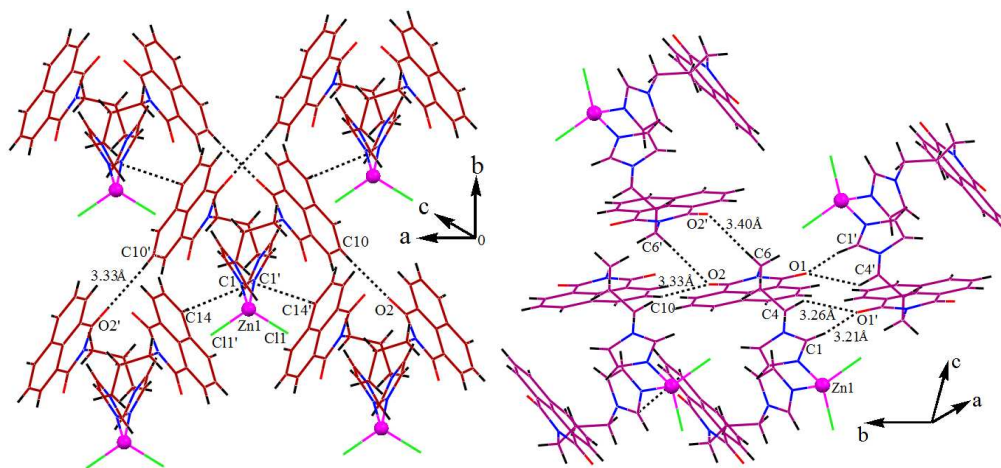


Figure 2S: Weak interactions in the crystal lattice of the complex **1** from two different projections.

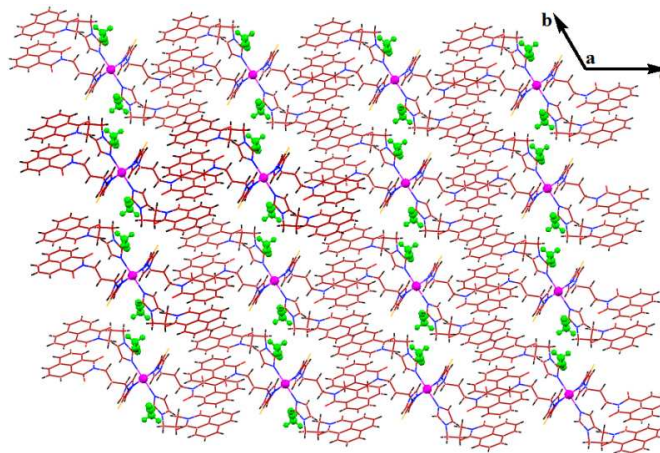


Figure 3S: 3D supramolecular network along a-axis. in the lattice of complex **4**.

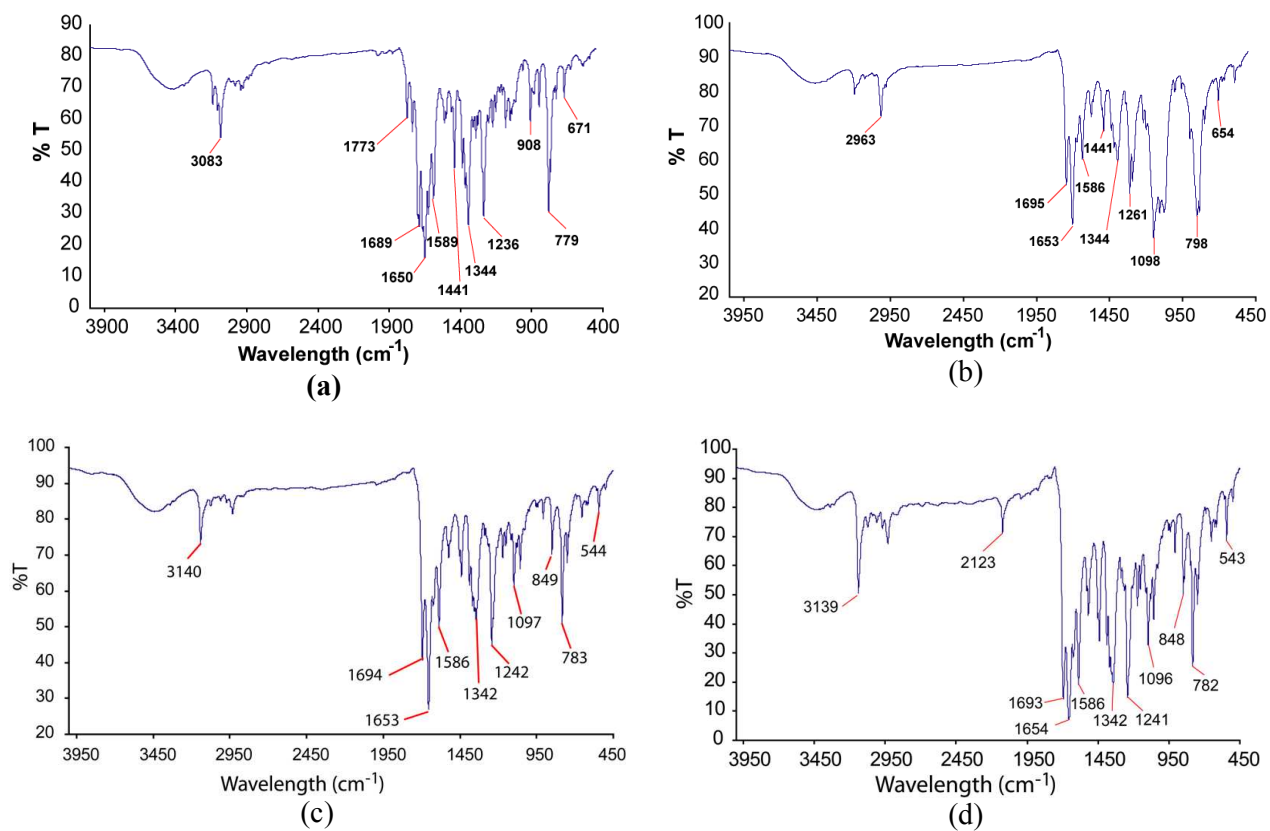


Figure 4S1: FT-IR (KBr) spectra of the (a) ligand, **L**, (b) Complex **1**, (c) Complex **2**, (d) Complex **3**.

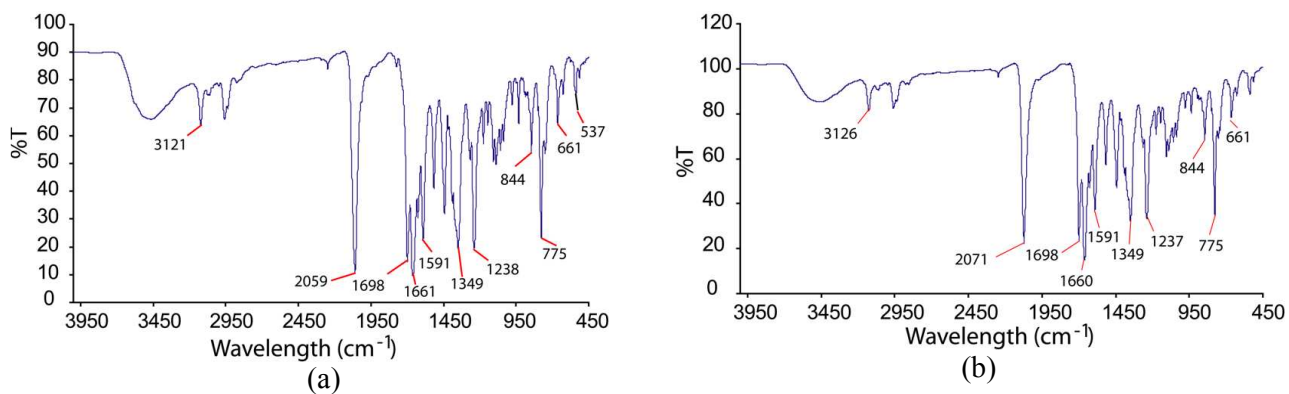


Figure 4S2: FT-IR spectra (KBr) of the (a) Complex **4** and (b) Complex **5**.

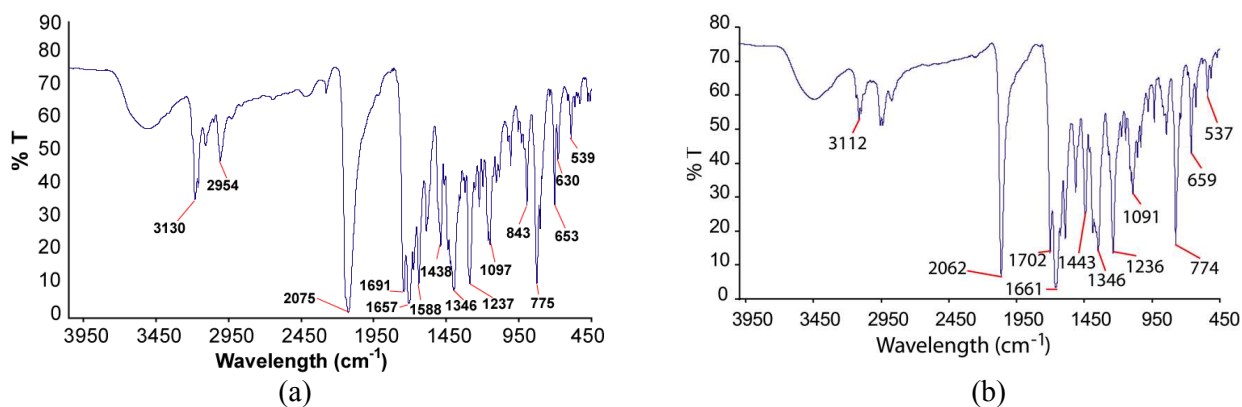


Figure 4S3: FT-IR spectra (KBr) of the (a) complex **6** and (b) Complex **7**

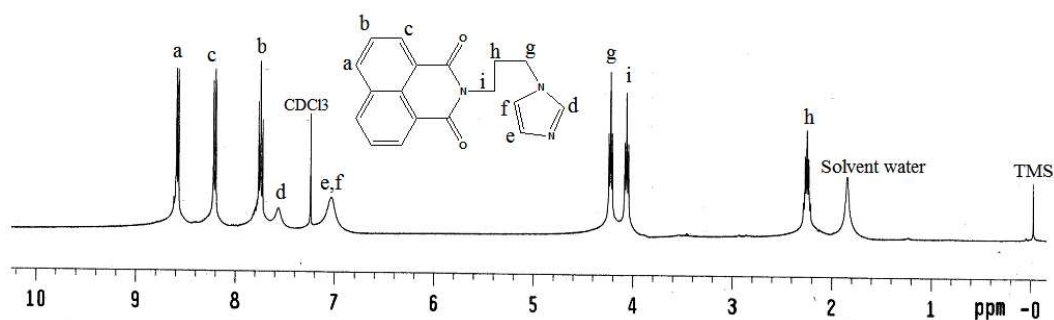


Figure 5S: ^1H NMR (400MHz, CDCl_3) spectrum of the ligand, **L**

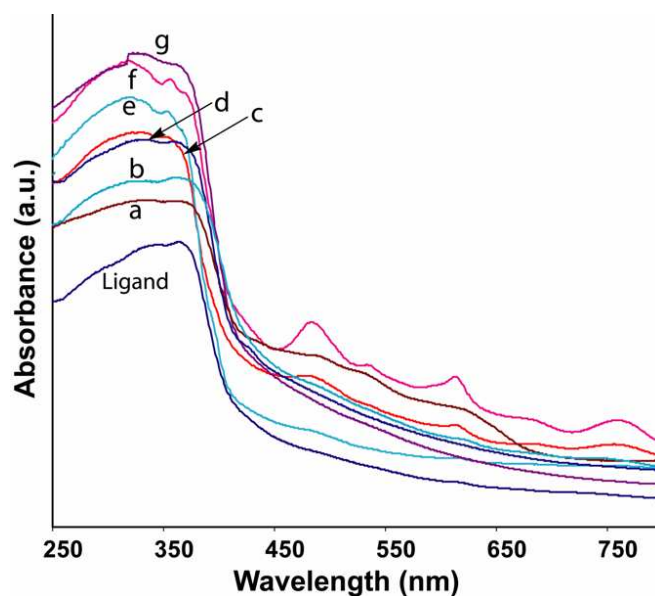


Figure 6S: Solid state UV-vis spectra of (a) complex **5**, (b) complex **7**, (c) complex **6**, (d) complex **2**, (e) complex **3**, (f) complex **1**, and (g) complex **4**.

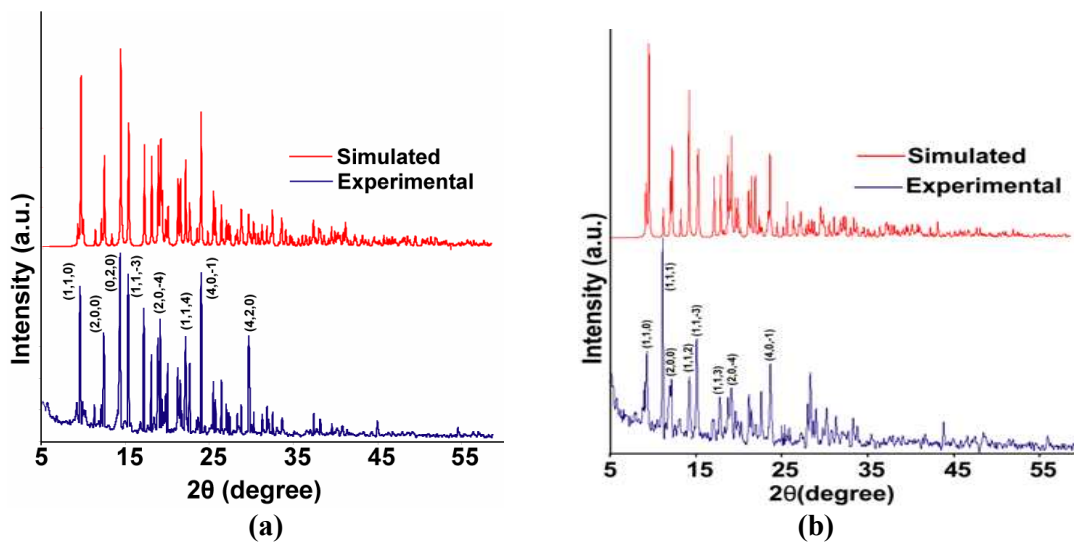


Figure 7S: PXRD pattern of the (a) complex 2 and (b) Complex 3

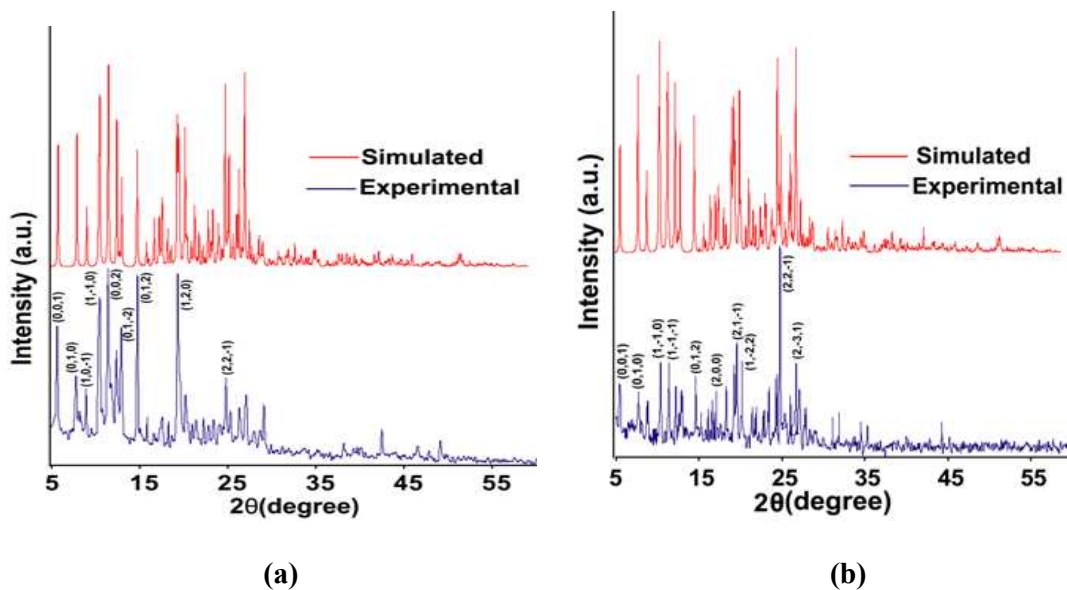


Figure 8S: PXRD pattern of the (a) complex 4 and (b) Complex 5

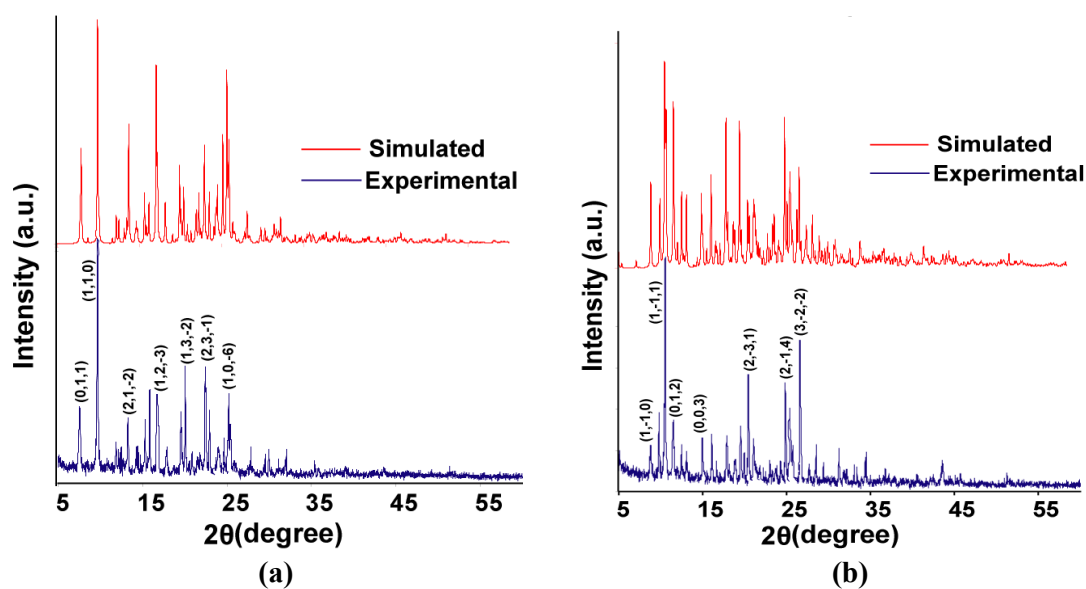


Figure 9S: PXRD pattern of the (a) complex 6 and (b) complex 7

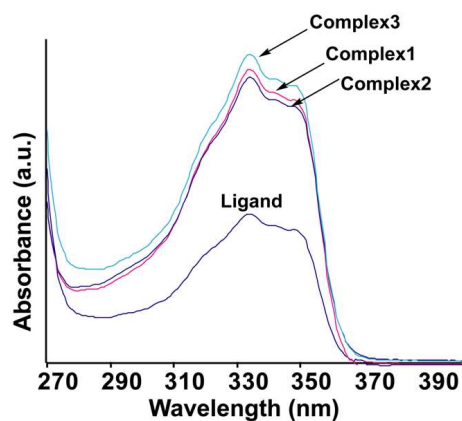


Figure 10S : UV-Vis spectra of the ligand, complex 1, complex 2 and complex 3 in DMF (concentration of 10^{-6} M each)

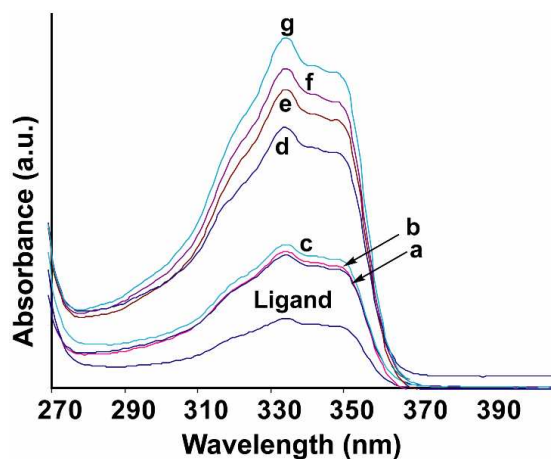


Figure 11S: UV-Vis spectra of the ligand, (a) complex 2; (b) complex 1; (c) complex 3; (d) complex 6; (e) complex 5; (f) complex 4; (g) complex 7; in DMF (concentration of 10^{-6} M each).

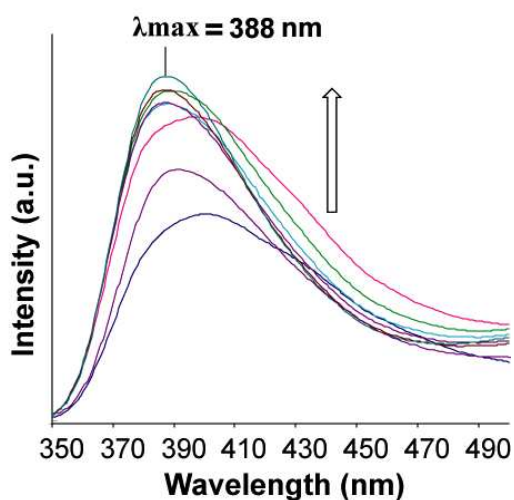


Figure 12S: Temperature dependent fluorescence spectra of the ligand, L. Fluorescence intensity increases with increasing temperature (30°C to 100°C, 0.1mM solution in DMF, $\lambda_{ex} = 340$ nm)

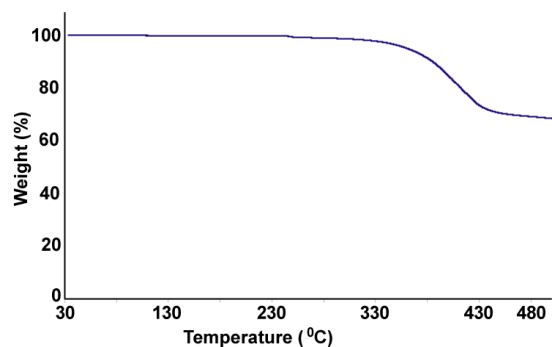


Figure 13S: Thermogravimetry of the complex 1

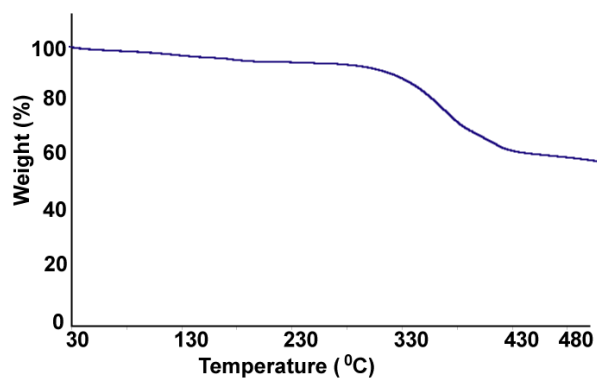


Figure 14S: Thermogravimetry of the complex 2. In case of the complex 2, the decomposition of the organic ligand started from 280 °C

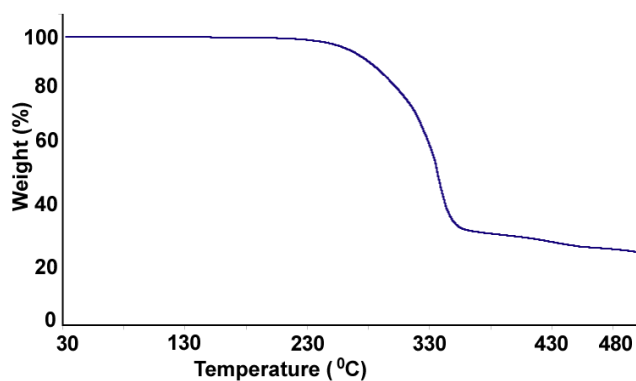


Figure 15S: Thermogravimetry of the complex 3

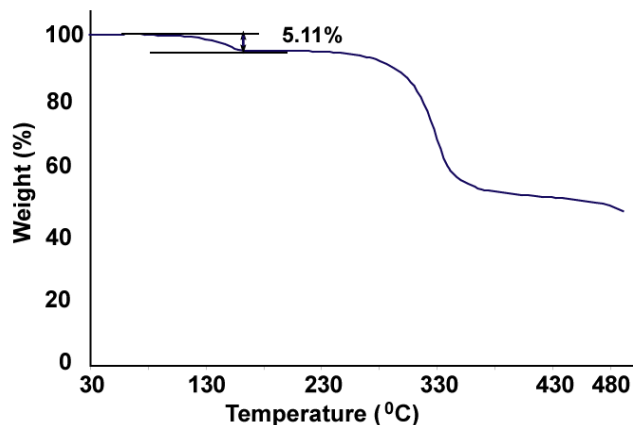


Figure 16S: Thermogravimetry of the complex **4** (For the complex **4**, one step weight loss due to the two solvent acetonitrile molecules takes place in the temperature range 70–170 °C corresponding to a weight loss of 5.11% (calcd 5.56%). The decomposition of ligand at 250 °C-460 °C.

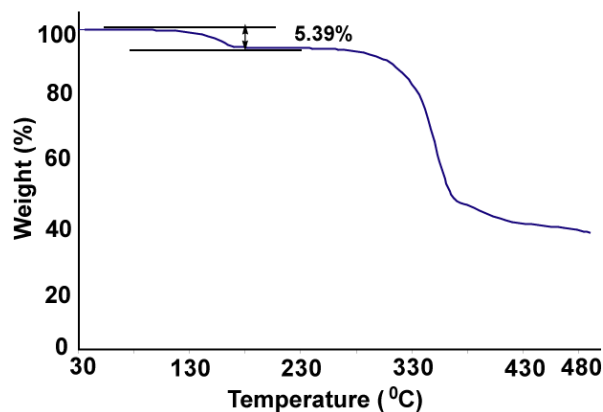


Figure 17S: Thermogravimetry of the complex **5**. The two solvent acetonitrile molecules are lost in the range 88-200 °C corresponding to a weight loss of 5.39 % (calcd. 5.55 %) and the decomposition of organic ligands at 260 °C-460 °C.

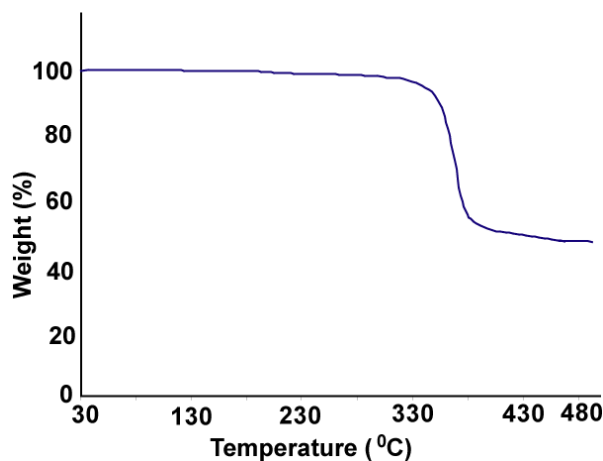


Figure 18S: Thermogravimetry of the complex **6**. Complex **6** shows a gradual one step weight loss due to the degradation of organic ligands in the temperature range 130-460 °C.

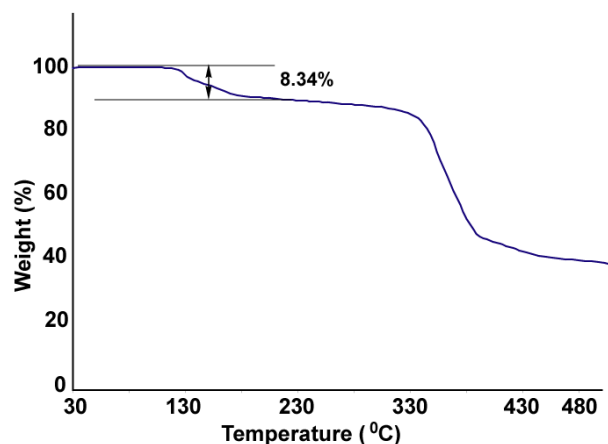


Figure 19S: Thermogravimetry of the complex **7**. The complex **7** shows weight loss of 8.34 wt % (calcd. 8.98 wt%) in the range of 120-182 °C corresponds to the loss of one lattice dimethylformamide molecule and one coordinated dimethylformamide molecule.

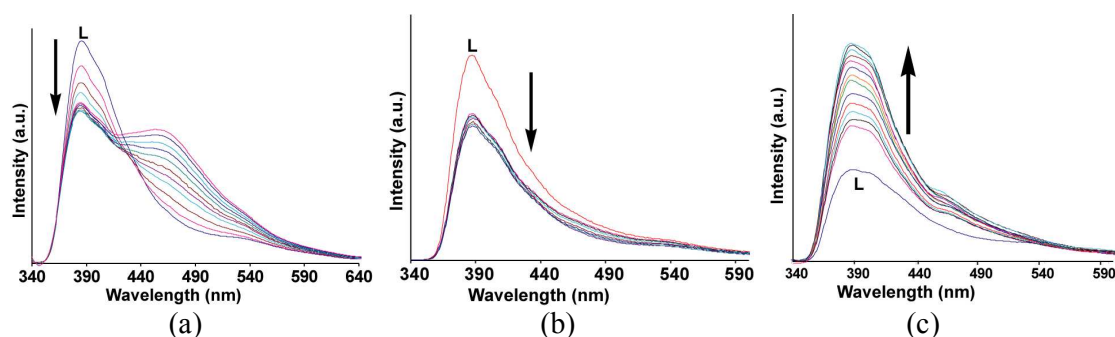


Figure 20S: The changes in the intensity of fluorescence emission ($\lambda_{\text{ex}} = 340\text{nm}$) of the ligand, **L** (2ml of 10^{-4} M solution in DMF) on addition of (a) ZnCl_2 , (b) CdCl_2 and (c) HgCl_2 ($5\mu\text{l}$ aliquots of 10^{-2} M solution in methanol).

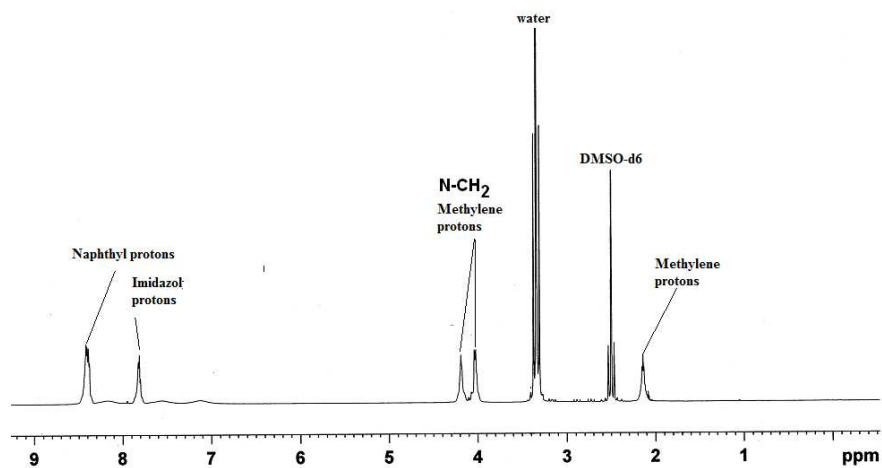


Figure 21S: $^1\text{H-NMR}$ (600 MHz, DMSO-d_6) spectra of the complex **6**.

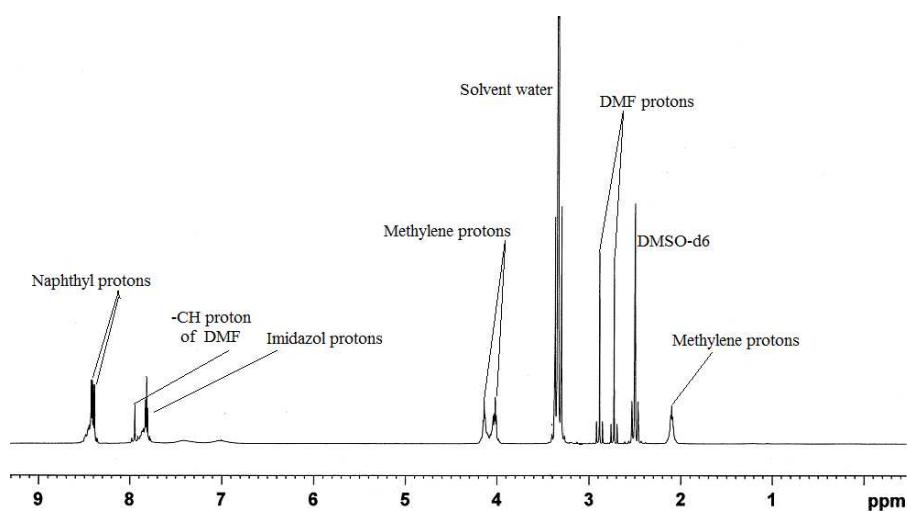
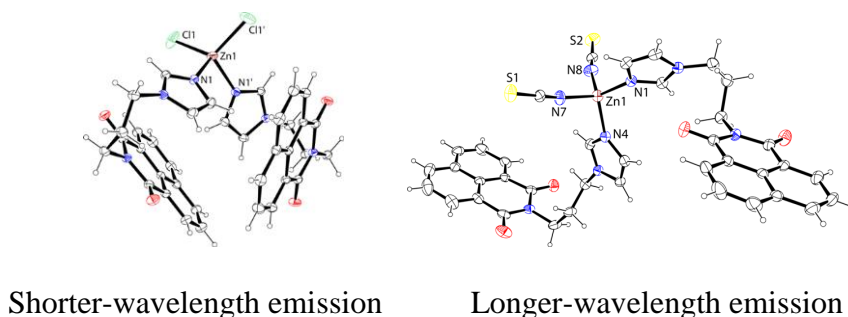


Figure 22S: $^1\text{H-NMR}$ (600 MHz, DMSO-d_6) spectra of the complex **7**.

Twisted conformations in complexes of N-(3-imidazol-1-yl-propyl)-1,8-naphthalimide and fluorescence properties



Shorter-wavelength emission

Longer-wavelength emission

Jayanta Kumar Nath and Jubaraj B. Baruah

Twisted conformations in complexes of N-(3-imidazol-1-yl-propyl)-1,8-naphthalimide and fluorescence properties

Jayanta Kumar Nath and Jubaraj B. Baruah*

Department of Chemistry, Indian Institute of Technology Guwahati, Guwahati 781 039 Assam, India, Fax: +91-361-2690762; Ph. +91-361-2582311; email: juba@iitg.ernet.in

<http://www.iitg.ernet.in/juba>

Keywords:

Naphthalimide; Imidazole, Isomorphous structures; fluorescence; Metal-imidazole complexes.

Abstract:

A series of complexes of N-(3-imidazol-1-yl-propyl)-1,8-naphthalimide (**L**) with divalent ions of manganese, cobalt, zinc, cadmium and mercury are structurally characterized. The metal complexes $[ML_2Cl_2]$ {M = Zn (**1**), Cd (**2**), Hg (**3**)} are isomorphous and have distorted tetrahedral geometry with bent conformation of **L**. The thiocyanate complex $[ZnL_2(SCN)_2]$ has a distorted tetrahedral geometry with **L** in bent but different geometry from that in the structure of complex **1**. The manganese and cobalt thiocyanate complexes $[ML_4(SCN)_2] \cdot 2CH_3CN$ (M = Mn, Co) are isomorphous and have distorted octahedral geometry with the thiocyanate ligands occupying the axial positions. The cadmium complex $CdL_3(SCN)_2DMF \cdot DMF$ has a distorted octahedral geometry with thiocyanate ligands in the axial positions. The tetrahedral complexes $[ML_2Cl_2]$ {M = Zn (**1**), Cd (**2**)} in solid state shows emission at shorter wavelength than the single emission peak observed from the ligand; whereas the fluorescence emission of $[ML_2(SCN)_2]$ {M = Zn (**1**), Cd (**2**)} occurred at longer wavelength than **L**. On the other hand, $[HgL_2Cl_2]$ (**3**) showed single emission peak with higher intensity but at 31 nm shorter wavelength

than the emission peak of the parent ligand. Two types of bend orientations of the ligand **L** namely, parallel arrangement of imidazole with 1,8-naphthalimide ring and non-parallel arrangement in the tetrahedral complexes are observed. Former case favors intra-molecular charge transfer to shows shorter wavelength emission, whereas the non-parallel arrangements facilitate exciplex leading to emission at longer wavelength.

Introduction:

Naphthalimide derivatives are commonly used as fluorescence probes¹ and optical materials.² Structurally modified naphthalimide compounds show selectivity in binding ions.³ The nature of self-assemblies formed by naphthalimide derivatives are guided by functional groups.⁴ Study on chromogenic properties of naphthalimide derivatives helps to understand biological interactions.⁵ Naphthalimides have vast photochemistry⁶ and they are used to make bio-model for anion transport.⁷ Solar cells are developed based on ruthenium complexes of naphthalimides.⁸ Stacking interactions between naphthalimides generate interesting structures.⁹ Naphthalimides also bind to DNA¹⁰ and act as anticancer agents.¹¹ Naphthalimide based dyads are potent inhibitor against human N-acetyl- β -hexosaminidase.¹² Imidazole based naphthalimide has been shown to have interesting DNA binding, and anticancer activity.¹³ Beside these, the N-functionalised 1,8-naphthalimide compounds having nitrogen-heterocyclic tether finds special interest for their interesting dual fluorescence properties. Such compounds show dual fluorescence originating from charge transfer via excited state with extended conjugation (ESEC).¹⁴ In such cases it was shown that the different orientation of N-heterocyclic ring

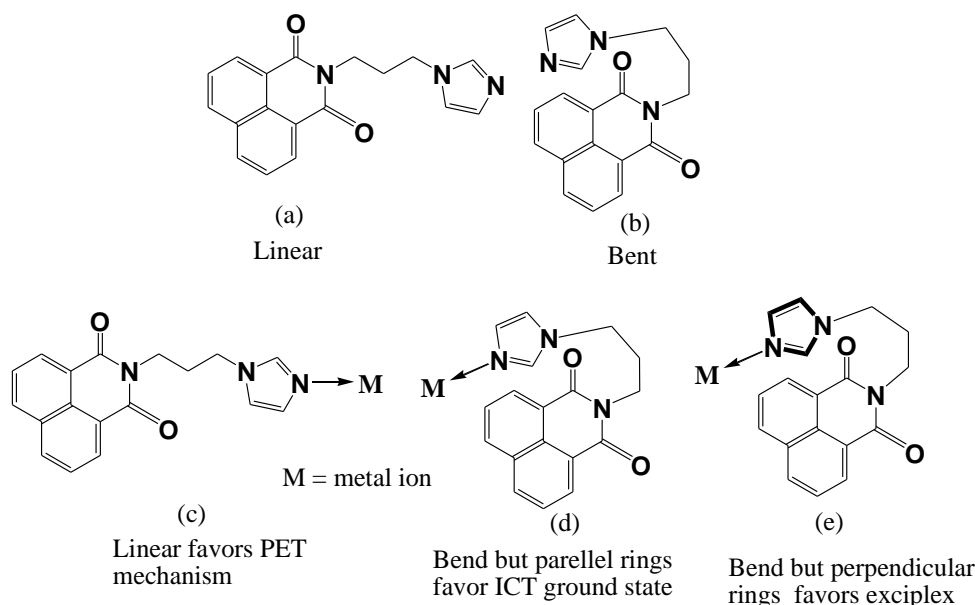


Figure 1: (a) linear and (b) bend form of the ligand **L**. Geometries of ligand **L** attached to a metal ion (c) linear form; and bend forms having (d) parallel or (e) non-parallel orientation of imidazole ring over 1,8-naphthalimide ring.

over a 1,8-naphthalimide ring can change the intensity as well as position of the absorptions. It was earlier shown by us that the anion- π interactions guide the fluorescence emission of imidazole tethered 1,8-naphthalimide derivatives. Since variation of anions resulted in change of fluorescence, it is essential to understand the role of cation in stabilization of different geometries of ligand such as **L** (figure 1) and understand their fluorescence properties. So far, such observations are not related to coordination effect of metal ions, as for example an N-functionalised 1,8-naphthalimide ligand such as **L** having flexible chain to connect the 1,8-naphthalimide with an imidazole ring would have provision to adopt linear or bend structure as illustrated in figure 1. Such geometry may be guided by a metal ion coordinating the orientation of the ligand to affect the intramolecular charge transfer or photo-electron transfer mechanism operative in such system to show characteristic fluorescence emission.³ While pursuing our study with metal complexes of **L**, we observe such structures in metal complexes of the ligand **L** and as a consequence characteristic fluorescence emissions are observed. Thus, we present here the results of such a study to establish correlation between the fluorescence and structures.

Experimental

All reagents and solvents were obtained from commercial sources. The IR spectra were recorded on a Perkin-Elmer SpectrumOne FT-IR spectrometer in the range 4000-400 cm^{-1} . The $^1\text{H-NMR}$ spectra were recorded using a Varian Mercury plus 400 MHz and Bruker 600 MHz instrument. Powder X-ray Diffraction (PXRD) were recorded using a Bruker D2 phaser with Cu- $K\alpha$ source ($\lambda = 154 \text{ \AA}$) on glass surfaces of air dried samples. Thermogravimetric analyses (TGA) were performed on a Mettler Toledo TGA/SDTA 851e module. Samples were placed in open alumina pans in the temperature range 25-600 $^{\circ}\text{C}$ and were purged with a stream of dry N_2 flowing at 100 mL min^{-1} with heating rate 5 $^{\circ}\text{C}$. The UV-Vis and solid state fluorescence emission spectra were recorded on a Perkin-Elmer-Lambda 750 UV-Vis spectrometer and Fluoromax-4 fluorimeter respectively at room temperature. The solid state fluorescence emission spectra of the samples were recorded of powdered samples in each case of equal weight (30 mg).

The quantum yield of fluorescence was determined by using quinine sulphate as a reference in water at room temperature.

$$\text{Quantum Yield} = \frac{\text{Area of the compound}}{\text{Area of Q.S}} \times \frac{\text{Absorbance at 333nm (Q.S)}}{\text{Absorbance at 333nm (Compound)}} \times \frac{\text{R.I of DMF}}{\text{R.I of water}} \times 0.54$$

The Q.S, DMF and R.I are quinine sulphate, dimethylformamide and refractive index respectively. And area means the area covered by fluorescence curve of the respective compound.

The N-(3-imidazol-1-yl-propyl)-1,8-naphthalimide (**L**) was synthesized by a reported procedure^{3f} using DMF as solvent and refluxing at 100 °C for 12 hs. Then the reaction mixture was cooled and ice cold water was added to it. Silky white precipitate of **L** formed was filtered and dried.

[ZnL₂Cl₂] (1): The ligand, **L** (0.61 g, 2 mmol) was dissolved in warmed DMF and added to a methanolic solution of zinc chloride (0.136 g, 1 mmol). The reaction mixture was refluxed for 4 hours and cooled it to room temperature and the filtered solution was kept undisturbed for crystallization. After one week white crystals appeared. Yield, 51%. Elemental anal calcd. For C₃₆H₃₀Cl₂N₆O₄Zn, C, 57.89; H, 4.05; N, 11.25; found C, 57.95, H, 4.07, N, 11.45. IR (KBr, cm⁻¹): 3414 (br), 2963 (s), 1695 (s), 1653 (s), 1586 (s), 1441 (m), 1344 (m), 1261 (s), 1242 (m), 1170 (w), 1098 (s), 1057 (w), 1026 (w), 850 (w), 801 (m), 785 (m), 654 (w), 544 (w). ¹H-NMR (600 MHz, DMSO-d₆): 8.48(d, 1H, 6.6 Hz), 8.42(br, 1H), 7.84(t, 1H, 7.8 Hz), 7.44(s, 1H), 7.02(s, 1H), 4.17(t, 2H, 6.6Hz), 4.10(t, 2H, 5.4Hz), 2.12(m, 2H, 6.6Hz).

[CdL₂Cl₂] (2): Complex **2** was prepared by a similar procedure as that of the complex **1**. Cadmium chloride was used instead of zinc chloride. One week later colourless crystals of **2** were obtained. Yield, 39 %. Elemental anal calcd. C₃₆H₃₀Cl₂N₆O₄Cd; C, 54.46; H,3.81; N, 10.58 found C, 54.51, H, 3.82, N, 10.61. IR (KBr, cm⁻¹): 3140 (m), 1694 (m), 1653 (s), 1586 (m), 1440 (w), 1342 (m), 1242 (s), 1170 (w), 1097 (m), 849 (m), 783 (s), 750 (w), 544 (w). ¹H-NMR (600 MHz, DMSO-d₆): 8.51(d, 1H, 24Hz), 7.87 (bs, 1H), 7.71(br, 1H), 7.22(s, 1H), 6.88(s, 1H), 4.08(t, 2H, 6Hz), 4.05 (t, 2H, 7.2Hz), 2.08 (bs, 2H).

[HgL₂Cl₂] (3): Complex **3** was prepared by the similar procedure as that of the complex **1** but mercuric chloride was used instead of cadmium chloride. On standing for 6-7 days, colorless crystals were observed. Isolated yield, 41%. Elemental anal calcd. C₃₆H₃₀Cl₂N₆O₄Hg, C, 49.01; H, 3.43; N, 9.53; found C, 49.10; H, 3.44; N, 9.61. IR (KBr, cm⁻¹): 3139 (s), 2123 (w), 1693 (m), 1654 (m), 1625 (s), 1518 (m), 1440 (m), 1342 (m), 1241 (s), 1096 (m), 1170 (w), 1096 (m), 1056 (w), 848 (s), 782 (s), 543 (m). ¹HNMR (600 MHz, DMSO-d₆): 8.47 (d, 1H, 7.2 Hz), 8.42 (d, 1H, 8.5Hz), 7.83 (t, 1H, 7.8Hz), 7.31 (s, 1H), 6.93 (s, 1H), 4.10 (t, 2H, 7.2 Hz), 4.03 (t, 2H, 7.2Hz), 2.08 (m, 2H, 7.2Hz).

[MnL₄(SCN)₂].2CH₃CN (4): To a binary mixture solution of acetonitrile and methanol of **L** (0.61 g, 2 mmol), manganese chloride tetrahydrate (0.10 g, 0.5 mmol) was added. After stirring the mixture for five minutes, potassium thiocyanate (0.10 g, 1 mmol) was added. Refluxing the reaction mixture for 4 hours, it was cooled, filtered and allowed to evaporate at room temperature. Brown colored crystals were observed after a week. Isolated yield, 54 %. Elemental anal calcd. C₇₈H₆₆N₁₆O₈S₂Mn C, 63.53, H, 4.51; N, 15.20 found C, 63.73, H, 4.61; N, 16.01. IR (KBr, cm⁻¹): 3466 (bs), 3121 (m), 2958 (w), 2059 (s), 1698 (m), 1661(s), 1591 (s), 1515 (s), 1443 (s), 1349 (s), 1238(s), 1174 (w), 1088 (w), 931 (m), 844

(s), 775 (s), 661 (m), 537 (w). Thermogravimetry: loss of 5.11% weight in the temperature range 70-170 °C (calcd 5.56 % for loss of acetonitrile molecules).

[CoL₄(SCN)₂].2CH₃CN (5): Complex **5** was synthesized in the same procedure as that of the complex **4**, cobalt chloride hexahydrate (0.12g, 0.5mmol) was used instead of MnCl₂.4H₂O. Yield, 51%. Elemental anal. calcd. C₇₈H₆₆N₁₆O₈S₂Co; C, 63.36, H, 4.50; N, 15.16; found C, 63.38; H, 4.51; N, 15.34. IR (KBr, cm⁻¹): 3444 (br), 3126 (w), 2071 (s), 1698 (s), 1660 (s), 1591 (s), 1515 (s), 1442 (s), 1349 (s), 1237 (s), 1174 (m), 1104 (w), 1089 (w), 935 (w), 844 (m), 775 (s), 661 (m), 537 (w). Thermogravimetry: Loss of the 5.39 % weight for acetonitrile molecules in the range 88-200 °C (calcd 5.55 %).

[ZnL₂(SCN)₂] (6): It was synthesized by a similar procedure as that of the compound **6** where zinc nitrate hexahydrate was used. Colorless crystals were obtained after 7-8 days. Isolated yield, 39%. Elemental anal. calcd. C₃₇H₃₀N₈O₄S₂Zn, C, 56.96; H, 3.88; N, 14.36; found C, 56.49; H, 3.87; N, 14.23. IR(KBr, cm⁻¹): 3130 (m), 2954 (w), 2075 (s), 1691 (w), 1657 (m), 1588 (m), 1535 (m), 1438 (s), 1346 (w), 1237 (s), 1173 (w), 844 (s), 755 (s), 653 (s), 630 (m), 539 (w), 409 (w). ¹H-NMR (600 MHz, DMSO-d₆): 8.42-8.39 (m, 6H, naphthalene protons), 7.81-7.56 (m, 3H, imidazole protons), 4.19 (m, 2H N-CH₂), 4.04 (t, 2H, 4.8Hz N-CH₂), 2.15 (m, 2H, -CH₂-).

[CdL₃(SCN)₂DMF].DMF (7): It was synthesized by a similar procedure as that of the compound **7** where cadmium nitrate tetrahydrate was used instead of zinc nitrate hexahydrate. Brown crystals were formed after 8 days. Isolated yield, 45 %. IR (KBr, cm⁻¹): 3112 (w), 2954 (w), 2062 (s), 1702 (m), 1661 (s), 1590 (m), 1513 (s), 1443 (s), 1236 (s), 1091 (m), 843 (m), 774 (s), 659 (s), 539 (m). ¹H-NMR (600 MHz, DMSO-d₆): 8.45-8.41 (m, 18H, naphthalene protons), 7.94 (s, 2H, OC-H of DMF), 7.83-7.43 (m, 9H imidazole protons), 4.15 (t, 6H, 6.6Hz, NCH₂), 4.02 (t, 6H, 7.2Hz, NCH₂), 2.88 (s, 6H CH₃ of DMF), 2.72 (s, 6H, CH₃ of DMF), 2.10 (m, 6H -CH₂-). Thermogravimetry: Weight loss of 8.34 % in the range of 120-182 °C corresponds to the loss of two dimethylformamide molecules (calcd. 8.98 %).

Structure determination:

The X-ray single crystal diffraction data for the complex **1**, complex **3**, complex **4** and the complex **7** were collected at 298 K with Mo K α radiation ($\lambda = 0.71073 \text{ \AA}$) with the use of a Bruker Nonius SMART APEX CCD diffractometer equipped with a graphite monochromator an Apex CCD camera; SMART software was used for data collection and also for indexing the reflections and determining the unit cell parameters^{15a}; whereas the data of complex **2**, **5** and **6** were collected on a Oxford SuperNova diffractometer. For the data collected on the SuperNova diffractometer, data refinement and cell reductions were carried out by CrysAlisPro.^{15b} Data reduction and cell refinement were performed using SAINT software.^{15a} The structures were solved by direct methods

and refined by full-matrix least-squares calculations using SHELXTL software. All the non-H atoms were refined in the anisotropic approximation against F^2 of all reflections. The H-atoms were placed at their calculated positions and refined in the isotropic approximation; those attached to nitrogen and oxygen atoms were located in the difference Fourier maps and refined with isotropic displacement coefficients. Crystallographic data collection was done at room temperature, and the data are tabulated in Table 1.

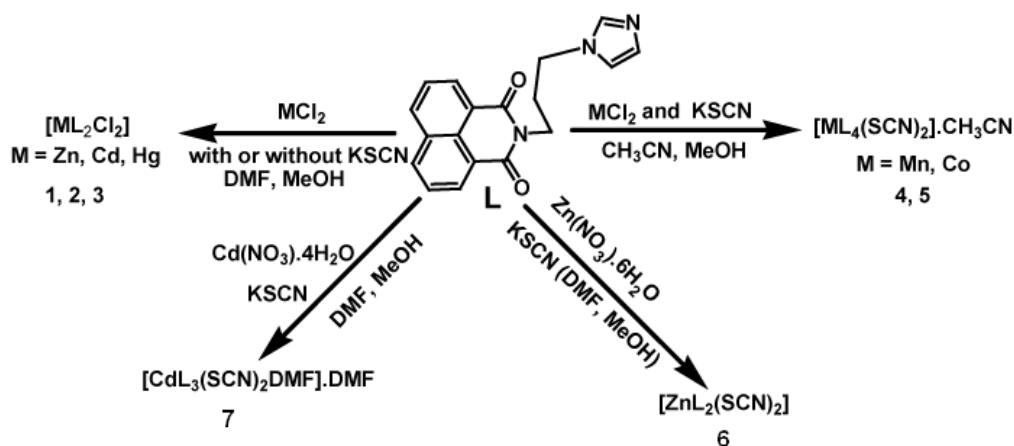
Table 1: Crystallographic parameters of complexes **1-7**

Compound No	Complex 1	Complex 2	Complex 3	Complex 4	Complex 5	Complex 6	Complex 7
Formulae	$C_{36}H_{30}Cl_2N_6O_4Zn$	$C_{36}H_{30}Cl_2N_6O_4Cd$	$C_{36}H_{30}Cl_2N_6O_4Hg$	$C_{78}H_{66}N_{16}O_8S_2Mn$	$C_{78}H_{66}N_{16}O_8S_2Co$	$C_{38}H_{30}N_8O_4S_2Zn$	$C_{62}H_{59}N_{13}O_8S_2Cd$
CCDC Nos.	928185	928178	928182	928183	928180	928184	928179
Mol. wt.	746.93	793.96	882.15	1474.53	1478.52	792.19	1290.74
Crystal system	Monoclinic	Monoclinic	Monoclinic	Triclinic	Triclinic	Monoclinic	Triclinic
Space group	$C2/c$	$C2/c$	$C2/c$	$P-1$	$P-1$	$P2_1/c$	$P-1$
$a/\text{\AA}$	14.6120(18)	14.6314(6)	14.7824(3)	10.6242(7)	10.6146(8)	14.5214(4)	10.3324(3)
$b/\text{\AA}$	11.9825(18)	11.9993(4)	12.0395(3)	11.2787(6)	11.2239(12)	14.1478(5)	16.9948(4)
$c/\text{\AA}$	19.488(3)	19.7572(8)	19.7994(5)	15.7505(9)	15.7625(14)	22.8454(8)	17.5964(4)
$\alpha/^\circ$	90.00	90.00	90.00	95.575(4)	95.493(8)	90.00	91.4080(10)
$\beta/^\circ$	104.612(11)	105.630(4)	104.923(2)	103.794(4)	104.366(7)	128.618(2)	95.6650(10)
$\gamma/^\circ$	90.00	90.00	90.00	99.258(4)	99.105(8)	90.00	106.9570(10)
$V/\text{\AA}^3$	3276.9(8)	3340.4(2)	3404.91(14)	1790.86(18)	1778.3(3)	3667.1(2)	2936.48(13)
Z	4	4	4	1	1	4	2
Density g.cm^{-3}	1.514	1.579	1.721	1.367	1.381	1.435	1.460
Abs. Coeff. $/\text{mm}^{-1}$	0.964	0.864	4.727	0.312	0.370	0.836	0.511
F(000)	1536	1608	1736	767	769	1632	1332
Total no. of reflections	2919	3032	3066	6370	6422	6629	10470
Reflections, $I > 2\sigma(I)$	2156	2638	2402	4095	4116	4765	7921
Max. $2\theta/^\circ$	50.50	50.50	50.48	50.50	50.50	50.50	50.50
Ranges (h, k, l)	$-16 \leq h \leq 17$ $-14 \leq k \leq 12$ $-22 \leq l \leq 22$	$-17 \leq h \leq 17$ $-14 \leq k \leq 10$ $-23 \leq l \leq 23$	$-17 \leq h \leq 17$ $-13 \leq k \leq 14$ $-23 \leq l \leq 23$	$-12 \leq h \leq 12$ $-13 \leq k \leq 13$ $-18 \leq l \leq 18$	$-12 \leq h \leq 12$ $-11 \leq k \leq 13$ $-18 \leq l \leq 18$	$-16 \leq h \leq 17$ $-16 \leq k \leq 16$ $-26 \leq l \leq 27$	$-12 \leq h \leq 12$ $-19 \leq k \leq 18$ $-21 \leq l \leq 20$
Complete to 2 θ (%)	98.1	99.8	99.0	98.3	99.8	99.8	98.3
Data/Restraints/Parameters	2919/0/222	3032/0/255	3066/0/222	6370/0/476	6422/0/476	6629/0/478	10470/0/779
Goof (F^2)	0.984	1.043	1.104	1.005	1.019	1.114	1.044
R indices [$I > 2\sigma(I)$]	0.0488	0.0351	0.0720	0.0433	0.0699	0.0473	0.0320
R indices (all data)	0.0627	0.0427	0.1093	0.0790	0.1076	0.0732	0.0450
WR ₂ [$I > 2\sigma(I)$]	0.1353	0.0793	0.1346	0.0676	0.1426	0.0774	0.0714
WR ₂ (all data)	0.1446	0.0835	0.1432	0.0781	0.1624	0.0863	0.0811

Results and discussion:

A series of divalent metal (M = Mn, Co, Zn, Cd, Hg) complexes of the ligand **L** with various compositions as depicted in scheme 1 were synthesized and characterized by various spectroscopic techniques and finally by single crystal X-ray diffraction. The powder XRD of all samples were recorded and compared with the simulated spectra; which showed the purity of the bulk samples in solid state. For the sake of comparison the powder pattern of the complex **1** is shown figure 1a and

others are available as supporting information. The metal chlorides of zinc, cadmium and mercury independently reacted with **L** led to a series of isomorphous complexes $[ML_2Cl_2]$ $\{M = Zn$ (**1**), Cd (**2**), Hg (**3**) $\}$. Each of the three complexes adopts distorted tetrahedral geometry. Since these three



Scheme 1: Different metal complexes of **L**

complexes are structurally similar, only the representative structure of the zinc complex (**1**) is shown in figure 2. In the solid state structure the zinc ion lies on a two-fold axis. The ligand **L** in these cases adopts a bend structure and such bend form of the ligand is stabilized by weak C-H \cdots O and π -

Table 1: The metal-ligand bond parameters in complexes **1-3**

Complex	M-L	Bond-length(Å)	< L-M-L	Angle (°)	< L-M-L	Angle (°)
Complex 1	Zn1- N1	2.028(2)	N1- Zn1- N1	99.41(13)	N1- Zn1- Cl1	112.63(7)
	Zn1- Cl1	2.2378(11)	N1- Zn1- Cl1	107.74(7)	Cl1- Zn1- Cl1	115.58(8)
Complex 2	Cd1- N1	2.231(2)	N1- Cd1- N1	94.99(12)	N1- Cd1- Cl1	112.84(7)
	Cd1 Cl1	2.4131(10)	N1- Cd1- Cl1	107.93(7)	Cl1- Cd1- Cl1	118.00(7)
Complex 3	Hg1- N1	2.268(7)	N1- Hg1- N1	92.3(4)	N1- Hg1- Cl1	111.5(2)
	Hg1- Cl1	2.451(5)	N1- Hg1- Cl1	106.3(2)	Cl1- Hg1- Cl1	124.2(3)

stacking interactions (supporting figure 2S). Such interactions arise from intermolecular interactions between the carbonyl group of 1,8-naphthalimide with one C-H of the propylene attached to an imidazole unit. Another C-H bond of the propylene group at the α -position next to the imidazole also interacts with carbonyl group of 1,8-naphthalimide group. The formation of intra-molecular stacks of imidazole and naphthalene rings is favored by flexible propylene group. The metal-ligand bond parameters of the complexes **1-3** are listed in table 1. From the table 1 it is clear that metal-ligand bond distances are in the sequence $Zn < Cd < Hg$. The observed trend is due to the increase in the size of the metal ions.

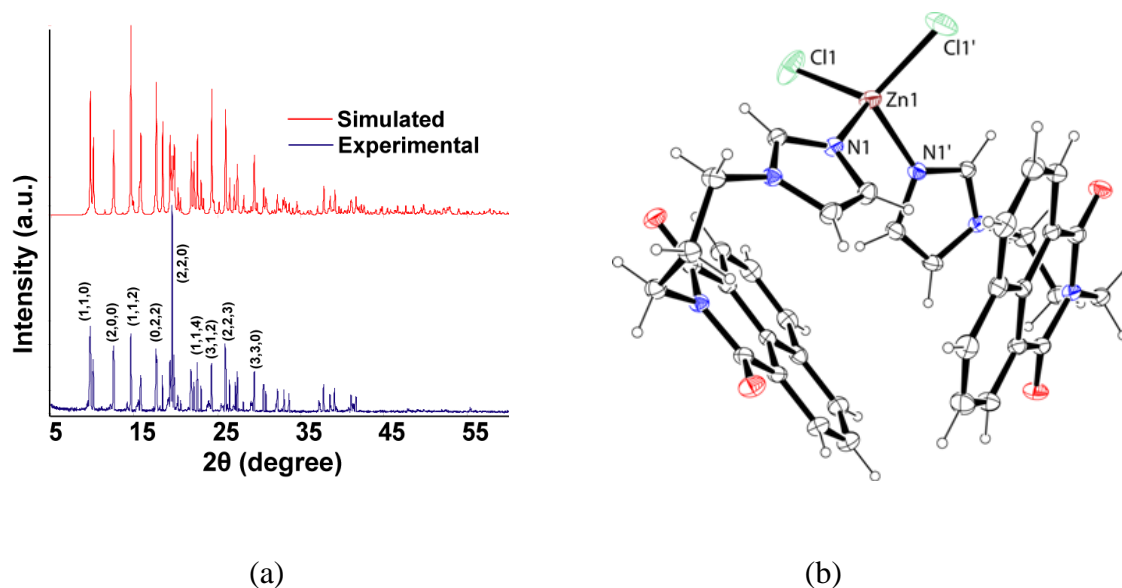


Figure 2: (a) Powder-XRD of the complex **1** (top : simulated, bottom : experimental). (b) Crystal structure of the complex **1** (ORTEP drawn with 30 % probability; equivalent symmetry is generated through 2-x, y, 1/2-z)

Table 2: The Metal-ligand bond parameters of complexes **4-7**

Complex No.	M-X	Bond-length (Å)	< L-M-L	Angle (°)	< L-M-L	Angle (°)
Complex 4	Mn1- N1	2.2758(19)	N1- Mn1- N4	88.12	N1'- Mn1- N4'	91.88
	Mn1- N4	2.2606(19)	N1- Mn1- N7	89.67	N1'- Mn1- N7	90.33
	Mn1- N7	2.236(2)	N4- Mn1- N7	92.67	N4'- Mn1- N7	87.33
Complex 5	Co1- N1	2.169(4)	N1- Co1- N4	88.92	N1'- Mn1- N4	91.08
	Co1- N4	2.161(4)	N1- Co1- N7	90.37	N1'- Mn1- N7	89.63
	Co1- N7	2.157(4)	N4- Co1- N7	92.64	N4'- Mn1- N7	87.46
Complex 6	Zn1-N1	1.986(3)	N1-Zn1 -N4	114.52(10)	N4 -Zn1-N8	102.27(11)
	Zn1-N4	1.997(3)	N1-Zn1 -N7	103.77(11)	N7- Zn1-N8	111.58(12)
	Zn1-N7	1.972(3)	N1-Zn1 -N8	115.03(12)		
	Zn1-N8	1.940(3)	N4-Zn1 -N7	109.85(12)		
Complex 7	Cd1-N1	2.327(2)	N1-Cd1-N4	178.09(7)	N4-Cd1-N11	90.36(8)
	Cd1-N4	2.335(2)	N1-Cd1-O7	88.72(8)	N4-Cd1-N7	87.37(7)
	Cd1-N7	2.339(2)	N1-Cd1-N11	91.18(9)	N4-Cd1-N10	90.92(8)
	Cd1-N10	2.340(3)	N1-Cd1-N7	93.77(7)	N7-Cd1-N10	92.63(9)
	Cd1-N11	2.343(3)	N1-Cd1-N10	87.50(9)	N11-Cd1-N10	177.69(9)
	Cd1-O7	2.337(2)	N4-Cd1-O7	90.20(8)	O7-Cd1-N7	176.79(8)
			O7-Cd1-N11	88.57(9)	O7-Cd1-N10	89.50(9)

In the thiocyanate containing metal complexes the ratio of the ligand to the metal ions varies. For example 1: 2 complex was formed in the case of zinc, 1 : 3 in cadmium and 1 : 4 in the case of manganese and cobalt. The metal complexes bearing thiocyanate ligand has special interest from their ease of degradability and due to their labile nature.¹⁶ The manganese complex **4** and cobalt complex **5** have a similar compositions, namely $[ML_4(SCN)_2] \cdot 2CH_3CN$ and they are isomorphous (Figure 3).

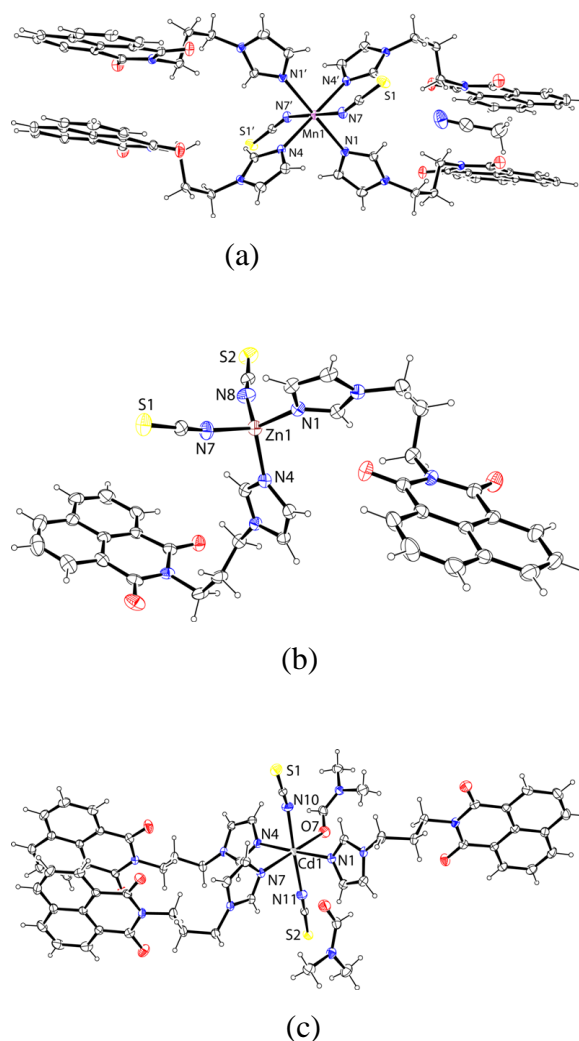


Figure 3: The structure of the complex (a) **4** (symmetry of equivalent atoms $-x, 1-y, -z$); (b) **6** and (c) **7** (ORTEP drawn with 30% thermal ellipsoid)

The manganese atom in the complex **4** and the cobalt atom in the complex **5** lies on an inversion centre. These hexa-coordinated complexes **4** and **5** have distorted octahedral geometry with four nitrogen atoms of the imidazole in one plane forming dative bond with a metal ion (Figure 3a). The monodentate thiocyanate ligands coordinating through nitrogen atoms occupy the axial positions. The structure of the complex **4** contains a center of inversion. The interesting feature of the structure is that the naphthalimide rings are π -stacked with another naphthalimide ring of neighboring molecules on each side so that layered structures are formed. The ligand **L** adopts a linear structure in the complex. While forming such structure the imidazole rings are not in one plane with respect to each other across the metal centers. The zinc thiocyanate complex $[\text{ZnL}_2(\text{SCN})_2]$ (**6**) is a tetra-coordinated complex (Figure 3b) with a distorted tetrahedral geometry. The complex is stable in solution and the $^1\text{H-NMR}$ show significant shift from the parent ligand, the spectra is shown in figure 21s of supporting information. On the other hand the $[\text{CdL}_3(\text{SCN})_2\text{DMF}]\cdot\text{DMF}$ (**7**) is a hexa-coordinated complex with three ligands (**L**) and one DMF occupying one plane and two thiocyanate occupying the axial positions

of a distorted octahedron (Figure 3c). The complex **7** is also characterized by its $^1\text{H-NMR}$ which is shown in the supporting figure 22S. It shows methyl signals for two DMF molecules, one corresponding to coordinated other free dimethylformamide appears at 2.88 and 2.72 ppm. This is supportive of the structure determined by X-ray crystallography. From the integration compound shows presence of two molecules of DMF per molecule. In thermogravimetry complex **7** shows weight loss of 8.34 wt % (calcd. 8.98 wt %) in the range of 120-182 °C corresponds to the loss of one lattice dimethylformamide molecule and one coordinated dimethylformamide molecule. The IR spectra of thiocyanate complexes showed characteristic stretching frequencies in the region of 2051-2075 cm^{-1} . The values support the coordination thiocyanate through nitrogen atom in each case.¹⁷

The complexes have UV-visible absorptions in the range of 315-360 nm originating from the ligand. By comparing with analogous compound it may be suggested to originate from $n \rightarrow \pi^*$ transition.¹⁸ The naphthalimide derivatives are fluorescent¹⁹ and in solid state the ligand **L** shows a strong emission at 461 nm. The solid samples of the complexes **1-5** showed emissions in the range of 425-481 nm upon excitation at 350 nm [Figure 4(i)-(ii)]. The complexes **3**, **6** or **7** show fluorescence enhancement with

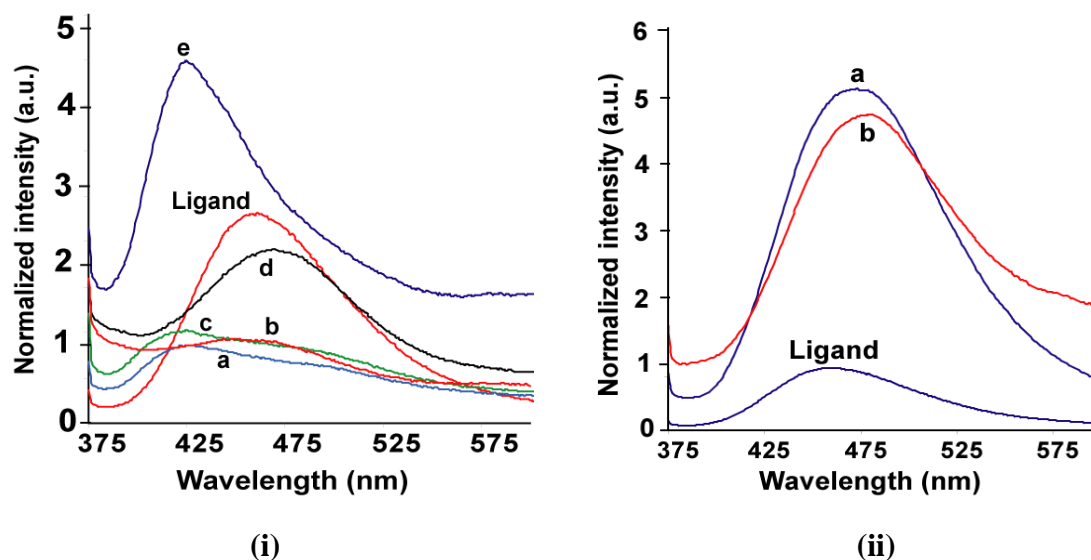
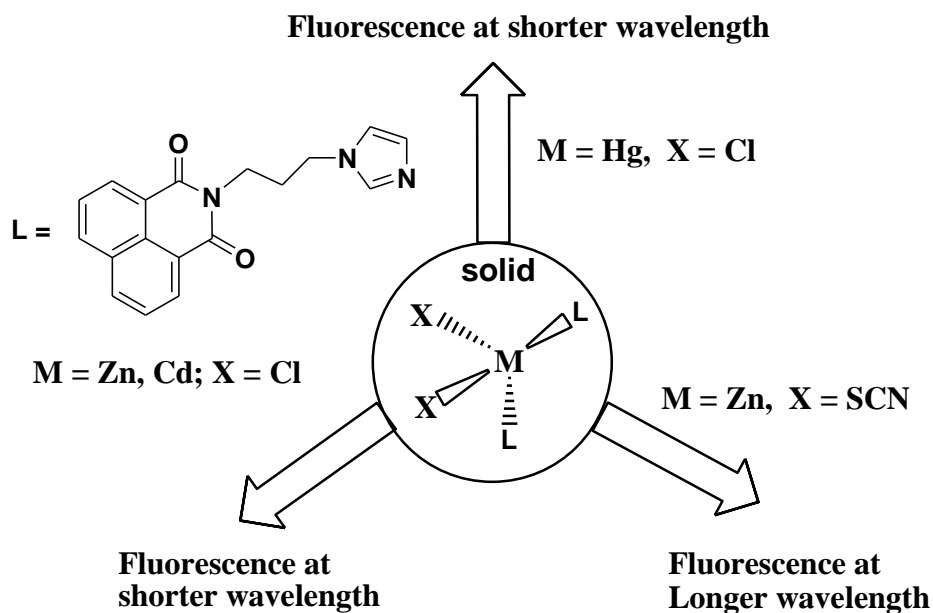


Figure 4: (i) Solid state fluorescence emission of ligand **L** and complexes (a) complex **1**; (b) complex **5**; (c) complex **2**; (d) complex **4**, (e) complex **3**. In each case the intensity are normalized with respect to the lowest emission intensity shown by complex **1**. (ii) Solid state fluorescence emission of (a) complex **6**; (b) complex **7** at room temperature ($\lambda_{\text{ex}} = 350 \text{ nm}$) with intensities normalised with respect to ligand.

respect to the ligand (**L**). On the other hand the complex **4** and **5** shows quenching of fluorescence with a small shift towards longer wavelength. The central metal ion in the complex **4** and complex **5** are manganese (d^5 , high-spin) and cobalt (d^7) in + 2 oxidation state respectively, which are paramagnetic

Both complexes show lower fluorescence intensity than the parent ligand due to the paramagnetic nature of the ions^{1f}. These complexes have stretched conformations of the ligand; hence follow conventional fluorescence emission resembling the emission of parent ligand.



Scheme 2: The fluorescence selectivity in four coordinated complexes of **L**

The fluorescence emission changes of solid samples of these tetrahedral complexes are interesting; they show characteristic emission on variation of anions and cations. The increase and decrease in intensity of fluorescence emission shown by these complexes are schematically presented in scheme 2. The complexes **1-3** have chloride ions, among them, the complex **1** or **2** show fluorescence emission at 428 nm and 425 nm respectively which are lower than the fluorescence emission of the ligand at 451 nm. The emission peak of mercury complex **3** has higher intensity than the free ligand occurs at 433 nm which is 31 nm less than the fluorescence emission of the ligand at solid state. On the other hand, the complexes **6** as well as **7** have fluorescence emission longer wavelength than the parent ligand. A close examination of the structure **1**, **2** and **6**, shows that the orientation of 1,8-naphthalimide rings are similar in the complex **1** and **2** but different from complexes **6** and **7**. Whereas, the complexes **6** has a non-parallel bent orientation, but complex **7** has a stretched orientation of ligand **L**. Thus, twisting of the ligand to adopt near parallel orientation between the imidazole ring and 1,8-naphthalimide rings favors shorter-wavelength emission due to stabilization of the ground state by intramolecular charge transfer. The stretched orientation or an orientation not favoring stabilization of ground state of **7** would help in stabilization of inter-molecular charge transfer excited state, taking the emission to longer wavelength. The mercury being large and have more diffused charge have intra-molecular

interaction between imidazole and naphthalimide ring, helps in the stabilization of the ground state, accordingly it emits at shorter wavelength.

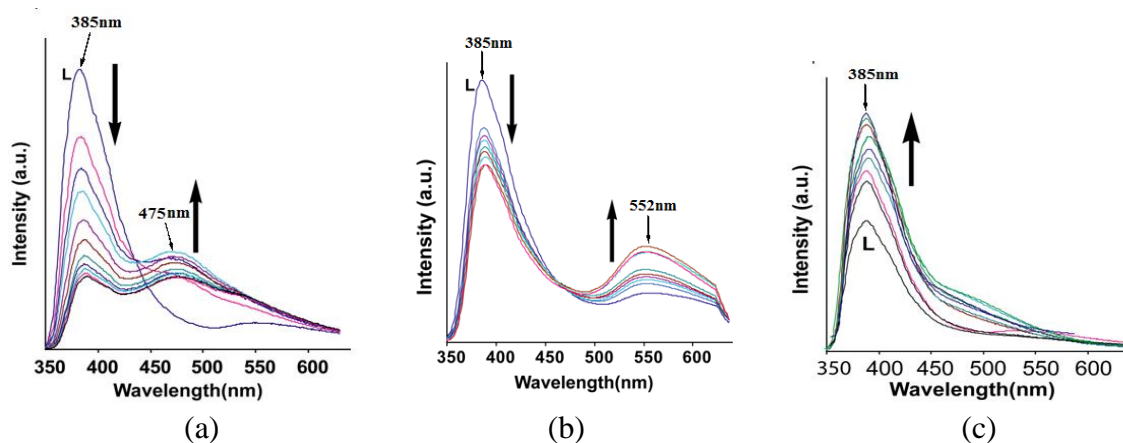


Figure 5: The changes in fluorescence emission intensity of ($\lambda_{\text{ex}} = 340 \text{ nm}$) of the ligand, **L** (2 ml of 10^{-4} M solution in DMF) on addition of (a) zinc chloride, (b) cadmium chloride and (c) mercuric chloride (5 μl aliquots of a 10^{-2} M solution in water).

The fluorescence emission of **L** in DMF solution by adding aqueous solution of chloride salts of zinc, cadmium or mercury were independently studied with complexes **1-3** (figure 5). As anticipated addition of mercury ions showed enhancement of fluorescence whereas the addition of zinc chloride or cadmium chloride quenched the emission causing emission at two wavelengths (Figure 5a, 5b). We find analogy between solution and solid state fluorescence emission study from the observed changes. The ligand single emission peak changed on titration with zinc chloride, and at the end of titration we observed emission at 385 nm and 475 nm; whereas similar titration with cadmium chloride yielded emission at 385 nm and 552 nm respectively. The role of anions in the fluorescence emission of naphthalimide fluorophores interacting with various anions is well established.^{2b} Heagy and coworkers have shown that depending on the orientations of pyridine over a naphthalimide ring causes fluorescence either shift to shorter wavelength (SW) or to longer wavelength (LW).¹⁴ Thus, in solution the addition zinc ions facilitated the stretching of the ligand leading to emission at longer wavelength occur from stabilization of exciplex through intermolecular π - π interactions.^{3f}

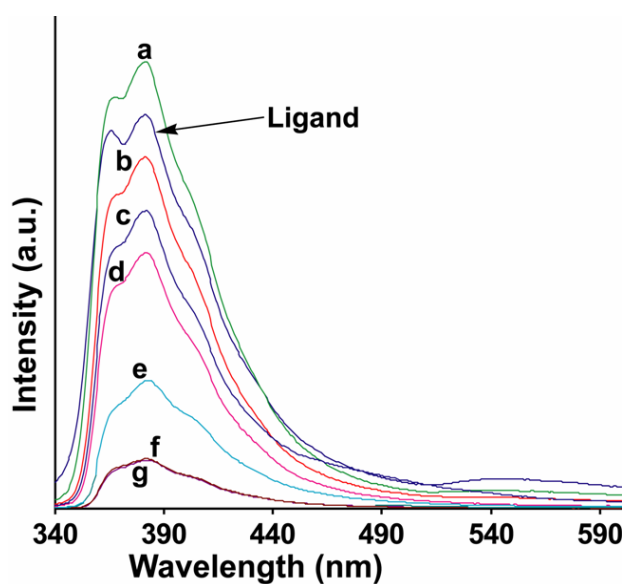


Figure 6 : Fluorescence emission spectra (λ_{ex} 330 nm) of the (a) complex **3**, (b) complex **2**; (c) complex **6**; (d) complex **1**; (e) complex **7**; (f) complex **5**; (g) complex **4** and ligand (**L**) in dimethylformamide (concentration of 10^{-4}M each)

The fluorescence emission spectra of the complexes in solutions were determined and are shown in figure 6. It is clear from the figure 6 that that the fluorescence quenching with respect to the ligand occurred in solution in each metal complex. However the exception was the mercury complex **3** which showed fluorescence enhancement. There are multiple components of fluorescence in each case pointing out number of orientations present in solutions. This makes clear distinction of mercury from other ions. There are terpyridine ligands distinguish mercury²⁰ in aqueous medium; but, our system also can distinguish mercury in aqueous solution from aqueous solution of cadmium and zinc ions. The quantum yields of the ligand as well as all the complexes were determined from their respective solution in dimethylformamide (table 2s of supporting information). The quantum yield of the ligand is 0.36 and the complexes lies in the range of 0.37-0.50.

To understand the effect of temperature on the fluorescence changes, we recorded the temperature dependent fluorescence emissions at different temperatures for the complexes **1-3** and compared these data with the ligand. This is carried out with the anticipation that as the thermal energy increases the ligand would open up from a bend geometry, which disfavors intramolecular charge transfer

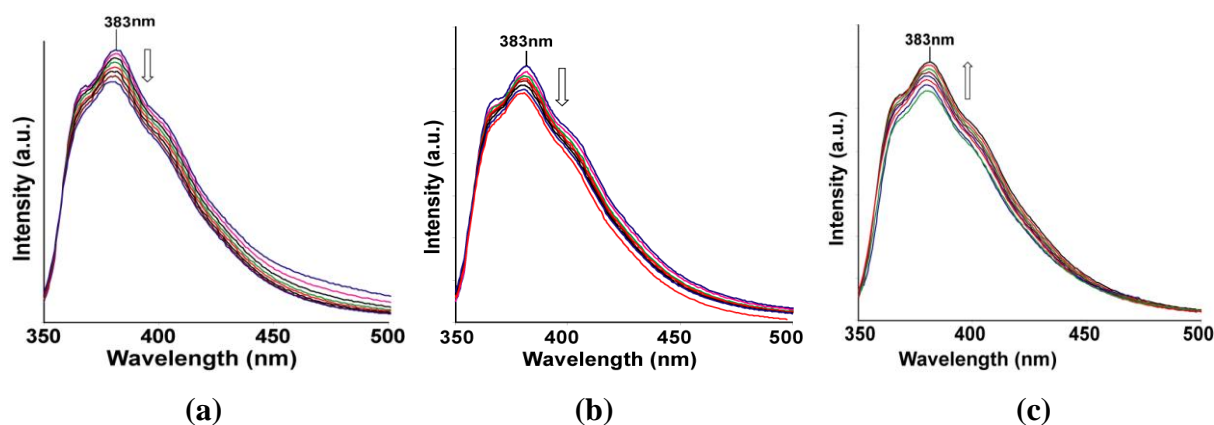


Figure 7: Temperature dependent fluorescence spectra of the (a) complex **1** ; (b) complex **2** and (c) complex **3**. (30 °C to 100 °C at 10 °C interval of temperature; 0.1 mM solution each in DMF; $\lambda_{\text{ex}}=330$ nm, downward arrow shows decrease in intensity).

interaction. Three illustrative examples on the changes of fluorescence in solution with respect to temperatures are shown figures 7. Quenching of fluorescence in the case of complex **1** and **2** were observed as the temperature was increased. While the mercury complex **3** showed enhancement of fluorescence emission as the temperature was increased. It may be mentioned that the nitrogen heterocycles attached to 1,8-naphthalimides are important as some of them show dual fluorescence and these are related to coplanar or orthogonal geometries of the 1,8-naphthalimide part with respect to the nitrogen containing heterocyclic units attached to them^{2c,14b}. Thus, the complex **1** and **2** shows decrease of fluorescence intensity on heating, suggesting the decrease in photo-electron energy transfer contribution to the emission process by change of orientation. Whereas, the mercury complex having a folded structure, stretches out on heating to show increase in the fluorescence emission intensity. When there is no metal ion to guide the orientation the ligand **L**, the lone pair of electrons present on the nitrogen atom of imidazole contributes to photo-electron energy transfer (PET) mechanism, causing a partially quenched state at start of heating, on heating the orientation of **L** changes, accordingly the intensity grows.

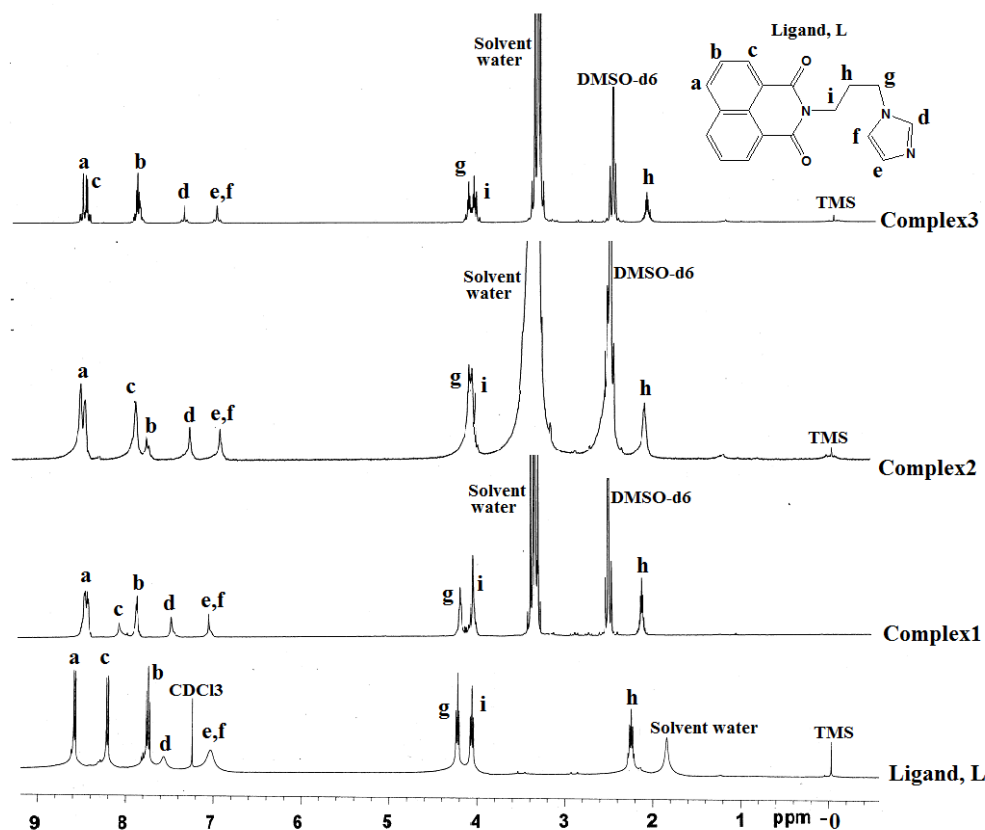


Figure 8: $^1\text{H-NMR}$ spectra of the ligand and (400MHz, CDCl_3) and the complex **1-3** (600MHz, DMSO-d_6)

The stability of the complexes in solution was ascertained from the respective $^1\text{H-NMR}$ spectra of the complexes **1-3**, **6** and **7**. The $^1\text{H-NMR}$ spectra of the complex **1-3** and ligand are compared in figure 8, which clearly indicates, that the complexes are stable in solution and on complexation of the ligand to zinc or cadmium, the chemical shift of the methylene group adjacent to imidazole is affected and so are the protons on the imidazole ring. Analogously, the complexes **6** and **7** also shows clear shifts of the $^1\text{H-NMR}$ peaks and some of the peaks were broadened in these complexes as shown in supporting information (figure 21S and 22S).

In conclusions, the structures in solid state have helped us to explain the fluorescence behavior of such complexes by invoking intramolecular charge-transfer (ICT) to stabilize ground state in bent geometry (d of figure 1) to cause emission at lower wave-length, whereas a stretched ligand helps exciplex through π -stacking of 1,8-naphthalimides to show emission at long wavelength (e of figure 1). The free ligand as well as the complexes in solution shows fluorescence enhancement on heating shows enhancement of fluorescence intensity through a PET mechanism²¹ arising from the lone pair of electrons on nitrogen atom of imidazole. On heating conformational changes disfavor participation of lone pair on nitrogen atom of imidazole in such process, hence enhancement of intensity of fluorescence of the ligand was observed. Whereas, in solid state the coordination of the ligand to d^{10} -

metal ions provide orientation to the ligand so as to favor or disfavor intra-molecular charge-transfer emission (d, e of figure 1). The mercury ions show fluorescence enhancement over the cadmium or zinc ions hence it is distinguishable from the later. From the series of study it is clear that the conformation shown as d of figure 1 favors the low wavelength emission, while the other stretched geometry helps in exciplex formation taking the fluorescence to longer wavelength.

Supporting information: The packing diagrams, powder XRD-patterns and their comparison with simulated patterns, solid state and solution UV-Vis spectra and thermogravimetric analysis are available. The CIF files are deposited to Cambridge Crystallographic database and have the CCDC numbers The CCDC numbers of the CIF of **1-7** are 928178, 928179, 928180, 928182, 928183, 928184 and 9281885.

References:

- (a) R. M. Duke, E. M. Veale, F. M. Pfeffer, P. E. Kruger, T. Gunnlaugsson, *Chem. Soc. Rev.*, 2010, **39**, 3936-3953. (b) T. Gunnlaugsson, P. E. Kruger, P. Jensen, F. M. Pfeffer, G.M. Hussey, *Tetrahedron Lett.*, 2003, **44**, 8909-8913. (c) X. Poteau, A. I. Brown, R. G. Brown, C. Holmes, D. Matthew, *Dyes and Pigments*, 2000, **47**, 91-105. (d) A. P. De Silva, H. Q. N. Gunaratne, T. Gunnlaugsson, A. J. M. Huxley, C. P. McCoy, J. T. Rademacher, T. E. Rice, *Chem. Rev.*, 1997, **97**, 1515-1566. (e) S. Guha, P. S. Goodson, L. J. Corson, S. Saha, *J. Am. Chem. Soc.*, 2012, **134**, 13679-13691. (f) Z. Xu, J. Yoon, P. R. Spring *Chem. Commun.*, 2010, **46**, 2563-2565.
- (a) K-Y. Lee, *Chem. Rev.*, 1993, **93**, 449-486. (b) H. D. P. Ali, P. E. Kruger, T. Gunnlaugsson, *New J. Chem.*, 2008, **32**, 1153-1161. (c) P. Nandhikonda, M. P. Begaye, Z. Cao, M. D. Heagy, *Chem. Commun.*, 2009, 4941-4943. (d) J. Gan, H. Tian, Z. Wang, K. Chen, J. Hill, P. A. Lane, M. D. Rahn, A. M. Fox, D.D.C. Bradley, *J. Organomet. Chem.*, 2002, **645**, 168-175.
- (a) Z. Liu, C. Zhang, X. Wang, W. He, Z. Guo, *Org. Lett.*, 2012, **14**, 4378-4381. (b) M. Formica, V. Fusi, L. Giorgi, M. Micheloni, *Coord. Chem. Rev.*, 2012, **256**, 170-192. (c) V. F. Pais, P. Remon, D. Collado, J. Andersson, E. Perez-Inestros, U. Pischel, *Org. Lett.*, 2011, **13**, 5572-5575. (d) L. Prodi, F. Bolletta, M. Montali, N. Zaccheroni, *Coord. Chem. Rev.*, 2000, **205**, 59-85. (e) S. Guha, S. Saha, *J. Am. Chem. Soc.*, 2010, **132**, 17674-17677. (f) J. K. Nath, J. B. Baruah, *New J. Chem.*, 2013, **37**, 1509-1519. (g) J. Nath, J.B. Baruah, *J. Fluoresc.* DOI 10.1007/s10895-014-1353-8.
- (a) C. Thalacker, A. Miura, S. De Feyter, F. De Schryver, F. Wurthner, *Org. Biomol. Chem.*, 2005, **3**, 414-422. (b) D. L. Reger, J. D. Elgin, R. F. Semeniuc, P. J. Pellechia, M. D. Smith, *Chem. Commun.*, 2005, 4068-4070.
- (a) G. Loving, B. Imperiali, *Bioconjugate Chem.*, 2009, **20**, 2133-2141. (b) M. E. Vazques, J. B. Blanco, B. Imperiali, *J. Am. Chem. Soc.*, 2005, **127**, 1300-1306. (c) G. Loving, B. Imperiali, *J. Am. Chem. Soc.*, 2008, **130**, 13630-13638.

6. (a) D.W. Cho, M. Fujisuka, K. H. Choi, M. J. Park, U. C. Yoon, T. Majima, *J. Phys. Chem. B*, 2006, **110**, 4576-4582. (b) Y. Xu, X. Qian, W. Yao, P. Mao, J. Cui, *Bioorg. Med. Chem.*, 2003, **11**, 5427-5433.
7. (a) V. Gorteau, G. Bollot, J. Mareda, A. Perez-valasco, S. Matile, *J. Am. Chem. Soc.*, 2005, **125**, 14788-14789. (b) J. T. Davis, *Nature Chem.*, 2010, **2**, 516-517. (c) R. E. Sawson, A. Hennig, D. P. Weimann, D. Emery, V. Ravikumar, J. Montenegro, T. Takeuchi, S. Gabutti, M. Mayor, J. Mareda, A. Schalley, S. Matile, *Nature Chem.*, 2010, **2**, 533-538.
8. D. V. Pogozhev, M. J. Bezdek, P. A. Schauer, C. P. Berlinguette, *Inorg. Chem.*, 2013, **52**, 3001-3006.
- 9.(a) D. L. Reger, A. Debreczeni, B. Reinecke, V. Rasslov, M. D. Smith, *Inorg. Chem.*, 2009, **48**, 8911-8924. (b) D. L. Reger, A. Debreczeni, M. D. Smith, *Inorg. Chim. Acta*, 2010, **364**, 10-15. (c) D. L. Reger, J. J. Horger, A. Debreczeni, M. D. Smith, *Inorg. Chem.*, 2011, **50**, 4669-4670. (d) R. J. Sarmá, C. Tamuly, N. Barooah, J. B. Baruah, *J. Mol. Struct.*, 2007, **829**, 29-36. (e) D. Singh, J. B. Baruah, *Cryst. Growth Des.*, 2012, **12**, 2109-2121. (c) D. Singh, J. B. Baruah, *Inorg. Chim. Acta* 2012, **390**, 37-40.
10. (a) I. Saito, M. Takayama, H. Sugiyama, K. Nakatani, *J. Am. Chem. Soc.*, 1995, **117**, 6406-6407. (b) M. F. Brafia, M. Cacho, A. Ramos, M. T. Dominguez, J. M. Pozuelo, C. Abradelo, M. F. Rey-Stolle, M. Yuste, C. Carrasco, C. Bailly, *Org. Biomol. Chem.*, 2003, **1**, 648-654. (c) E. B. Veale, T. Gunnlaugsson, *J. Org. Chem.*, 2010, **75**, 5513-5525.
11. (a) L. Ingrassia, F. Lefranc, R. Kiss, T. Mijatovic, *Curr. Med. Chem.*, 2009, **161**, 192-121. (b) M. Ly, H. Xu, *Curr. Med. Chem.*, 2009, **16**, 797-813. (c) J. L. Nitiss, J. Zhou, A. Rose, Y. Huiung, K. C. Gale, N. Osheroff, *BioChem.*, 1998, **37**, 3078-3085. (d) S. Banerjee, E. B. Veale, C. M. Phelan, S. A. Murphy, G. M. Tocci, L. J. Gillespie, D. O. Frimannsson, J. M. Kelly, T. Gunnlaugsson, *Chem. Soc. Rev.*, 2013, **42**, 1601-1618. (e) K. Wang, Y. Wang, X. Yan, H. Chen, G. Ma, P. Zhang, J. Li, X. Li, P. Zhang, *Bioorg. Med. Chem. Lett.*, 2012, **22**, 937-941. (f) P. Gasioski, K. S. Danel, M. Matusiewicz, J. Uchacz, W. Kuznik, A. V. Kityk, *J. Fluoresc.*, 2012, 81-91.
12. P. Guo, Q. Chen, T. Liu, L. Xu, Q. Yang, X. Qian, *Med. Chem. Lett.*, 2013, **4**, 527-531.
13. K. J. Kilpin, C. M. Clavel, F. Edefe, P. J. Dyson, *Organometallics*, 2012, **31**, 7031-7039.
14. (a) S. Paudel, P. Nandhikonda, M. D. Heagy, *J. Fluoresc.*, 2009, **19**, 681-691. (b) P. Nandhikonda, M. P. Begaye, Z. Chao, M. D. Heagy, *Org. Biomol. Chem.*, 2010, **8**, 3195-3201. (c) L. Biczok, P. Valat, V. Wintgens, *Phys. Chem. Chem. Phys.*, 1999, **1**, 4759-4766. (d) H. Cao, V. Chang, R. Hernandez, M. D. Heagy, *J. Org. Chem.*, 2005, **70**, 4929-4934. (e) J. V. Mello, N. S. Finney, *Angew. Chem. Int. Ed.* 2001, **40**, 1536-1538.

15. (a) G. M. Sheldrick, *Acta Crystallogr.*, 2008, **A64**, 112-122. (b) CrysAlisPro, Oxford Diffraction Ltd., version 1,171. 33. 34d (release crysAlis 171.NET) 2009.
16. A. Abedi, V. Amani, R. Boca, L. Dlhan, H. K. Khavasi, N. Safari, *Inorg. Chim. Acta*, 2013, **395**, 58-66.
17. P. C. H. Mitchell, R. J. P. Williams, *J. Chem. Soc.*, 1960, 1912-1918.
18. P. Kucheryavy, G. Li, S. Vyas, C. Hadad, K. D. Glusac, *J. Phys. Chem. A*, 2009, **113**, 6453-646.
19. (a) D. L. Reger, A. Debreczeni, J. J. Horger, M. D. Smith, *Cryst. Growth Des.*, 2011, **11**, 4068-4079. (b) D. L. Reger, A. Debreczeni, A. E. Pascui, M. D. Smith, *Polyhedron*, 2013, **52**, 1317-1322. (c) S.-M. Fang, Q. Zhang, M. Hu, X.-G. Yang, L.-M. Zhou, M. Du, C.-S. Liu, *Cryst. Growth Des.*, 2010, **10**, 4773-4785. (d) S.-L. Zheng, J. -H. Yang, X. -L. Yu, X. -M. Chen, W. -T. Wong, *Inorg. Chem.*, 2004, **43**, 830-838.
20. (a) R. Shunmugam, G. J. Gabriel, C. E. Smith, K. A. Aamer, G. N. Tew, *Chem. Eur. J.*, 2008, **14**, 3904-3907. (b) H. N. Kim, W. X. Ren, J. S. Kim, J. Yoon, *Chem. Soc. Rev.*, 2012, **41**, 3210-3244.
21. D.W. Cho, M. Fujisuka, A. Sugimoto, U.C. Yoon, P.S. Mariano, T. Majima, *J. Phys. Chem. B* 2006, **110**, 11062-11068.

Inorganic Chemistry Frontiers Accepted Manuscript

Twisted conformations in complexes of N-(3-imidazol-1-yl-propyl)-1,8-naphthalimide and
fluorescence properties

J. K. Nath and J. B. Baruah

Supporting Information

Table 1S: Absorption and emission of complexes # **1-7**

Complex / ligand	Absorption in solid (nm)	Emission in solid (nm)
L	361	461
1	315, 353	428
2	330	425
3	318, 351	426
4	323	470
5	361	452
6	357	473
7	360	481

Table 2S : The quantum yield of the complexes determined in DMF solution

S.I No.	Compound	Quantum yield
1	Ligand, L	0.36
2	Complex 1	0.37
3	Complex 2	0.35
4	Complex 3	0.40
5	Complex 4	0.38
6	Complex 5	0.41
7	Complex 6	0.50
8	Complex 7	0.46

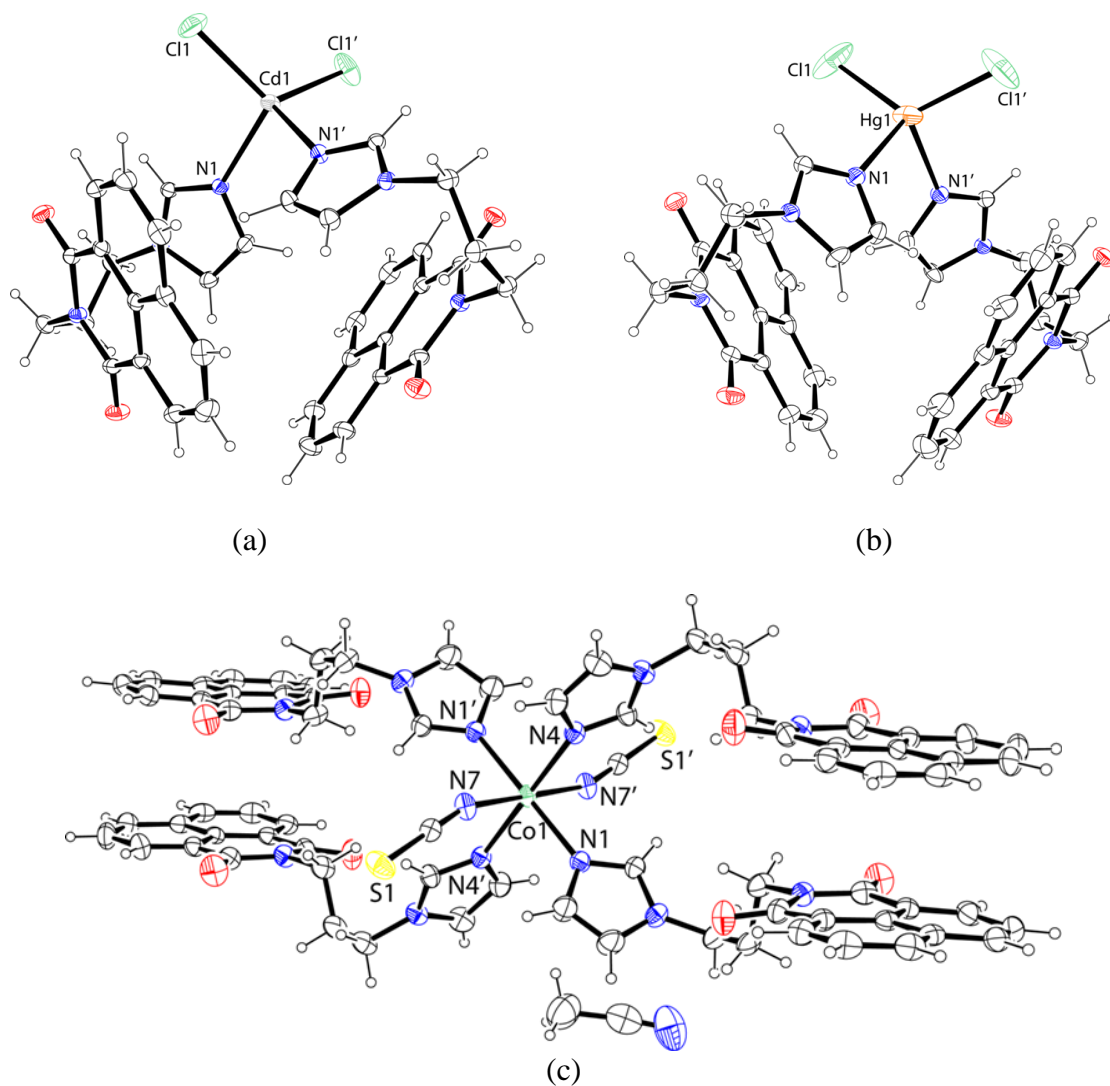


Figure 1S: ORTEP diagram of (a) complex **2**, (b) complex **3**, (c) complex **5** (symmetry of equivalent atoms $x,-y,-z$)

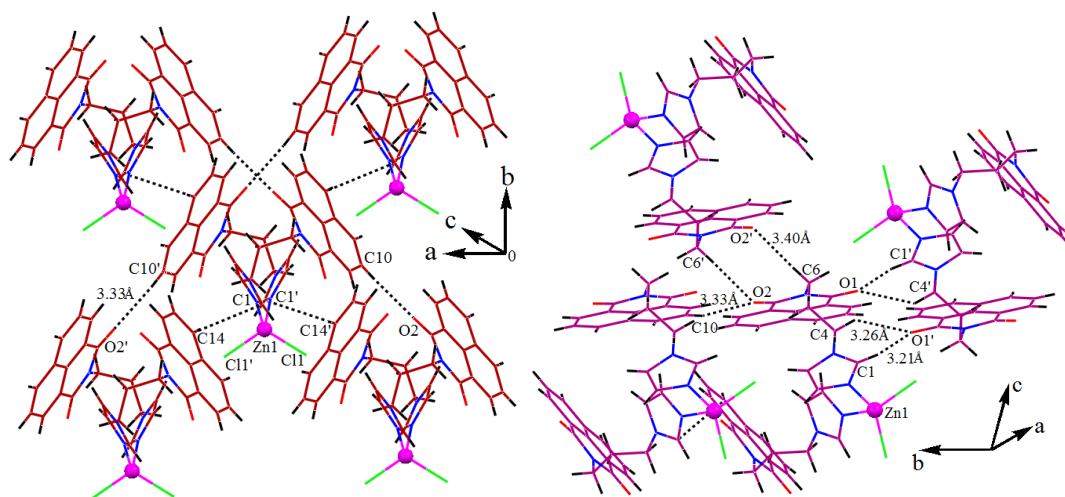


Figure 2S: Weak interactions in the crystal lattice of the complex **1** from two different projections.

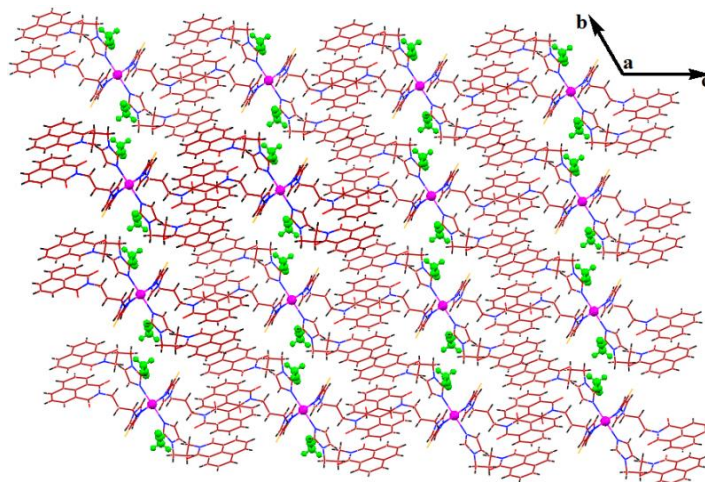


Figure 3S: 3D supramolecular network along a-axis. in the lattice of complex **4**.

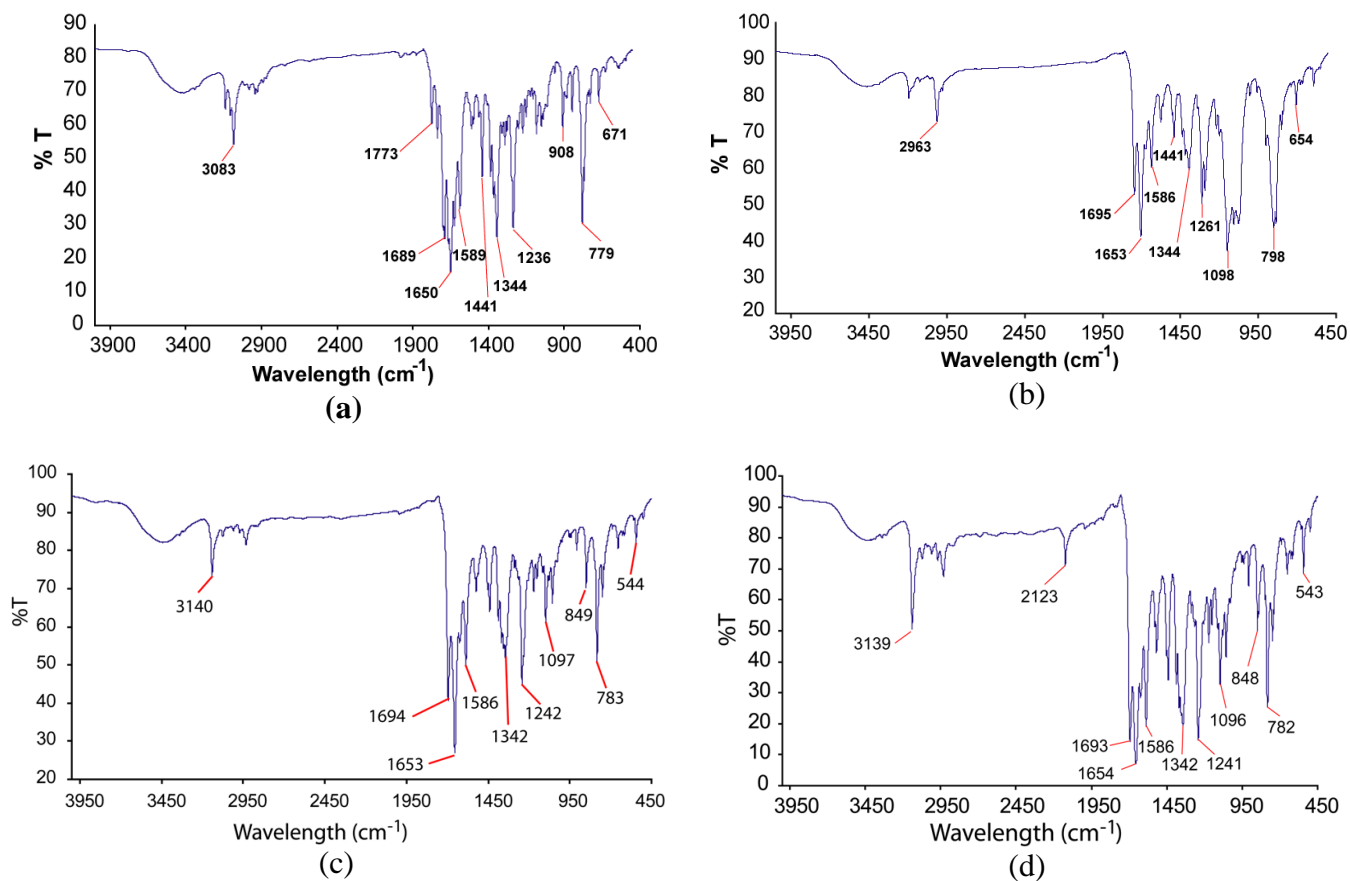


Figure 4S1: FT-IR (KBr) spectra of the (a) ligand, **L**, (b) Complex **1**, (c) Complex **2**, (d) Complex **3**.

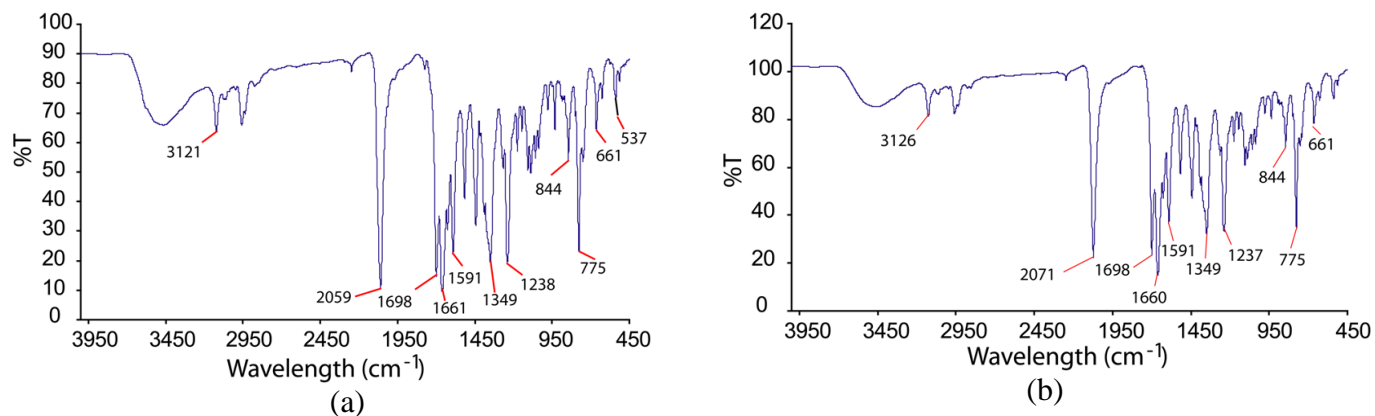


Figure 4S2: FT-IR spectra (KBr) of the (a) Complex **4** and (b) Complex **5**.

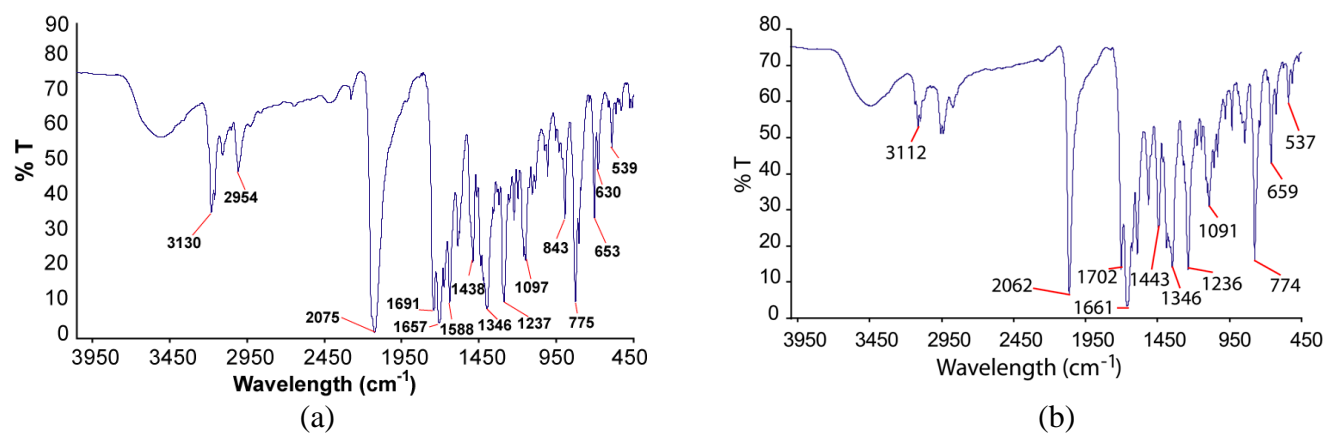


Figure 4S3: FT-IR spectra (KBr) of the (a) complex **6** and (b) Complex **7**

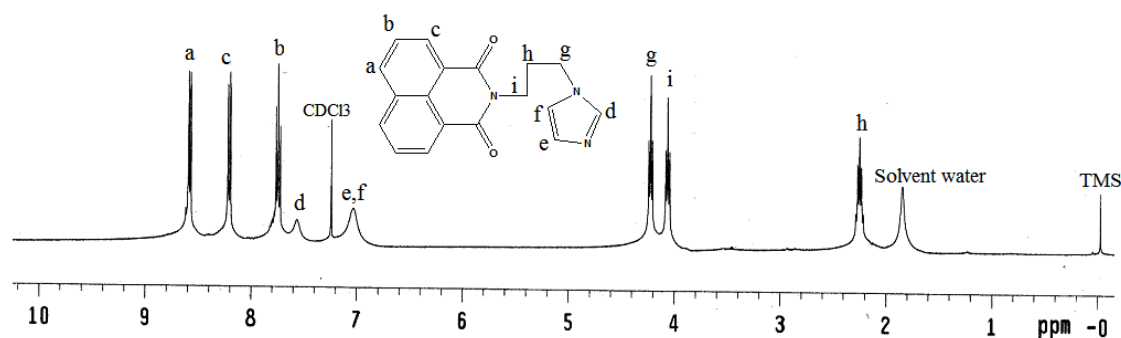


Figure 5S: ^1H NMR (400MHz, CDCl_3) spectrum of the ligand, **L**

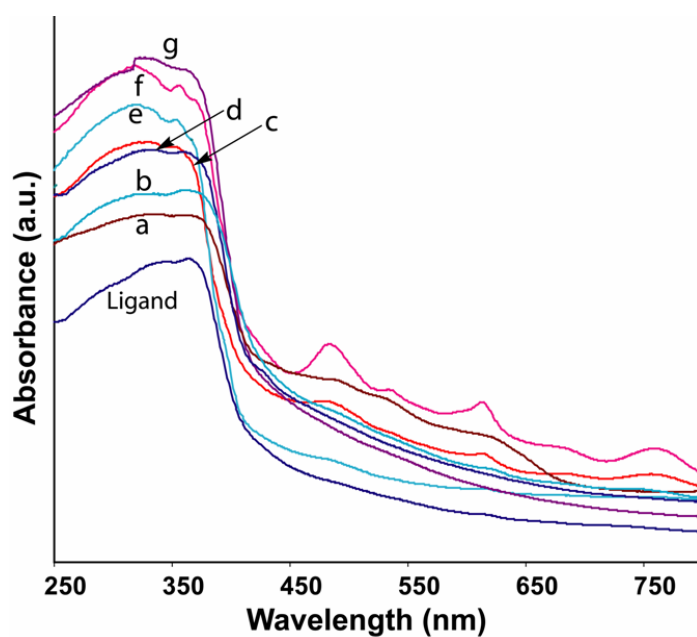


Figure 6S: Solid state UV-vis spectra of (a) complex **5**, (b) complex **7**, (c) complex **6**, (d) complex **2**, (e) complex **3**, (f) complex **1**, and (g) complex **4**.

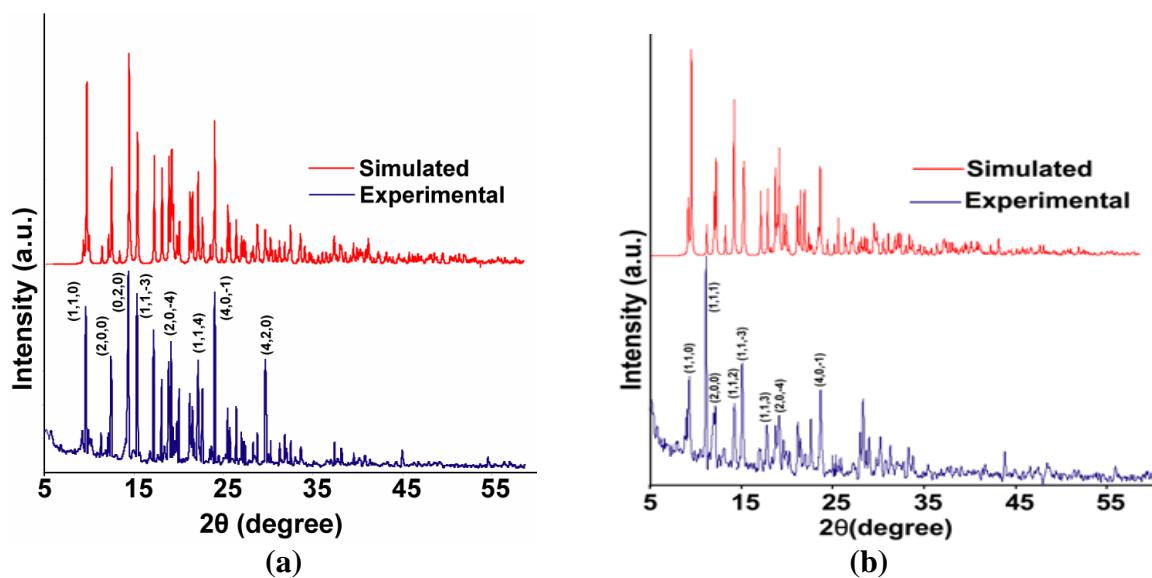


Figure 7S: PXRD pattern of the (a) complex 2 and (b) Complex 3

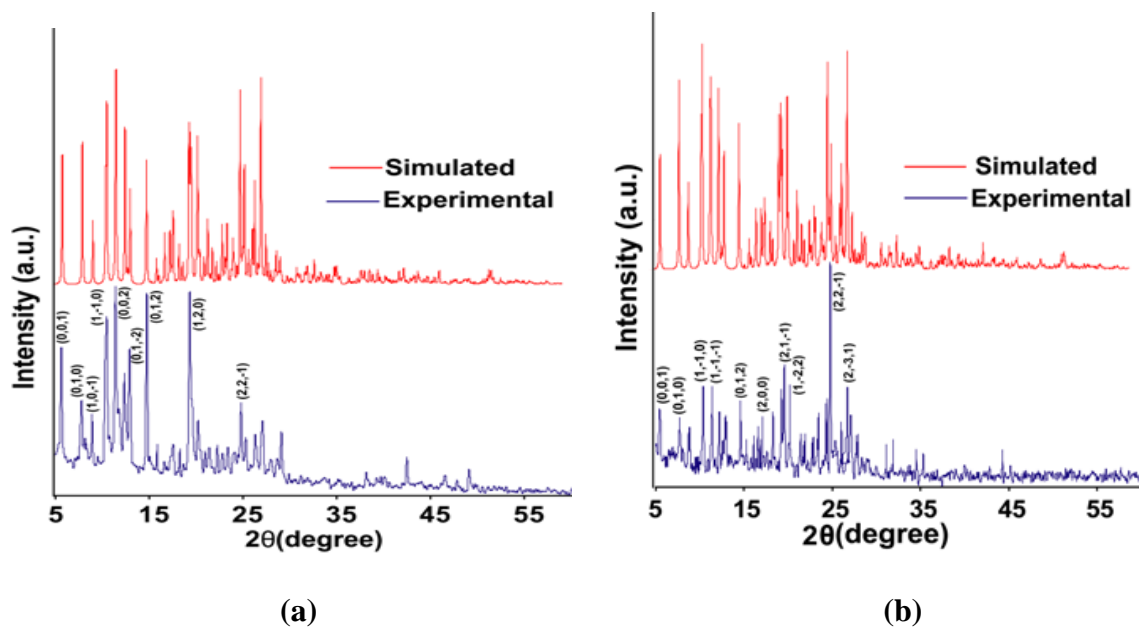


Figure 8S: PXRD pattern of the (a) complex 4 and (b) Complex 5

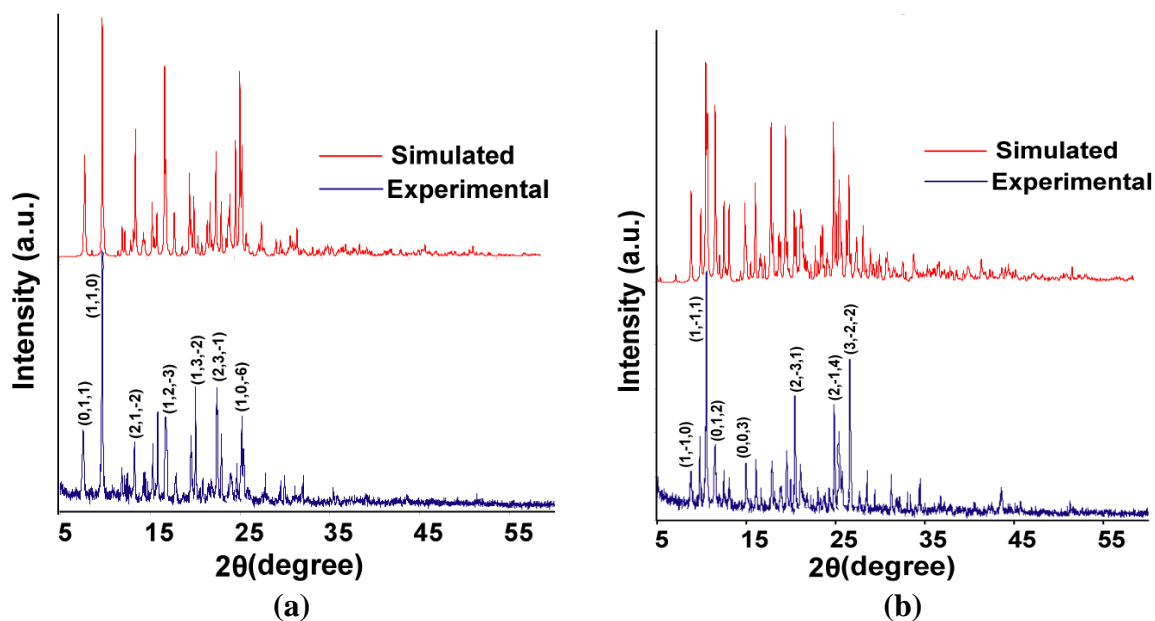


Figure 9S: PXRD pattern of the (a) complex 6 and (b) complex 7

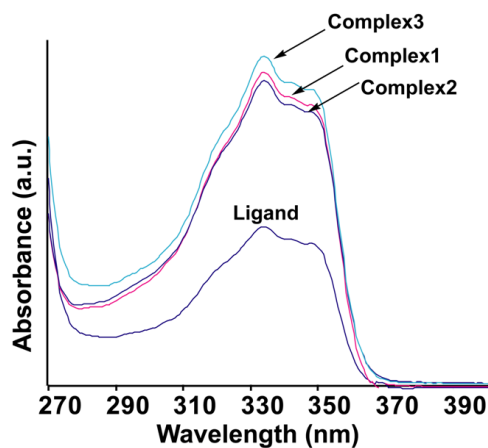


Figure 10S : UV-Vis spectra of the ligand, complex 1, complex 2 and complex 3 in DMF (concentration of 10^{-6} M each)

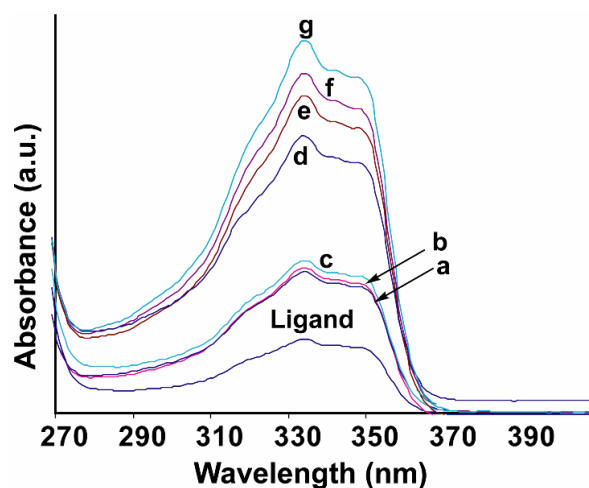


Figure 11S: UV-Vis spectra of the ligand, (a) complex **2**; (b) complex **1**; (c) complex **3**; (d) complex **6**; (e) complex **5**; (f) complex **4**; (g) complex **7**; in DMF (concentration of 10^{-6} M each).

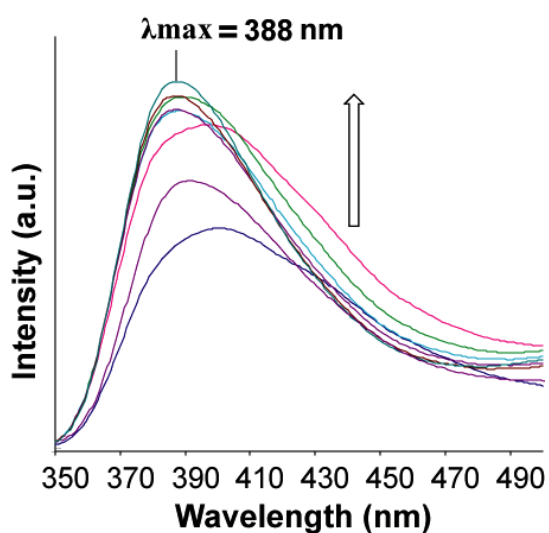


Figure 12S: Temperature dependent fluorescence spectra of the ligand, **L**. Fluorescence intensity increases with increasing temperature (30°C to 100°C, 0.1mM solution in DMF, $\lambda_{ex} = 340$ nm)

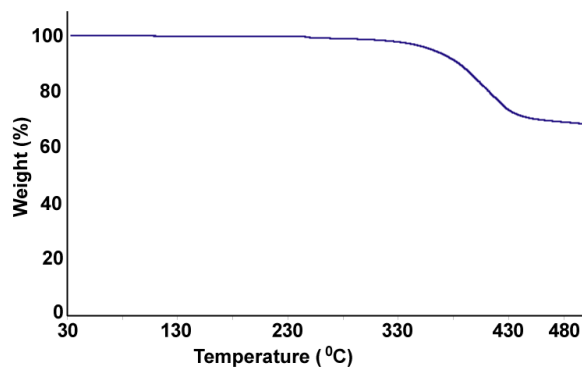


Figure 13S: Thermogravimetry of the complex **1**

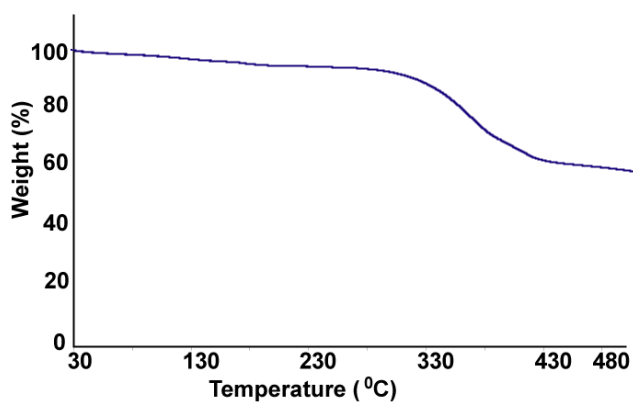


Figure 14S: Thermogravimetry of the complex **2**. In case of the complex **2**, the decomposition of the organic ligand started from 280 °C

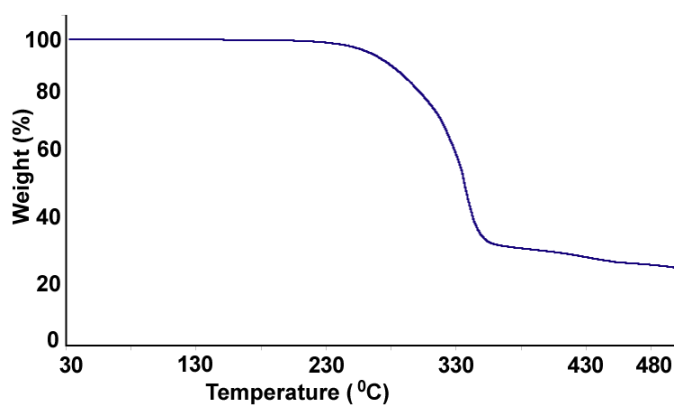


Figure 15S: Thermogravimetry of the complex **3**

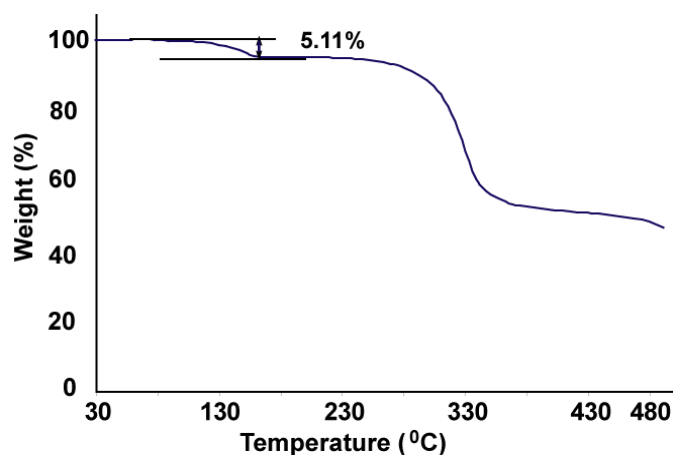


Figure 16S: Thermogravimetry of the complex **4** (For the complex **4**, one step weight loss due to the two solvent acetonitrile molecules takes place in the temperature range 70–170 °C corresponding to a weight loss of 5.11% (calcd 5.56%). The decomposition of ligand at 250 °C–460 °C.

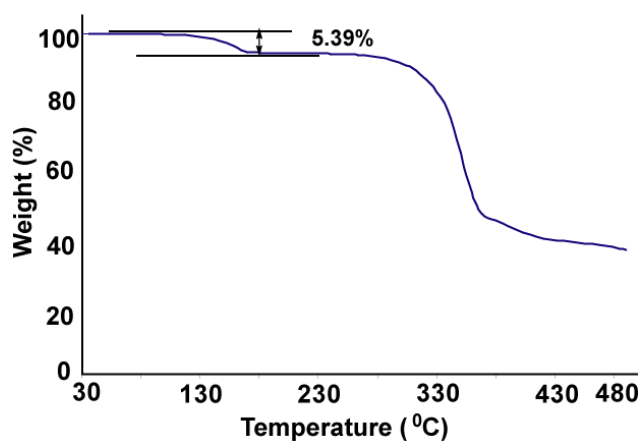


Figure 17S: Thermogravimetry of the complex **5**. The two solvent acetonitrile molecules are lost in the range 88–200 °C corresponding to a weight loss of 5.39 % (calcd. 5.55 %) and the decomposition of organic ligands at 260 °C–460 °C.

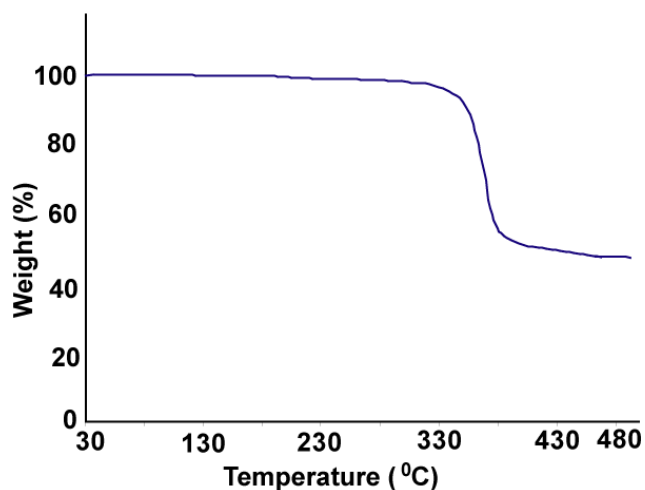


Figure 18S: Thermogravimetry of the complex **6**. Complex **6** shows a gradual one step weight loss due to the degradation of organic ligands in the temperature range 130-460 °C.

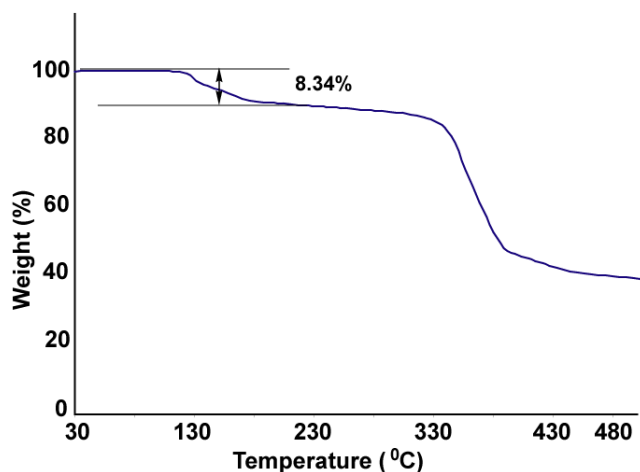


Figure 19S: Thermogravimetry of the complex **7**. The complex **7** shows weight loss of 8.34 wt % (calcd. 8.98 wt%) in the range of 120-182 °C corresponds to the loss of one lattice dimethylformamide molecule and one coordinated dimethylformamide molecule.

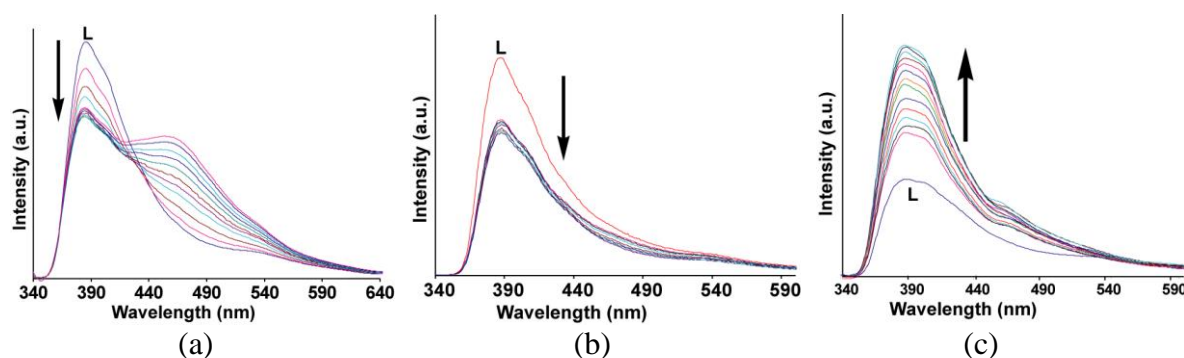


Figure 20S: The changes in the intensity of fluorescence emission ($\lambda_{\text{ex}} = 340\text{nm}$) of the ligand, **L** (2ml of 10^{-4} M solution in DMF) on addition of (a) ZnCl_2 , (b) CdCl_2 and (c) HgCl_2 (5 μl aliquots of 10^{-2} M solution in methanol) .

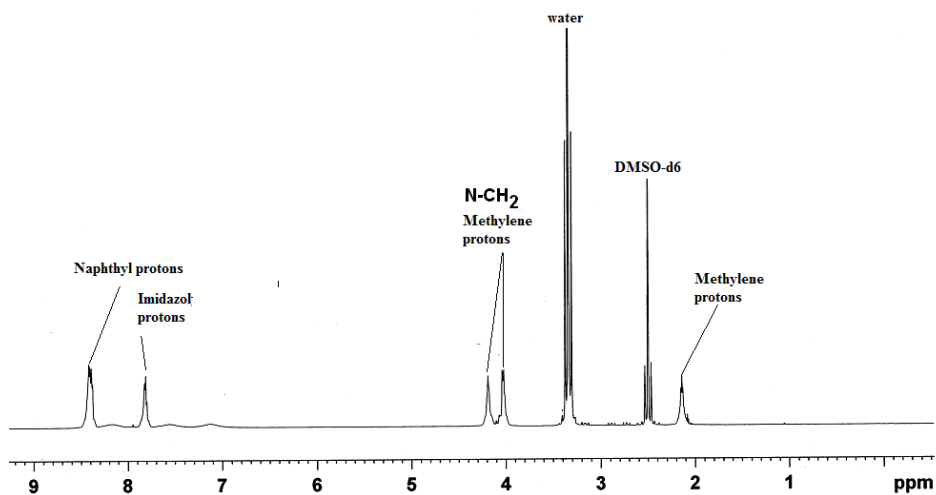


Figure 21S: $^1\text{H-NMR}$ (600 MHz, DMSO-d_6) spectra of the complex **6**.

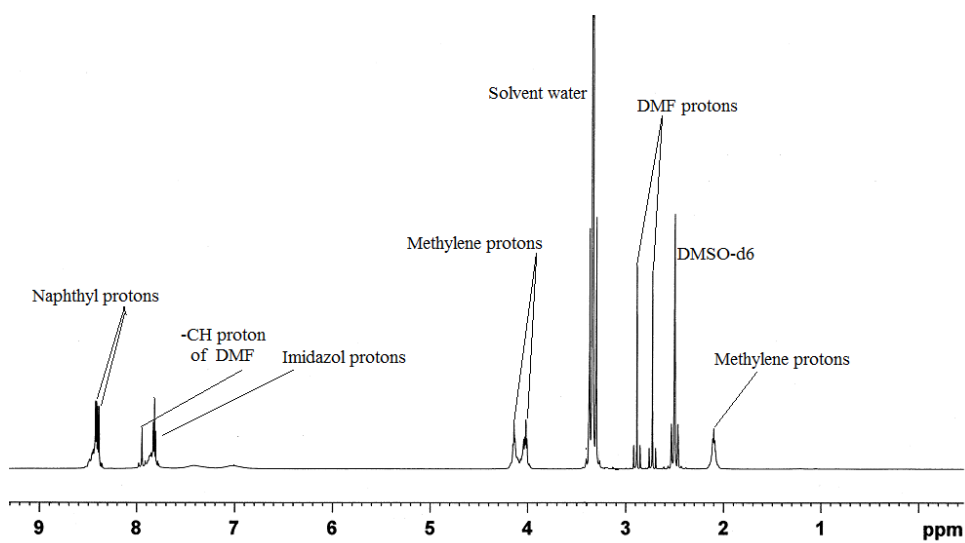


Figure 22S: $^1\text{H-NMR}$ (600 MHz, DMSO-d_6) spectra of the complex **7**.